# Edith Cowan University

# Copyright Warning

# MICROSTRUCTURE AND MECHANICAL BEHAVIOR OF METASTABLE BETA TYPE TITANIUM ALLOYS

This thesis is presented for the degree of

**Doctor of Philosophy**

By:

**Chirag Dhirajlal Rabadia**

Principal supervisor:

**Professor Lai-Chang Zhang**

Associate supervisor:

**Professor Hongqi Sun**

**School of Engineering,**

**Edith Cowan University (ECU)**

**2020**

**Page deliberately left blank**

# Abstract

Current biomaterials such as stainless steel, Co-Cr alloys, commercially pure titanium and Ti-6Al-4V either possess poor mechanical compatibility and/or produce toxic effects in the human body after several years of usage. Consequently, there is an enormous demand for long-lasting biomaterials which provide a better combination of mechanical, corrosion and biological properties. In addition to this, alloys used in high-strength applications possess either high-strength or large plasticity. However, a high-strength alloy should possess a better blend of both strength and plasticity when used in high-strength applications. Metastable β-titanium alloys are the best suited alloys for biomedical and high-strength applications because they demonstrate a wide range of superior mechanical, corrosion and biological properties.

In this PhD study, the Ti-27Nb-7Fe-xCr (x = 0, 2, 4, 6, 8 wt%) alloys using inexpensive elements (Fe, Mn, Cr etc.) have been designed to check their suitability for biomedical applications, whereas the Ti-33Zr-xFe-yCr (x = 3, 5, 7 and y = 2, 4 wt%), Ti-35Zr-5Fe-xMn (x = 0, 2, 4, 6, 8 wt%) and Ti-xZr-7Fe-ySn (x = 25, 30, 35 and y = 2, 4 wt%) alloys have been designed to check their suitability for high-strength applications. Later, all the investigated alloys have been cast using a cold crucible levitation melting technique.

In the Ti-27Nb-7Fe-xCr alloys, only 2 wt% quantity of Cr is enough to retain a single β phase. Young's moduli of the Ti-27Nb-7Fe-xCr alloys decrease from 116 GPa (in Ti-27Nb-7Fe) to 72 GPa (in Ti-27Nb-7Fe-8Cr) as the β stability improves. The Ti-33Zr-xFe-yCr alloys, except Ti-33Zr-3Fe-2Cr alloy, demonstrate a C15 type Laves phase and a dominating β phase. Moreover, the Ti-35Zr-5Fe-xMn and Ti-xZr-7Fe-ySn alloys show C14 type Laves and β phases. It is quite interesting to investigate the deformation and strength characteristics of hexagonal close-packed C14 and face-centered cubic C15 type Laves phases in the soft β matrix. Therefore, the deformation and strength characteristics of C14 phase in Ti-35Zr-5Fe-6Mn and C15 phase in Ti-33Zr-7Fe-4Cr, considering the same volume fraction of Laves phase (~7.0%) have been evaluated and compared using a micro-indentation method. Remarkably, dislocation activity and plastic deformation features are evident in the C15 phase, whereas the C14 phase strongly blocks dislocation motion.

The Ti-33Zr-xFe-yCr, Ti-35Zr-5Fe-xMn and Ti-xZr-7Fe-ySn alloys, designed for high-strength applications, demonstrate yield strength from 1048 to 1580 MPa, ultimate compressive strength from 1498 to 2140 MPa and plastic strain from 2.6 to 33.6%. Further, the appropriate variation in the volume fraction of Laves phase helps in achieving an improved trade-off between strength and plasticity. Moreover, fracture analyses have also been executed for the Ti-33Zr-xFe-yCr, Ti-35Zr-5Fe-xMn and Ti-xZr-7Fe-ySn alloys. It has been found that the crack propagates along the corresponding Laves phase present in these alloys. The results of the investigated alloys suggest that Ti-27Nb-7Fe-8Cr is suitable for biomedical applications, whereas Ti-33Zr-7Fe-4Cr, Ti-35Zr-5Fe-8Mn and Ti-35Zr-7Fe-2Sn are suitable for high-strength structural applications. This research is useful to understand the microstructure, mechanical and fracture behavior of titanium alloys used in industries such as biomedical, aerospace, automobile etc.

# Declaration

I certify that this PhD thesis does not, to the best of my knowledge and belief:

I. Incorporate without acknowledgment any material previously submitted for a degree or diploma in any institution of higher education;
II. Contain any material previously published or written by another person except where due reference is made in the text of this thesis; or
III. Contain any defamatory material.

Chirag Dhirajlal Rabadia

07/01/2020

# Acknowledgements

First and foremost, I would like to thank Almighty God for giving me strength, knowledge, ability and opportunity to undertake this doctoral study and to persevere and complete it satisfactorily.

I would like to express my heartiest gratitude to my supervisor and a well-known academician Prof. Lai-Chang Zhang for giving me the opportunity to be a part of his research group. He always supported and motivated me to execute my PhD study with high efficiency and effectiveness. He treated me as his younger brother and allowed me to share my innermost thoughts and emotions with him. I have significantly enhanced my research and other academic skills only based on his skilled advice and comments. It is my great honor to carry out my study under his valuable supervision. He always gave me his valuable time not only during office hours but even after office-hours until late night and during weekends as well. I have to say that it was not possible for me to achieve such high research outcomes without his guidance. I really hope that I will always be your student or younger brother in the future as well. I would also like to thank Prof. Hongqi Sun for being my co-supervisor and giving me helpful suggestions. I am also grateful for the financial support from the ECU HDR Scholarship which helped me in managing my research and living expenses.

I want to extend my gratitude to my senior colleague Dr. Yujing Liu who helped me in doing many experiments at The University of Western Australia, gave me his valuable time for my experimental work and many insightful suggestions related to my research. I am also thankful to my colleagues Mr. Syed Faraz Jawed, Mr. Shunxing Liang, Mr. Jincheng Wang and Mr. Peng Qin for their kind support and help throughout my study.

I would like to express my heartily gratitude to my beautiful wife Nisha for her endless love and unconditional support throughout this entire process. She has made countless sacrifices and encouraged me to get this point. I am sincerely grateful to my parents and parents-in-law for their invaluable support, encouragement and blessings. Without their love and attention none of this would have been possible.

I dedicate my PhD thesis to all of them. I wish they would be proud of my doctoral research and efforts.

# List of publications arising from this work

## A) First-authored peer-reviewed publications

[1] **C.D. Rabadia**, Y.J. Liu, G.H. Cao, Y.H. Li, C.W. Zhang, T.B. Sercombe, H. Sun, L.C. Zhang, High-strength β stabilized Ti-Nb-Fe-Cr alloys with large plasticity, *Materials Science and Engineering: A* 732 (2018) 368-377. https://doi.org/10.1016/j.msea.2018.07.031

**(Main source of Chapter 5)**

[2] **C.D. Rabadia**, Y.J. Liu, L. Wang, H. Sun, L.C. Zhang, Laves phase precipitation in Ti-Zr-Fe-Cr alloys with high strength and large plasticity, *Materials & Design* 154 (2018) 228-238. https://doi.org/10.1016/j.matdes.2018.05.035.

**(Main source of Chapter 6)**

[3] **C.D. Rabadia**, Y.J. Liu, S.F. Jawed, L. Wang, Y.H. Li, X.H. Zhang, T.B. Sercombe, H. Sun, L.C. Zhang, Improved deformation behavior in Ti-Zr-Fe-Mn alloys comprising the C14 type Laves and β phases, *Materials & Design* 160 (2018) 1059-1070. https://doi.org/10.1016/j.matdes.2018.10.049.

**(Main source of Chapter 7)**

[4] **C.D. Rabadia**, Y.J. Liu, L.Y. Chen, S.F. Jawed, L.Q. Wang, H. Sun, L.C. Zhang, Deformation and strength characteristics of Laves phases in titanium alloys, *Materials & Design* 179 (2019) 107891. https://doi.org/10.1016/j.matdes.2019.107891.

**(Main source of Chapter 8)**

[5] **C.D. Rabadia**, Y.J. Liu, C.H. Zhao, J.C. Wang, S.F. Jawed, L.Q. Wang, L.Y. Chen, H. Sun, L.C. Zhang, Improved trade-off between strength and plasticity in titanium based metastable beta type Ti-Zr-Fe-Sn alloys, *Materials Science and Engineering:* A 766 (2019) 138340. https://doi.org/10.1016/j.msea.2019.138340.

**(Main source of Chapter 9)**

## B) Collaborative peer-reviewed publications

[1] S.F. Jawed, **C.D. Rabadia**, Y.J. Liu, L.Q. Wang, Y.H. Li, X.H. Zhang, L.C. Zhang, Mechanical characterization and deformation behavior of β-stabilized Ti-Nb-Sn-Cr alloys, *Journal of Alloys and Compounds* 792 (2019) 684-693. https://doi.org/10.1016/j.jallcom.2019.04.079.

[2] S.F. Jawed, **C.D. Rabadia**, Y.J. Liu, L. Wang, Y.H. Li, X.H. Zhang, L.C. Zhang, Beta-type Ti-Nb-Zr-Cr alloys with large plasticity and significant strain hardening, *Materials & Design* 181 (2019) 108064. https://doi.org/10.1016/j.matdes.2019.108064.

### C) First-authored conference publication

[1] **C.D. Rabadia**, Y.J. Liu, S.F. Jawed, L.Q. Wang, L.C. Zhang, Bulk deformation and toughness behavior of titanium alloys comprising the C15-type Laves and beta phases in "*International Conference on Materials Science and Engineering- 2019*" at Melbourne, Australia (Accepted in conference and under review for publication in *Materials Today Sustainability* journal).

# Table of Contents

# List of Abbreviations

| | |
|---|---|
| 316L SS | 316L stainless steel |
| $a$ | Lattice parameter |
| $a_{C14}$ | Lattice parameter of C14 phase |
| $a_{C15}$ | Lattice parameter of C15 phase |
| $a_{\beta}$ | Lattice parameter of β phase |
| bcc | Body-centered cubic |
| $Bo$ | Bond order |
| CCLM | Cold crucible levitation melting |
| Co-Cr | Cobalt-chromium |
| CP-Ti | Commercially pure titanium |
| $e/a$ | Valence electrons to atoms ratio |
| EDS | Energy dispersive X-ray spectroscopy |
| fcc | Face-centered cubic |
| hcp | Hexagonal close-packed |
| HV | Vickers hardness |
| $\lambda$ | The size of the subsurface deformation zone |
| $Md$ | Metal d-orbital energy level |
| $Mo_{eq}$ | Molybdenum equivalent |
| OM | Optical microscopy |
| PUSCS | Product of compressive strength and compressive strain |
| $S$ | Spacing between slip steps |
| SAED | Selected area electron diffraction |
| SEM | Scanning electron microscopy |
| T25S1 | Ti-25Zr-7Fe-1Sn (wt%) |
| T25S2 | Ti-25Zr-7Fe-2Sn (wt%) |
| T30S1 | Ti-30Zr-7Fe-1Sn (wt%) |
| T30S2 | Ti-35Zr-7Fe-1Sn (wt%) |
| T30S2 | Ti-30Zr-7Fe-2Sn (wt%) |
| T35S2 | Ti-35Zr-7Fe-2Sn (wt%) |
| TEM | Transmission electron microscopy |

| | |
|---|---|
| TNF0 | Ti-27Nb-7Fe (wt%) |
| TNF2 | Ti-27Nb-7Fe-2Cr (wt%) |
| TNF4 | Ti-27Nb-7Fe-4Cr (wt%) |
| TNF6 | Ti-27Nb-7Fe-6Cr (wt%) |
| TNF8 | Ti-27Nb-7Fe-8Cr (wt%) |
| TZ32 | Ti-33Zr-3Fe-2Cr (wt%) |
| TZ34 | Ti-33Zr-3Fe-4Cr (wt%) |
| TZ52 | Ti-33Zr-5Fe-2Cr (wt%) |
| TZ54 | Ti-33Zr-5Fe-4Cr (wt%) |
| TZ72 | Ti-33Zr-7Fe-2Cr (wt%) |
| TZ74 | Ti-33Zr-7Fe-4Cr (wt%) |
| TZF0 | Ti-35Zr-5Fe (wt%) |
| TZF2 | Ti-35Zr-5Fe-2Mn (wt%) |
| TZF4 | Ti-35Zr-5Fe-4Mn (wt%) |
| TZF6 | Ti-35Zr-5Fe-6Mn (wt%) |
| TZF8 | Ti-35Zr-5Fe-8Mn (wt%) |
| $V_f$ | Volume fraction |
| $V_{f,\,C14}$ | Volume fraction of C14 phase |
| $V_{f,\,C15}$ | Volume fraction of C15 phase |
| $V_{f,\,Laves}$ | Volume fraction of Laves phase |
| $V_{f,\,\beta}$ | Volume fraction of β phase |
| $V_{f,\,\alpha''}$ | Volume fraction of α" phase |
| XRD | X-ray diffraction |
| α | Alpha |
| α' | Alpha prime |
| α" | Alpha double prime |
| β | Beta |
| $\delta$ | The size of deformation zone around the indentations |
| $\rho_d$ | Dislocation density |
| $\sigma_{UTS}$ | Ultimate tensile strength |
| ω | Omega |

$\overline{Bo}$ Average value of bond order

$\overline{Md}$ Average value of metal d-orbital energy level

# List of Figures

# List of Tables

# Chapter 1. Introduction and significance

This chapter gives a brief overview on metastable titanium alloys and information on the problem statement of this research. This chapter also details the significance and innovation of the research.

## 1.1. Introduction and problem statement

The last two decades have witnessed an exponentially increasing demand in development of light-weight alloys for several engineering applications, especially in biomedical, aerospace and automobile industries [1]. Titanium alloys are the most preferred alloys amongst other metallic materials for these aforementioned applications due to their outstanding attributes, e.g., low density, high specific strength, superior work hardening ability, excellent abilities to resist corrosion along with very good fatigue behavior [2]. In general, it is difficult to achieve high strength and high plasticity together in metallic materials [3]. However, titanium alloys demonstrate an impressive trade-off between strength and plasticity. There are three fundamental types of titanium alloys: (i) α alloys, (ii) α + β alloys and (iii) β alloys. β type titanium alloys comprise the highest number of slip systems and therefore, β type titanium alloys exhibit the highest deformability amongst the three type of titanium alloys, followed by α + β alloys and α alloys [4]. The proportion of β phase greatly impacts the mechanical and corrosive properties of titanium alloys [5, 6]. Hence, β titanium alloys not only help to achieve an improved trade-off between strength and plasticity but they also help to achieve enhanced corrosion resistance and fatigue properties.

The stability of the β phase depends on the concentration of β stabilizers such as Nb, Fe, Mo, Cr, Ta, Mn etc. in titanium alloys [1]. Therefore, the selection of alloying elements and their corresponding concentrations are primarily important phenomena in designing titanium alloy compositions for a specific engineering application. Moreover, several electronic parameters such as bond order (*Bo*), metal d-orbital energy level (*Md*), valence electron concentration, molybdenum equivalent ($Mo_{eq}$) and atomic radius of alloying elements are also useful in designing titanium alloy compositions either for biomedical applications where low Young's modulus is an essential parameter for an alloy, or for structural applications where high strength is an essential parameter for an alloy [5, 7].

Commercially pure-titanium (CP-Ti) and Ti-6Al-4V are currently used in several biomedical and structural applications [8]. However, CP-Ti and Ti-6Al-4V are not ideally suited to biomedical and structural applications due to their poor mechanical behavior and biocompatibilities [8]. Other than CP-Ti and Ti-6Al-4V, many researchers have presented their scientific endeavors to date to develop titanium alloys with the required properties for biomedical and structural applications. However, researchers have bridged the gap between the actual and the required mechanical, biological and corrosive properties of titanium alloys up to a certain level. Hence, it is immensely desirable to design and develop new titanium alloys for biomedical and high-strength structural applications. In addition to this, the cost of an alloy should also be considered when designing new titanium alloys to lower the overall cost of titanium alloys. Thus, it is also necessary to design new alloys using inexpensive elements considering the prospective performance and the cost of the alloy simultaneously.

### 1.2. Significance and innovation

Amongst β stabilizers, elements such as Fe, Mn and Cr are eutectoid type β stabilizers, where elements such as Nb, Mo and Ta are isomorphous type β stabilizers [9]. Although Zr, Sn and Si are considered as neutral elements when added to titanium alloys, the established literature suggests that these elements enhance the β stability in titanium alloys [10]. Therefore, the elements for new titanium alloys should be selected in a manner where newly designed alloys demonstrate very good overall performance at a low-cost.

The essential requirements of titanium alloys for biomedical applications are to achieve comparable strength and low Young's modulus which should be near to that of human bone (~ 30 GPa) along with improved wear and corrosion resistance [1]. Nb is quite an effective alloying element in obtaining the required mechanical, biological and corrosive properties when alloyed with Ti for biomedical applications, whereas Fe and Cr are inexpensive and strong β stabilizers which improve strength and hardness and simultaneously, reduce Young's modulus [7]. Hence, the Ti-Nb-Fe-Cr alloys have been designed in the present work using aforementioned electronic parameters and $Mo_{eq}$ to investigate their suitability for biomedical applications.

The role of a strengthening phase remains crucial in enhancing strength and hardness of an alloy. Laves phases are intermetallic strengthening phases and effective in tailoring the mechanical properties of materials for several high-strength structural applications in aerospace and

automobile industries [11]. Laves phase precipitation in an alloy depends on (i) the atomic radii ratio of relatively larger and smaller atoms, (ii) average valence electron concentration and (iii) the difference in electronegativities of relatively larger and smaller atoms, where the values of these parameters rely on the type of alloying elements and their concentrations in an alloy [12]. Moreover, the binary and ternary phase diagrams of alloying elements also help in predicting the Laves phase precipitation in titanium alloys [12, 13]. Laves phases comprising Fe and Zr elements are popular and evident in many Ti-Zr-Fe alloys displaying the superior mechanical properties. Furthermore, Zr has a higher affinity to be soluble in Ti and other alloying elements, i.e., Fe, Mn, Cr and Sn are inexpensive but very reliable to enhance the mechanical properties in titanium alloys [5, 10]. Hence, Ti-Zr-Fe-Cr, Ti-Zr-Fe-Mn and Ti-Zr-Fe-Sn alloys have been designed in the present work with an aim to obtain Laves phase in the microstructure considering their corresponding ternary phase diagrams for several high-strength structural applications. Moreover, the corresponding microstructure and mechanical behavior of Laves phases in the designed titanium alloys have also been investigated.

### 1.3. Outline of the thesis

This doctorate thesis follows the "Thesis with Publication" format (available on ECU website). Chapters 5 to 9 of this thesis consist of work that has been published in peer-reviewed journals. The outline of the thesis is as follows:

- **Chapter 1** gives a brief overview on titanium alloys and defines the problem statement of this research. This chapter also details the significance and innovation of the research.
- **Chapter 2** provides a comprehensive literature review relating to titanium alloys suitable for biomedical and high-strength structural applications including the information on the microstructure and mechanical properties of the previously reported findings.
- **Chapter 3** describes the applicability and objectives of the present research, as based on the literature review.
- **Chapter 4** provides details on the materials and experimental methods used in the present work.
- **Chapter 5** provides the design and performance details of the Ti-27Nb-7Fe-xCr alloys, which have been designed for biomedical applications.

- **Chapters 6 to 9** provide various performance details of the Ti-33Zr-xFe-yCr, Ti-35Zr-5Fe-xMn and Ti-xZr-7Fe-ySn alloys, which have been designed for high-strength structural applications.
- **Chapter 10** summarizes the concluding remarks of the present research and also provides recommendations for future work.
- **Bibliography** of the present work is presented at the end of the thesis.

# Chapter 2. Literature review

This chapter provides a comprehensive literature review on titanium alloys including fundamental types of titanium alloys, microstructure and mechanical properties of titanium alloys and suitability of titanium alloys for biomedical and high-strength structural applications.

## 2.1. Introduction

Titanium is a transition metal in the periodic table of elements. Titanium alloys are metallic materials which contain titanium and other chemical element/s. Titanium alloys are generally considered as relatively new engineering materials because titanium alloys were discovered many years later than commonly used metallic materials [14, 15]. Titanium alloys became commercially available in 1940s, initially as structural applications and then, the usage of titanium alloys as metallic biomaterials expanded in the 1960s [14, 15]. Subsequently, the use of titanium and titanium alloys rapidly increased in many industries such as aerospace, nuclear, chemical, power generation, orthopedic, dental, sports etc. The strength of titanium alloys is almost the same as stainless steel but the density of titanium is almost half of the density of stainless steel [16]. Therefore, titanium alloys have been considered as light-metals. Titanium alloys also exhibit low elastic modulus and superior resistance to corrosion, wear and fatigue-loading [2, 6, 8]. In addition, the mechanical properties of titanium alloys can be tailored with a long range of options for strength and ductility through the addition of appropriate alloying elements, thermo-mechanical processing and additive manufacturing techniques [4, 17]. As a result, it is possible for titanium alloys to obtain the required blend of strength and ductility depending on the requirement of a specific application. Hence, titanium alloys have become a significantly preferred metallic material in many engineering applications.

Titanium possesses two allotropic phases, i.e., α phase and β phase [14]. The α phase of titanium forms below 883 °C with a hexagonal close-packed (hcp) structure, whereas the β phase of titanium forms above 883 °C with a body-centered cubic (bcc) structure [1, 18-20]. Therefore, the temperature of 883 °C is considered as phase transformation or transus temperature for titanium [1]. The allotropic transformation temperature of pure titanium either increases or decreases depending on the type of alloying elements added in titanium alloy compositions [18]. Alloying elements such as Al, O, N etc. increase the allotropic transformation temperature and stabilize the

α phase, which are known as α stabilizers. In contrast, some alloying elements such as Nb, Ta, Mo, Mg, V, W, Re, Fe, Ni, Cr, Co, Mn, Cu etc. decrease the allotropic transformation temperature and stabilize the β phase, which are known as β stabilizers [9, 18]. Amongst β stabilizers, elements such as V, Nb, Mo, Ta, Re etc. are considered as β isomorphous elements, where elements such as Cr, Mn, Fe, Cu, Ni, Cu etc. are considered as β eutectoid elements [9]. In addition to this, few elements such as Zr, Hf, Sn etc. are considered as neutral elements in which there is no noticeable change in allotropic transus temperature occurs. Hence, neutral elements technically do not stabilize either of the phases, i.e., α or β [1, 9]. Based on the volume fraction ($V_f$) of α ($V_{f,\alpha}$) and β ($V_{f,\beta}$) phases, titanium alloys are classified into four diverse groups: (a) α titanium alloys which comprise only α stabilizers in alloy compositions and consist a full α phase in the microstructure, (b) near α titanium alloys which comprise around 1 to 2% of β stabilizers in alloy compositions and show β fraction of around 5 to 10% in the microstructure, (c) α+β titanium alloys which hold a greater amount of β stabilizers in alloy compositions and display β fraction of around 10 to 40% in the microstructure and (d) β titanium alloys which possess a rich amount of β stabilizers in alloy compositions and display a single β phase in the microstructure [14, 21]. The stabilities of α and β phases and transformation temperature of titanium alloys mostly depend on the alloying elements present in the alloy composition. Fig. 2.1 and Fig. 2.2 schematically illustrate the effect of alloying elements on the phase stability of titanium alloys [14, 22]. It is apparent from Fig. 2.1 that the quantities of alloying elements and processing temperature greatly influence the formation of α and β phases in the microstructure and thereby, mechanical behavior as well. The addition of required quantities of β isomorphous and/or β eutectoid elements exhibit a stable β phase in the microstructure (Fig. 2.1). In case of titanium alloys with β eutectoid elements, the precipitation of intermetallic phases occurs either with α and/or with β phases due to eutectoid reactions.

In general, α and intermetallic phases are relatively brittle in nature, while the β phase is relatively soft in nature [16, 23-25]. This means that the deformability of the β phase remains better than that of other α and intermetallic phases. The deformability of a specific phase in the microstructure greatly relies on the crystal structure [3]. A greater number of slip systems remain active in a bcc structure compared to fcc and hcp structures and therefore, a phase with a bcc structure deforms a much more than a phase with either fcc or hcp structures [26, 27]. In contrast, a phase with fcc and/or hcp structures demonstrate high yield strength and hardness as compared to a phase with a bcc structure [26, 27]. This means that α and intermetallic phases are also beneficial to obtain high

yield strength and hardness. The requirements of mechanical and corrosion properties change depending on the type of applications, where these properties entirely rely on the microstructure of alloys. Therefore, it is necessary to understand the microstructure behavior of all three fundamental types of titanium alloys and their influencing parameters. A brief review on the three fundamental types of titanium alloys has been covered in Section 2.2.

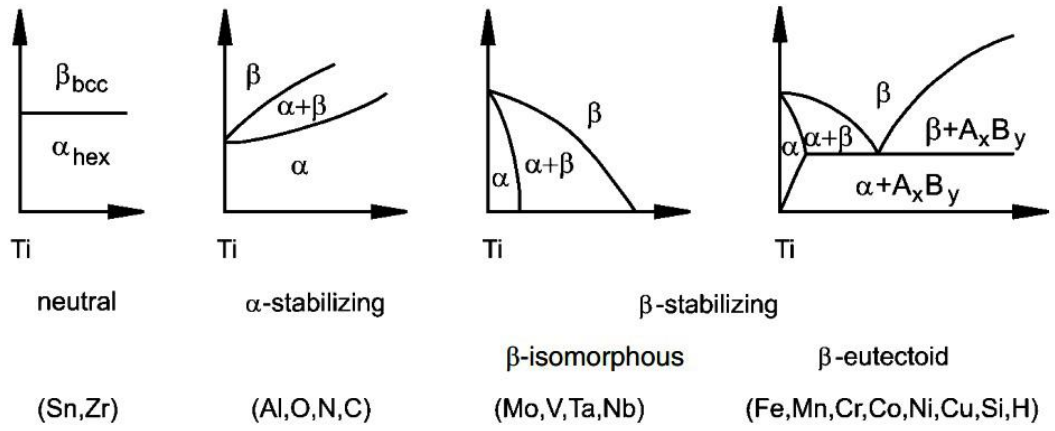


Fig. 2.1. The effect of alloying elements on the phase stability of titanium alloys [14, 22].

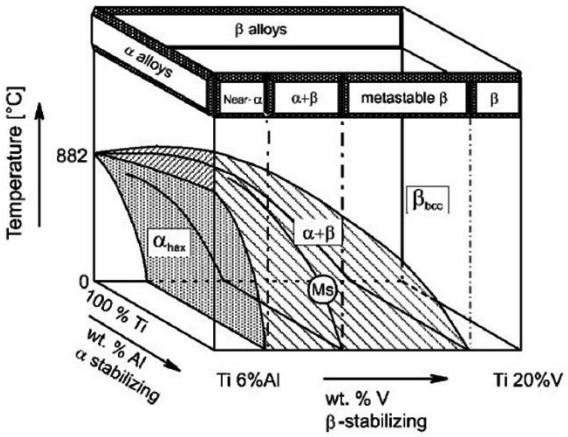


Fig. 2.2. The effect of α and β stabilizing elements on α and β stabilities of titanium alloys respectively [14, 22].

## 2.2. Fundamental types of titanium alloys

There are three fundamental types of titanium alloys: (a) α alloys, (b) α+β alloys and (c) β alloys. Table 2.1 [14] presents varied physical and mechanical properties of α, α+β and β titanium alloys which are useful in selecting a specific type of titanium alloys for a specific application.

### 2.2.1. α titanium alloys

Al is a popular α stabilizing element and its specific strength is about 50% of the specific strength of titanium [14]. Therefore, the density of α titanium alloys is less than that of β titanium alloys. In general, α titanium alloys are suitable for chemical and other processing industries due to comprising excellent corrosion resistance. Various grades of CP-Ti are commonly α type titanium alloys. The grades of CP-Ti are distinguishable based on the concentration of interstitial Fe and O as presented in Table 2.1 [14]. The quantities of interstitial O are intentionally varied in different grades of CP-Ti to obtain different values of strength and ductility, whereas the impurities of Fe, C, N and H come from the manufacturing process employed. As quantities of interstitial O increase, the strength of CP-Ti significantly increases, where the ductility significantly decreases.

Table 2.1. The physical and mechanical properties of α, α+β and β titanium alloys [14].

| **Properties** | **Titanium alloys** | | |
|---|---|---|---|
| | **α** | **α+β** | **β** |
| Density | + | + | − |
| Strength | − | + | ++ |
| Ductility | −/+ | + | +/− |
| Corrosion resistance | ++ | + | +/− |
| Oxidation resistance | ++ | +/− | − |
| Cod workability | −− | − | −/+ |
| Weldability | + | +/− | − |
| Creep strength | + | +/− | − |
| Fracture toughness | + | −/+ | +/− |

Table 2.2 [28] and Table 2.3 [17, 29-32] reveal that as the concentration of interstitial O increases in CP-Ti, the values of yield strength and ultimate tensile strength ($\sigma_{UTS}$) increase, whereas the values of elongation decrease. Due to comprising an hcp structure, α titanium alloys show high fracture toughness, reasonable strength, low forgeability and relatively high modulus. Therefore, α titanium alloys are used for low-temperature applications. Nonetheless, near α titanium alloys demonstrate superior creep behavior at high-temperatures and are considered as classical high-temperature alloys. Ti-8Al-1Mo-1V (known as Ti-8-1-1) was the first alloy that was used for high-temperature applications; however, this alloy also exhibits poor stress corrosion behavior. To overcome this problem, Ti-6Al-2Sn-4Zr-2Mo-0.1S (known as Ti-6-2-4-2-S) was developed by

TIMET, which exhibits improved creep behavior. Further research on Ti-6Al-2Sn-4Zr-2Mo-0.1S has revealed that the concentration of Si does not show any unfavorable effects in high-temperature applications when added up to 0.5 wt%. Subsequently, Ti-11Sn-5Zr-2.25Al-1Mo-0.25Si (known as IMI 679), Ti-6Al-5Zr-0.5Mo-0.25S (known as IMI 685) and Ti-5.8Al-4Sn-3.5Zr-0.7Nb-0.5Mo-0.35Si-0.06C (known as TIMETAL 834) were developed for high-temperature long-lasting applications targeting a service temperature of around 600 °C.

Table 2.2. The maximum concentrations of impurities present in various grades of CP-Ti [28].

| Materials | Maximum concentrations of impurities (wt%) | | | | |
|---|---|---|---|---|---|
| | Fe | O | C | N | H |
| CP-Ti grade 1 | 0.2 | 0.18 | 0.08 | 0.03 | 0.015 |
| CP-Ti grade 2 | 0.3 | 0.25 | 0.08 | 0.03 | 0.015 |
| CP-Ti grade 3 | 0.3 | 0.35 | 0.08 | 0.03 | 0.015 |
| CP-Ti grade 4 | 0.5 | 0.40 | 0.08 | 0.03 | 0.015 |

### 2.2.2. α+β titanium alloys

α+β titanium alloys have contributed significantly in increasing the popularity of titanium alloys because more than 50% of titanium alloys used commercially are α+β titanium alloys [14]. The properties of α+β titanium alloys can be tailored using various thermo-mechanical processing techniques. α+β titanium alloys demonstrate high yield, ultimate and fatigue strengths along with enhanced corrosion resistance as compared to α type CP-Ti [30]. Out of all the α+β titanium alloys, Ti-6Al-4V is the most prevalent α+β type titanium alloy for aerospace and biomedical applications as it possesses a better combination of above-mentioned properties [27]. Ti-6Al-4V was first developed in the United States in the early 1950s, where subsequently, various properties of Ti-6Al-4V have been rigorously investigated [15]. Ti-6Al-4V was initially used in aerospace applications and later applied to biomedical applications [17]. Moreover, the properties of Ti-6Al-4V were further improved by reducing the concentration of interstitial impurities (O, Fe, H, C and N) [33, 34]. The Ti-6Al-4V alloy with low interstitial impurities is known as Ti-6Al-4V ELI (Ti-6Al-4V with extra low interstitials) [34]. The presence of V in Ti-6Al-4V produces toxic reactions inside the human body [18]. Consequently, Ti-6Al-4V was initially replaced by Ti-6Al-7Nb and Ti-5Al-2.6Fe to improve the biocompatibility and corrosion behavior for biomedical applications [33, 34]. CP-Ti, Ti-6Al-4V, Ti-6Al-4V ELI, Ti-6Al-7Nb and Ti-5Al-2.6Fe are considered as the

first generation of biomaterials developed between the years of 1950 and 1990 [30, 35]. Ti-6Al-7Nb and Ti-5Al-2.6Fe exhibit better yield and tensile strength than Ti-6Al-4V and Ti-6Al-4V ELI at almost the same value of modulus [17].

Table 2.3. The tensile properties of α, α+β and β titanium alloys [17, 29-32]. Note that ultimate tensile strength, yield strength, elongation and elastic modulus are abbreviated as $\sigma_{UTS}$, $\sigma_{0.2}$, *El.* and *E* respectively in Table 2.3.

| Materials | $\sigma_{UTS}$ (MPa) | $\sigma_{0.2}$ (MPa) | *El.* (%) | *E* (GPa) |
|---|---|---|---|---|
| **α titanium alloys** | | | | |
| CP-Ti grade 1 (annealed) | 240 | 170 | 24 | 102 |
| CP-Ti grade 2 (annealed) | 345 | 275 | 20 | 102 |
| CP-Ti grade 3 (annealed) | 450 | 380 | 18 | 103 |
| CP-Ti grade 4 (annealed) | 550 | 485 | 15 | 104 |
| **α + β titanium alloys** | | | | |
| Ti-6Al-4V ELI (annealed) | 860-965 | 795-875 | 10 to 14 | 101-110 |
| Ti-6Al-4V (annealed) | 895-930 | 825-869 | 6 to 10 | 110-114 |
| Ti-6Al-7Nb (wrought) | 900-1050 | 880-950 | 8.1 to 15 | 114 |
| Ti-5Al-2.5Fe (cast) | 1020 | 895 | 15 | 112 |
| **β titanium alloys** | | | | |
| Ti-13Nb-13Zr (aged) | 973-1037 | 836-908 | 10 to 16 | 79-84 |
| Ti-12Mo-6Zr-2Fe (annealed) | 1060-1100 | 1000-1060 | 18-22 | 74-85 |
| Ti-15Mo (annealed) | 874 | 544 | 21 | 78 |
| Ti-15Mo-5Zr-3Al (solution treated/aged) | 852-1100 | 838-1060 | 18-25 | 80 |
| Ti-35Nb-7Zr-5Ta (annealed) | 597 | 547 | 19 | 55 |
| Ti-16Nb-10Hf (aged) | 851 | 736 | 10 | 81 |
| Ti-29Nb-13Ta-4.6Zr (aged) | 911 | 864 | 13.2 | 80 |
| Ti-15Mo-2.8Nb-0.2Si (annealed) | 979-999 | 945-987 | 16-18 | 83 |
| Ti-24Nb-4Zr-7.9Sn (hot forged) | 755 | 570 | 13 | 55 |
| Ti-24Nb-4Zr-7.9Sn (selective laser melting) | 665 | 563 | 14 | 53 |
| Ti-35Nb-7Zr-5Ta-0.4O (annealed) | 1010 | 976 | 19 | 66 |
| Ti-22.3Nb-4.6Zr-1.6Ta-6Fe (sintering/960 °C) | - | 2425 | 6.91 | 52 |

### 2.2.3. β titanium alloys

β titanium alloys contain enough quantities of β stabilizers in alloy compositions and depending on the quantities of β stabilizers, metastable β and stable β titanium alloys can be obtained [21, 30, 32]. The forgeability and heat treatability of β titanium alloys are better than those of α and α+β titanium alloys with a wide range of temperatures as β titanium alloys possess a greater amount of

β stabilizers [14]. The increase in $V_{f,\beta}$ leads to enhanced elongation, toughness, heat treatability and hardenability [30, 32]. Table 2.3 compares the tensile properties of β titanium alloys with α and α+β titanium alloys [17, 29-32]. It is evident from Table 2.3 that β titanium alloys display a very wide range of mechanical properties. This also suggests that it is easy to shape microstructures of β titanium alloys using several heat treatments, aging, rolling and cooling processes. Consequently, the mechanical properties for β titanium alloys can be tailored according to the requirement of a specific application. β titanium alloys demonstrate the lower elastic modulus and excellent corrosion resistance and biological behavior as compared to α and α+β titanium alloys [18, 23, 24, 30, 36]. As a result of these advantages, β titanium alloys have been extensively studied for biomedical applications over the last 30 years [1, 7, 17]. However, β titanium alloys still possess poor fatigue behavior and relatively high density compared to α and α+β titanium alloys [14]. Researchers in the last 10 years have applied their endevors to enhance the fatigue behavior and to reduce the density of β titanium alloys using additive manufacturing along with conventional thermo-mechanical processing techniques [4, 8, 10, 37-39]. It can be deduced that α and α+β titanium alloys can simply be replaced by β titanium alloys for most engineering applications.

### 2.3. Microstructures of titanium alloys

α titanium alloys are usually processed in the α phase field to control the grain size of the α phase [17]. Fig. 2.3 shows the microstructure of α phase in CP-Ti with two different grain sizes [21], i.e., (a) 10 μm which can be obtained after recrystallization at around 700-750 °C and (b) 50 μm which can be obtained after recrystallization at around 900 °C [21]. The mechanical properties directly relate with the grain size in the microstructure [7, 11]. This indicates that the processing temperature influences the mechanical properties of an alloy.

The α+β type Ti-6Al-4V alloys display lamellar, equiaxed and bimodal morphologies in their microstructures [14, 21, 32]. Lamellar morphologies form upon cooling from the β phase field, whereas equiaxed morphologies form as a result of recrystallization parameters used [14, 32]. In addition, the cooling medium and cooling rate usually influence the corresponding microstructure of Ti-6Al-4V. Slow cooling usually leads to the formation of pure lamellar structure with coarse morphologies [14, 32]. Fig. 2.4 shows the lamellar morphologies of Ti-6Al-4V at different

magnifications [21]. Further, the fast cooling/quenching leads to the formation of fine acicular morphologies, which are also presented in Fig. 2.4.

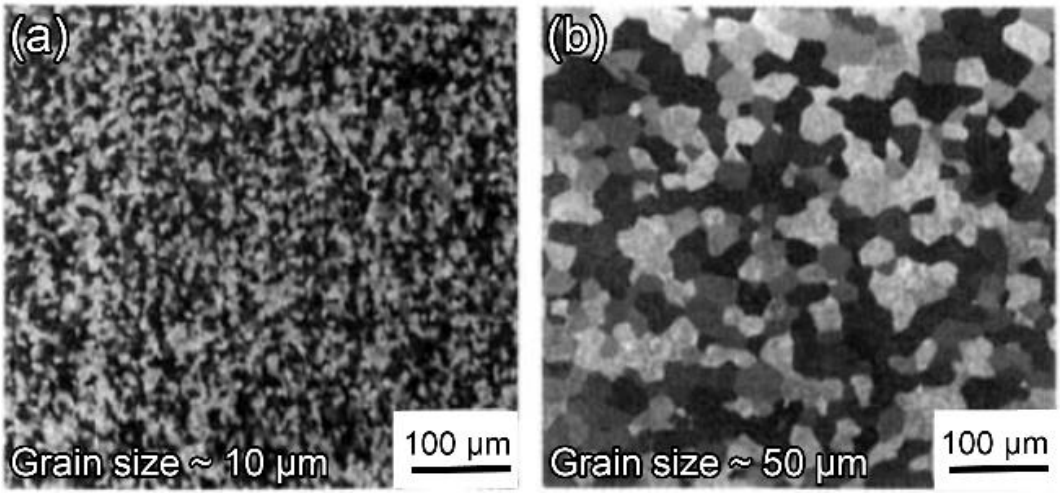


Fig. 2.3. The microstructures of α phase in CP-Ti with different grain size (a) 10 μm and (b) 50 μm [21].

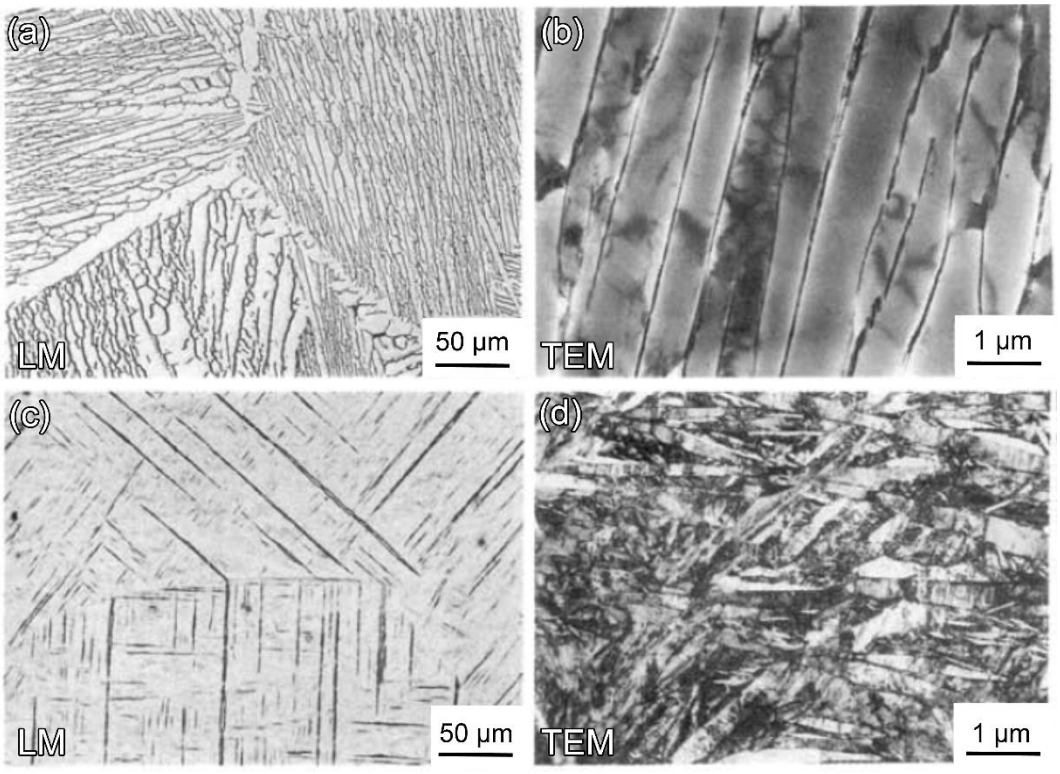


Fig. 2.4. (a) and (b) Lamellar morphologies of Ti-6Al-4V and (c) and (d) Acicular morphologies of Ti-6Al-4V [21]. Note that Low-magnification and transmission electron microscopy are abbreviated as LM and TEM respectively in Fig. 2.4.

The effects of the cooling medium and processing temperature on the microstructure morphologies of Ti-6Al-4V can be seen in Fig. 2.5 [14]. The rise in the cooling rate decreases the size of the α-lamellar structure [14, 21, 32]. As a result, the water quenched microstructure of Ti-6Al-4V displays a lower-sized α-lamellar structure than the furnace cooled ones (Fig. 2.5). The size of α lamellar colonies are directly related to the corresponding slip systems of an hcp structure and thereby, to the mechanical properties [32].

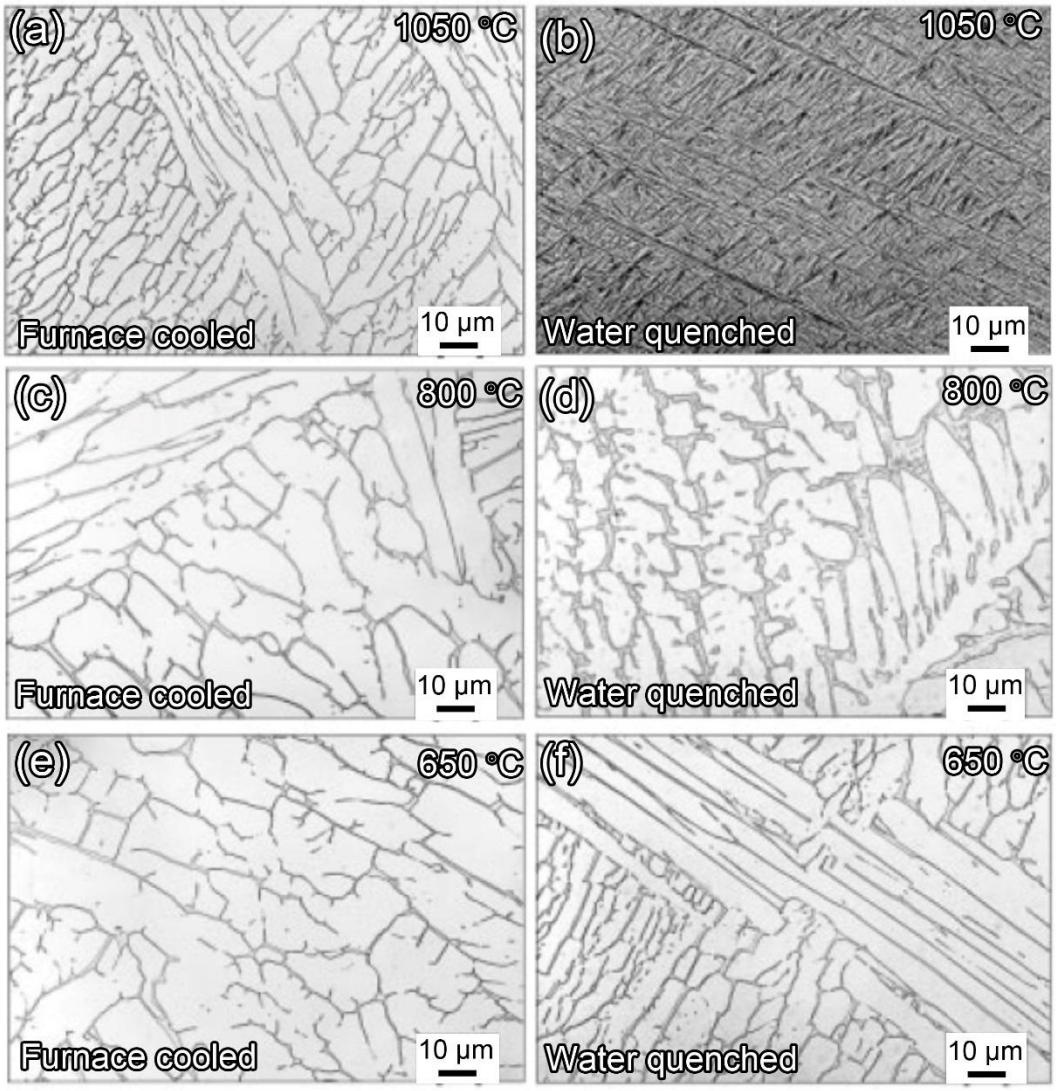


Fig. 2.5. The effects of cooling medium and processing temperature on the microstructure of Ti-6Al-4V [14].

The effect of three different cooling rates, i.e., 1 °C/min, 100 °C/min and 8000 °C/min, on the microstructure of Ti-6Al-4V is displayed in Fig. 2.6 [21]. The cooling rate is also an important

parameter to control the final lamellar morphologies of Ti-6Al-4V. High cooling rate usually displays a basket-weave or Widmanstätten microstructure, where new α plates form along the old α plates (Fig. 2.6b-c) [32]. The equiaxed and bimodal morphologies for Ti-6Al-4V are presented in Fig. 2.7 [14]. The formation of equiaxed structure in Ti-6Al-4V occurs upon executing solution treating above the martensitic transformation temperature (Fig. 2.7a) [14, 21]. The further coarsening of the equiaxed morphologies can usually be achieved by extending the duration of the annealing process (Fig. 2.7b) [14, 21]. The formation of a bimodal structure (equiaxed α in lamellar α+β matrix) occurs if the solution treating process is performed below the martensitic transformation temperature (Fig. 2.7c-d) [14, 21].

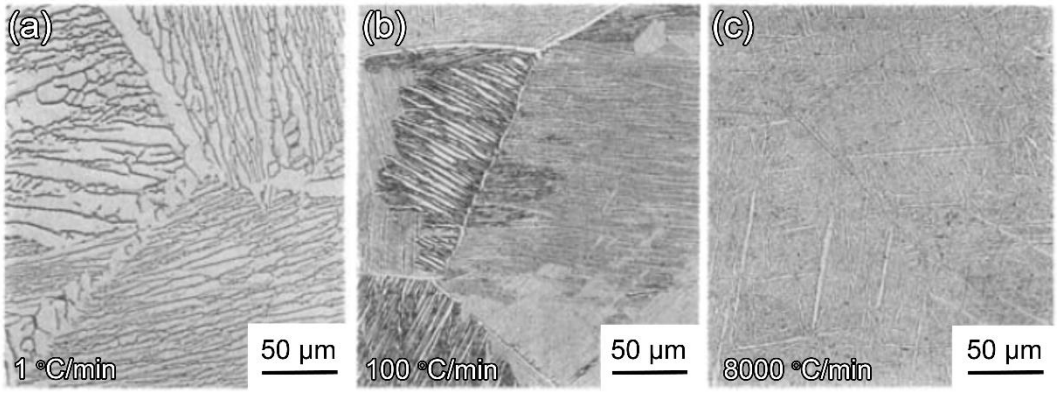


Fig. 2.6. The effect of different cooling rates on the microstructure of Ti-6Al-4V [21].

In β titanium alloys, the martensitic transformation occurs following the rapid cooling/quenching from the β phase field [7, 10, 40]. The martensitic transformation usually rely on the cooling rate and the quantities of alloying elements present in titanium alloy compositions [7]. Various non-equilibrium phases such as α' (with an hcp structure and a space group of $P6_3/mmc$), α" (with orthorhombic structure and a space group of *Cmcm*) and athermal ω (with an hcp structure and a space group of $P6_3/mmc$) form in the β matrix as a result of martensitic transformation [7, 10, 18, 23, 24, 36]. An α' phase generally forms with an irregularly distributed lath or needle like martensites with a size range from 0.5 μm to 100 μm [32, 40]. The size of the lath martensites increases as the concentration of β stabilizers in the alloy compositions decreases [40]. In contrast, fine-needle (acicular) like morphologies of α' phase form as the concentration of β stabilizers increases [40]. The further addition of β stabilizers leads to the loosening of symmetry in the hcp structure of α' phase, which finally leads to the formation of α" phase with an orthorhombic crystal

structure [40]. The orthorhombic α" phase is considered as an intermediate phase that forms between α' and β phases. In addition, the sufficient quantities of β stabilizers are added in titanium alloy compositions to suppress the martensitic transformation of β phase to α' and α" phases. Nonetheless, the formation of athermal ω phase occurs with a very tiny size of up to 5 nm. Another form of ω phase is isothermal ω phase which generally forms from athermal ω phase when annealing is executed in the ω+β phase field [40]. In previous research, two kinds of morphologies of the isothermal ω phase have been reported, i.e., ellipsoidal and cubic, which usually form evenly in the microstructure and therefore, produces the strengthening effect [40, 41]. As a result, the presence of ω phase in the microstructure enhances yield strength, elastic modulus and hardness but reduces ductility [42, 43]. Hence, the formation of ω phase is not favorable for an application where there is a requirement of low elastic modulus in an alloy, e.g., biomedical applications. In contrast, ω phase is favorable for an application where there is a requirement of high yield strength and hardness.

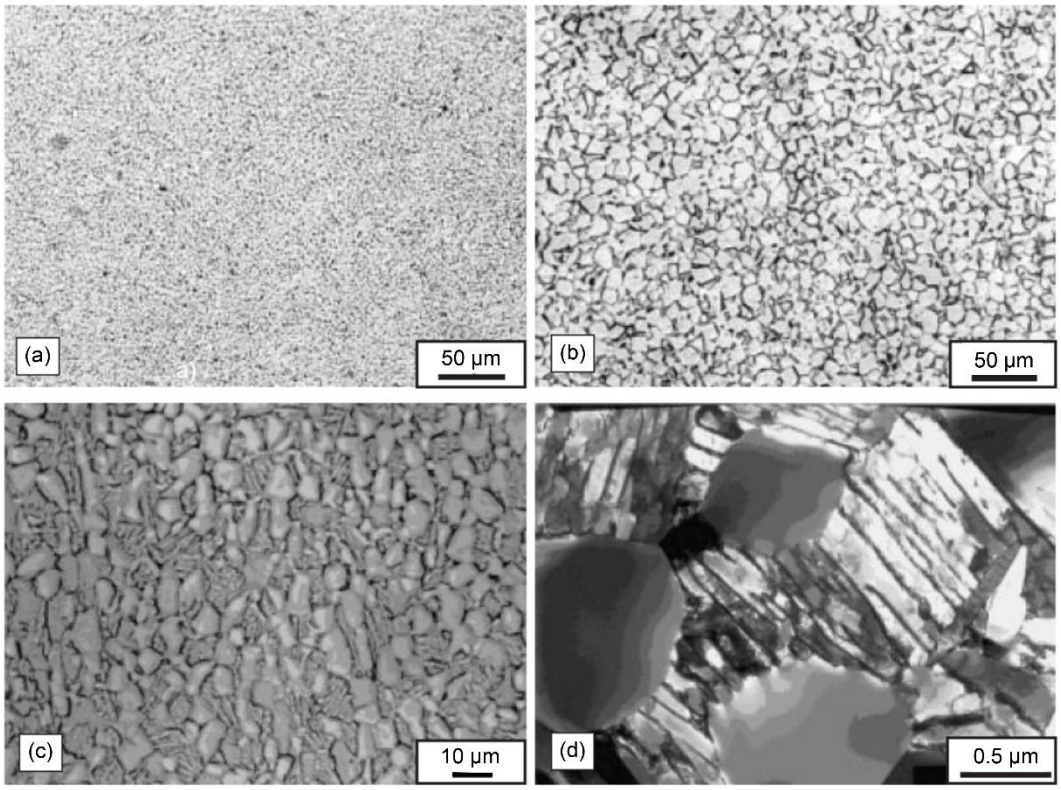


Fig. 2.7. Equiaxed and bimodal morphologies of Ti-6Al-4V: (a) fine equiaxed, (b) coarse equiaxed, (c) bimodal (OM) and (d) bimodal (TEM) [14].

Fig. 2.8 illustrates the transition of martensitic phases as well as the effect of β stabilizers on the microstructure of the Ti-11Nb-xFe alloys [36]. In Fig. 2.8a, Ti-11Nb-0.5Fe shows Widmanstätten type lamellar morphologies (dark) of α phase with the $V_f$ of 83% along with β phase (grey) in the microstructure [36]. The values of $V_{f,\alpha}$ decrease to 42% as the quantity of Fe increases from 0.5 to 3.5 wt% in the Ti-11Nb-3.5Fe alloy (Fig. 2.8b) [36]. Further increase in the quantity of Fe from 3.5 to 6 wt% leads to form the orthorhombic α" phase with the $V_f$ of 10% in the β matrix [36]. Interestingly, the β phase is fully retained in Ti-11Nb-9Fe as a result of increasing the quantity of Fe from 6 to 9 wt% [36].

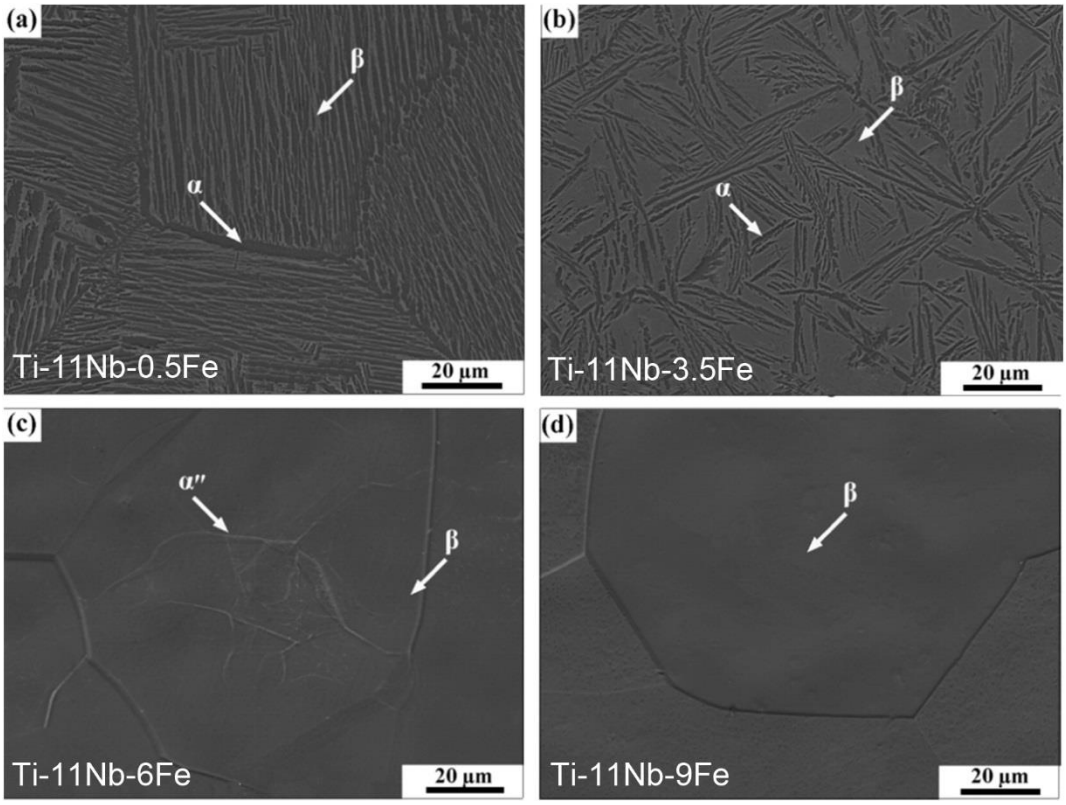


Fig. 2.8. The microstructures of the as-cast Ti-11Nb-xFe alloys [36].

The quantities of β stabilizers greatly affect the stability of β phase and their increased quantities suppress the $V_{f,\alpha''}$, which can also be seen in Fig. 2.9 [24]. It is evident in Fig. 2.9 that the values of $V_{f,\alpha''}$ decrease as the quantities of Nb increase in the Ti-xNb-7Fe alloys and therefore, the alloy with the highest amount of β stabilizers amongst the Ti-xNb-7Fe alloys, i.e., Ti-11Nb-7Fe retains the 100% $V_f$ of the β phase [24]. A similar trend is demonstrated in the Ti-xFe-yTa alloys where the values of $V_{f,\alpha''}$ decrease as the quantities of Fe and Ta increase in the Ti-xFe-yTa alloys and

Ti-10Fe-10Ta exhibits a single β phase microstructure as it comprises the highest amount of β stabilizers amongst the Ti-xFe-yTa alloys [18].

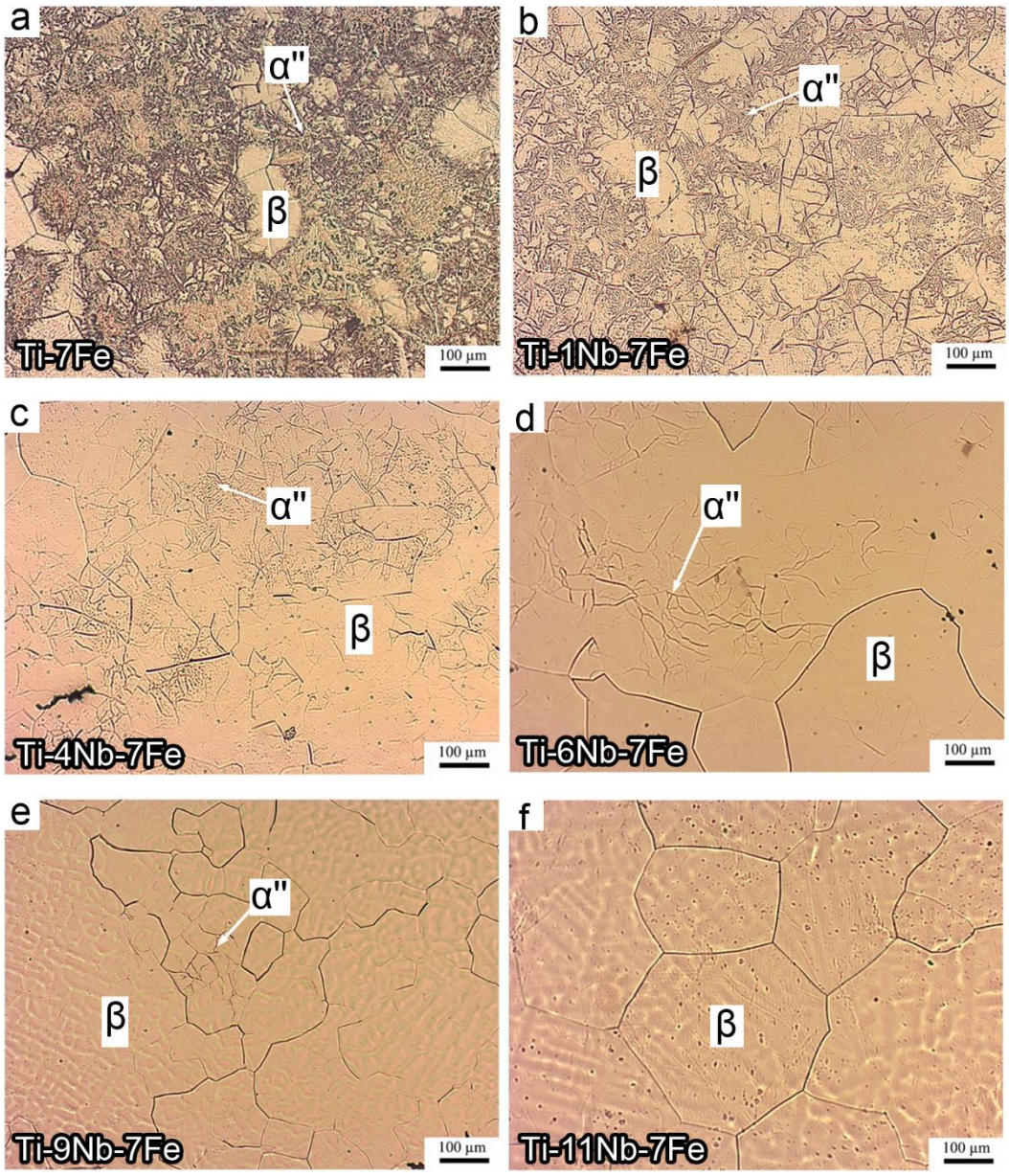


Fig. 2.9. The optical microstructures of the Ti-xNb-7Fe alloys [24].

The excess concentration of solute elements, e.g., Fe, Mn, Cr etc., which have atomic radius less than titanium in alloy compositions, form intermetallic phases in the microstructure [5, 11]. Fig. 2.10 shows the microstructure of $(Ti_{0.65}\text{-}Fe_{0.35})_{100\text{-}x}Sn_x$ (x = 0, 2.5, 5 at.%) alloys investigated by Zhang et al. [16, 44]. Figs. 2.10a and 2.10b reveal the formation of FeTi and (β-Ti+FeTi) type

eutectic phase in the microstructure of the $(Ti_{0.65}\text{-}Fe_{0.35})_{100}$ alloys with the $V_f$ of 35% and 65% respectively [16]. As the concentration of Sn increases from 0 to 2.5% in the $(Ti_{0.65}\text{-}Fe_{0.35})_{97.5}Sn_{2.5}$ alloy, the $V_f$ of eutectic (β-Ti+FeTi) phase increases to 72% and accordingly the $V_f$ of FeTi decreases to 28% (Fig. 2.10c-d) [16]. This further increase in the quantity of Sn in $(Ti_{0.65}\text{-}Fe_{0.35})_{95}Sn_5$ alloy leads to form one additional intermetallic phase, i.e., $Ti_3Sn$ along with FeTi and (β-Ti+FeTi) phases with $V_f$ values of 20%, 24% and 56%, respectively [16].

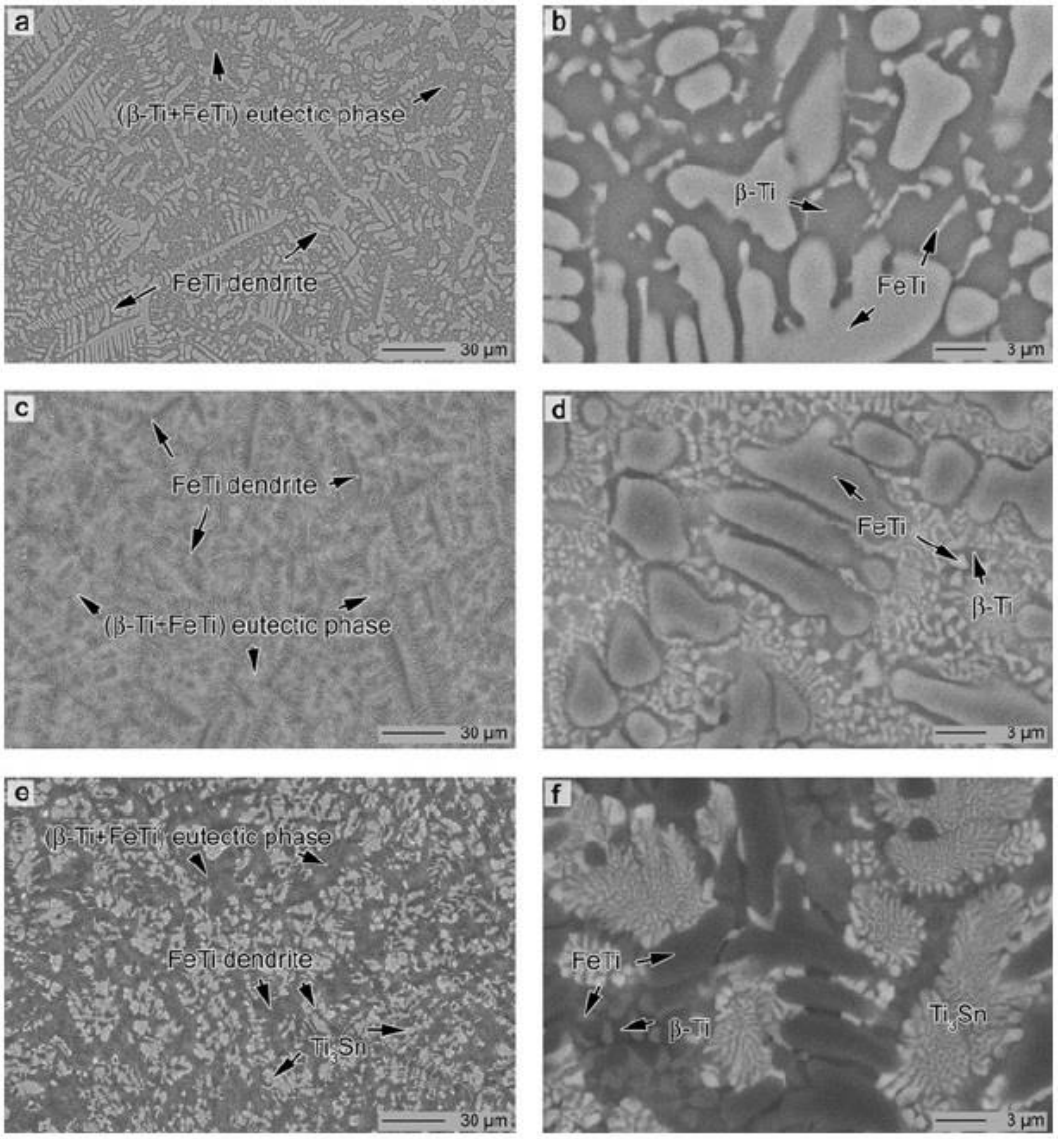


Fig. 2.10. The microstructures of Ti-Fe-Sn alloys: (a) and (b) $(Ti_{0.65}\text{-}Fe_{0.35})_{100}$ (at%), (c) and (d) $(Ti_{0.65}\text{-}Fe_{0.35})_{97.5}Sn_{2.5}$ (at%), (e) and (f) $(Ti_{0.65}\text{-}Fe_{0.35})95Sn5$ (at%) [16, 44].

Zhang et al. have also investigated $(Ti_{0.72}\text{-}Fe_{0.28})_{100-x}Ta_x$ (x = 0, 2 and 4 at%) alloys [44] and $(Ti_{0.655}Fe_{0.345})_{100-x}Nb_x$ (x =0, 3, 5, 7 at%) alloys [44]. The microstructures shown in Fig. 2.11 [44] display the ultrafine-grained (β-Ti+FeTi) eutectic phase with different lamellar spacing in the (β-Ti+FeTi) eutectic phase and the different $V_f$ of microstructural phases depending on the alloying elements present in the alloying compositions. It can be deduced from the microstructures presented in Figs. 2.10 and 2.11 that a high quantity of Fe in titanium alloys leads to form intermetallic phases in the microstructure due to the size misfit effect between atoms of Fe and Ti. The presence of intermetallic phases works as a strengthening phase and therefore, it is useful to increase yield strength and hardness of alloys [5, 11, 26].

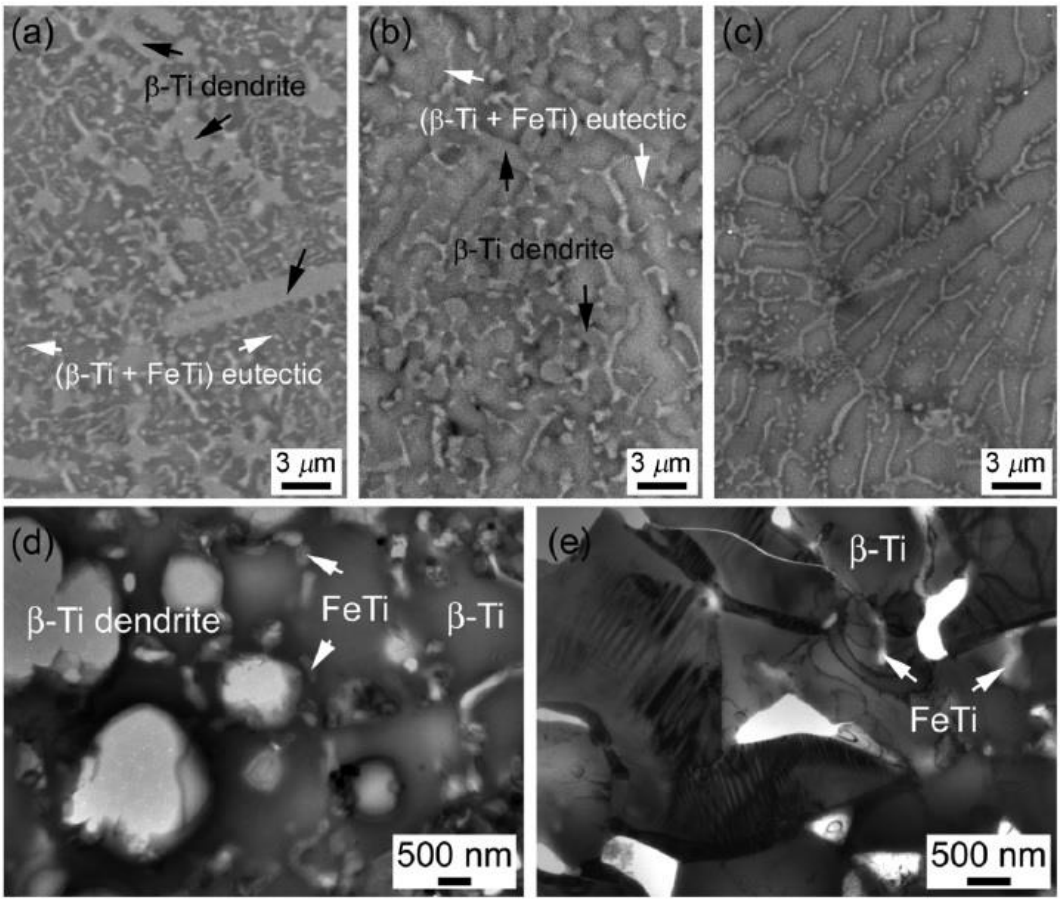


Fig. 2.11. The microstructures of $(Ti_{0.72}\text{-}Fe_{0.28})_{100-x}Ta_x$ alloys: (a) and (d) x = 0 (at%), (b) x = 2 (at%), (c) and (e) x = 4 (at%) [44].

## 2.4. Mechanical properties of titanium alloys

Amongst all the three type of titanium alloys, α+β and β titanium alloys have been used extensively for commercial biomedical, aerospace and many industrial applications as compared to α type titanium alloys because α+β and β titanium alloys demonstrate a wide range of mechanical, corrosion and biological properties [4, 17]. Table 2.3 demonstrates that α+β and β titanium alloys show high yield strength and $\sigma_{UTS}$ as compared to α type titanium alloys. It is also evident from Table 2.3 that α+β titanium alloy show less tensile elongation and almost same elastic modulus as compared to α type titanium alloys. However, β titanium alloys display low elastic modulus, high yield and ultimate strength and large elongation as compared to α and α+β titanium alloys [4, 17]. Therefore, β type titanium alloys have become the most favorable alloys for biomedical and many other high-strength structural applications [4, 17].

Table 2.4 presents the compressive mechanical properties of metastable β titanium alloys shown in Figs. 2.8 and 2.9 as well as other Ti-Fe-Ta alloys comprising the α" phase. Table 2.4 displays that the addition of a eutectoid type β stabilizer, i.e., Fe in titanium alloys increases yield strength and hardness, whereas the addition of isomorphous type β stabilizers, i.e., Nb and Ta in titanium alloys decrease yield strength and hardness. Moreover, the inverse relationship between the β stability and the values of ultimate compressive strain and elastic modulus is evident from Table 2.4. The increase in the β stability suppresses the formation of martensitic phases such as hcp α', orthorhombic α" and athermal hcp ω in titanium alloys. The elastic modulus of β phase remains lower than martensitic phases, i.e., $E_{\omega} > E_{\alpha'} > E_{\alpha''} > E_{\beta}$. Therefore, the enhancement of β stability decreases elastic modulus and ultimate compressive strain. The formation of aforementioned martensitic phases increases elastic modulus, which is not favorable phenomenon for biomedical titanium alloys. Thus, the β stability is an essential requirement for titanium alloys used in biomedical implant applications.

Moreover, the presence of second phases in the β matrix impedes the dislocation motion. Therefore, dislocation pileups occur at the phase boundaries of second phases, which increase yield strength and hardness. Nonetheless, second phases decrease the plasticity of an alloy due to their brittle nature. Fig. 2.12 presents the mechanical properties of titanium alloys shown in Figs. 2.10 and 2.11 as well as some other Ti-Fe-Nb alloys comprising high quantities of Fe and intermetallic phases. The alloys shown in Fig. 2.12 demonstrate an impressive yield strength from

around 1.2 GPa to 2.3 GPa and ultimate compressive strength from 2.1 GPa to 2.7 GPa as they are comprised of a high fraction of intermetallic phases. However, the plastic strain of the alloys presented in Fig. 2.12 remain low as compared to alloys comprising a single β phase [18, 24, 36].

Table 2.4. The compressive mechanical properties of metastable β titanium alloys. Note that yield strength, ultimate compressive strain, hardness and elastic modulus are abbreviated as $\sigma_{0.2}$, $\varepsilon_{max}$, $H$ and $E$ respectively in Table 2.4.

| **Alloys** | $\sigma_{0.2}$ **(MPa)** | $\varepsilon_{max}$ **(%)** | $H$ **(GPa)** | $E$ **(GPa)** | **Ref.** |
|---|---|---|---|---|---|
| Ti-11Nb-0.5Fe | 796 | 20.0 | 2.72 | 109 | [36] |
| Ti-11Nb-3.5Fe | 932 | 32.5 | 2.97 | 101 | [36] |
| Ti-11Nb-6Fe | 1137 | 40.0 | 3.50 | 89 | [36] |
| Ti-11Nb-9Fe | 1078 | 42.0 | 3.27 | 82 | [36] |
| Ti-7Fe | 1847 | 8.0 | 5.92 | 130 | [23, 24] |
| Ti-7Fe-1Nb | 1785 | 10.0 | 5.58 | 124 | [23, 24] |
| Ti-7Fe-4Nb | 1539 | 24.3 | 5.13 | 115 | [23, 24] |
| Ti-7Fe-6Nb | 1144 | 32.1 | 4.18 | 97 | [23, 24] |
| Ti-7Fe-9Nb | 1010 | 40.5 | 3.72 | 89 | [23, 24] |
| Ti-7Fe-11Nb | 985 | 41.5 | 3.57 | 86 | [23, 24] |
| Ti-8Fe | 1562 | 17.1 | 5.75 | 128 | [18, 45] |
| Ti-8Fe-5Ta | 1062 | 37.3 | 5.00 | 119 | [18, 45] |
| Ti-8Fe-8Ta | 1030 | 38.1 | 4.38 | 107 | [18, 45] |
| Ti-9Fe-9Ta | 1010 | 39.5 | 3.75 | 99 | [18, 45] |
| Ti-10Fe-10Ta | 1000 | 40.0 | 3.38 | 92 | [18, 45] |

It is remarkable based on the results of titanium alloys presented in Table 2.4 and Figs. 2.8-2.12 that the mechanical properties, e.g., yield strength, elastic modulus, ductility, hardness, ultimate strength and deformation behavior of titanium alloys can be effectively tailored using various strengthening second phases, i.e., martensitic α', α'', ω and intermetallic phases. The formation of martensitic and intermetallic phases depends on the alloying elements and their corresponding quantities. All these alloying elements have their own advantages and disadvantages in terms of performance and cost parameters for a specific application. Thus, it is a challenging task for researchers to obtain a balance of required properties for a specific application in titanium alloys.

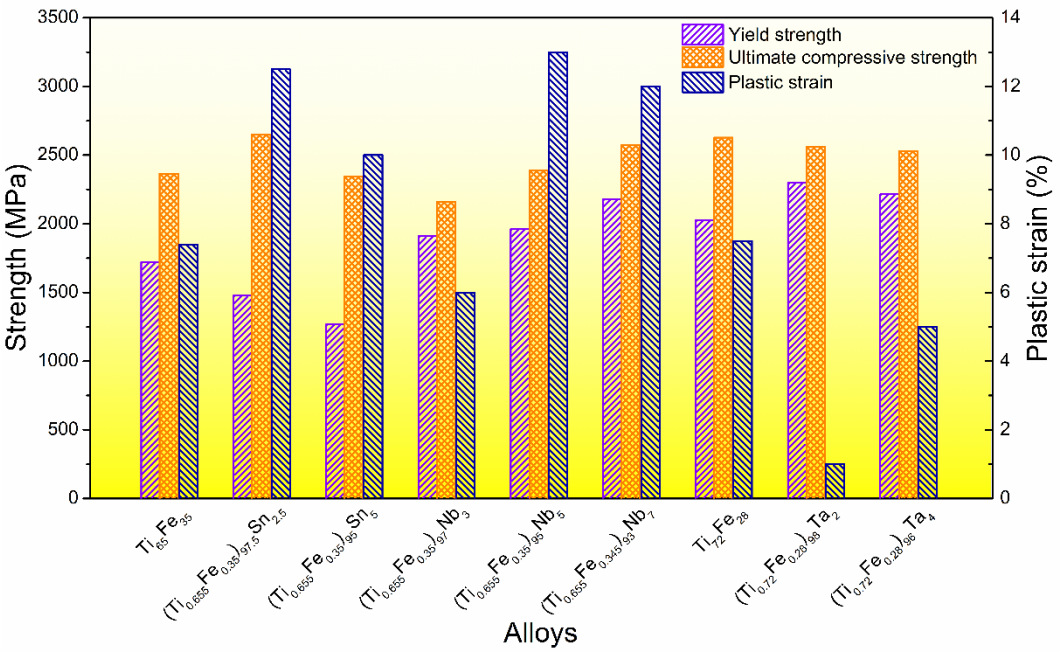


Fig. 2.12. The mechanical properties of high-strength titanium alloys comprising intermetallic phases [44].

Table 2.5. The effects of alloying elements, processing technique and phase constituents on $\sigma_{UTS}$ (ultimate tensile strength) and $E$ (elastic modulus) of binary metastable β titanium alloys.

| Binary titanium alloys | Processing technique | Phase constituents | $\sigma_{UTS}$ (MPa) | $E$ (GPa) | Ref. |
|---|---|---|---|---|---|
| Ti-16Nb | Solution treatment | α"/β | 613 | 58 | [46] |
| Ti-26Nb | Cold working | β | 420 | 50 | [47] |
| Ti-45Nb | Hot rolling | β | 527 | 64 | [48] |
| Ti-14Nb | Hot rolling | α/β | 700 | 99 | [49] |
| Ti-26Nb | Hot rolling | α/β | 760 | 78 | [49] |
| Ti-36Nb | Hot rolling | β | 810 | 80 | [49] |
| Ti-40Nb | Hot rolling | β | 630 | 57 | [49] |
| Ti-7.5Mo | As-cast | α" | 1019 | 70 | [50] |
| Ti-15Mo | As-cast | β | 921 | 84 | [50] |
| Ti-10Mo | Solution treatment | β | 731 | 93 | [51] |
| Ti-20Mo | Solution treatment | ω/β | 823 | 75 | [51] |
| Ti-10Ta | Solution treatment | α' | 500 | 99 | [42] |
| Ti-20Ta | Solution treatment | α' | 550 | 82 | [42] |
| Ti-30Ta | Solution treatment | α" | 570 | 69 | [42] |
| Ti-40Ta | Solution treatment | α" | 565 | 81 | [42] |
| Ti-30Ta | Ageing treatment | α"/β | 892 | 76 | [52] |
| Ti-50Ta | Ageing treatment | α"/β | 713 | 77 | [52] |

The effects of alloying elements, processing techniques and phase constituents on $\sigma_{UTS}$ and elastic modulus of binary and ternary titanium alloys can be seen in Table 2.5 and Table 2.6 respectively. The mechanical properties of an alloy remain different with varied processing methods, e.g., Ti-26Nb in Table 2.5 shows different values of $\sigma_{UTS}$ and elastic modulus due to the different processing techniques used. The type of processing method usually influences microstructural phases and thereby, mechanical properties. Therefore, Ti-26Nb demonstrates a single β phase when processed using a cold rolling method and the same alloy demonstrates dual phase morphologies of α and β phases when processed using a hot rolling method. It can also be seen in Table 2.5 that Ti-Nb alloys show a single β phase when more than 25 wt% quantity of Nb is added to binary titanium alloys, whereas a single β phase can be retained upon addition of 10 wt% quantity of Mo in binary titanium alloys.

Table 2.6. The effects of alloying elements, processing technique and phase constituents on $\sigma_{UTS}$ (ultimate tensile strength) and $E$ (elastic modulus) of metastable β titanium alloys comprising more than 2 alloying elements.

| **Ternary titanium alloys** | **Processing technique** | **Phase constituents** | $\sigma_{UTS}$ **(MPa)** | $E$ **(GPa)** | **Ref.** |
|---|---|---|---|---|---|
| Ti-35Nb-4Sn | Cold working | α"/β | 630 | 42 | [53] |
| Ti-35Nb-7.9Sn | Cold working | β | 600 | 57 | [53] |
| Ti-33.6Nb-4Sn | Hot rolling | α"/β | 800 | 40 | [54] |
| Ti-33Nb-4Sn | Solution treatment and cold rolling | α"/β | 853 | 36 | [55] |
| Ti-30Nb-18Ta | Cold working | α"/β | 530 | 71 | [56] |
| Ti-25Nb-25Ta | Solution treatment and cold rolling | β | 530 | 55 | [57] |
| Ti-35Nb-6Ta | Cold working | β | 820 | 50 | [58] |
| Ti-13Nb-13Zr | Cold working | α' | 732 | 65 | [59] |
| Ti-35Nb-5Zr | Ageing treatment | β | 660 | 60 | [60] |
| Ti-35Nb-15Zr | Ageing treatment | β | 700 | 63 | [60] |
| Ti-16Nb-10Zr | Cold working | α"/β | 520 | 70 | [61] |
| Ti-18Nb-8Zr | Cold working | α"/β | 550 | 75 | [61] |
| Ti-20Nb-6Zr | Cold working | ω/β | 470 | 60 | [61] |
| Ti-24Nb-2Zr | Cold working | β | 440 | 62 | [61] |
| Ti-23Nb-0.7Ta-2Zr | Solution treatment | α"/β | 400 | 55 | [62] |
| Ti-23Nb-0.7Ta-2Zr-1.2O | Solution treatment | β | 880 | 60 | [62] |
| Ti-32Nb-2Ta-3Zr-0.5O | Cold working | α"/β | 1370 | 55 | [63] |

According to previous studies, it is also beneficial to add O in titanium alloys because small quantities of O suppress the formation of martensitic phases and improve the β stability, e.g., Ti-23Nb-0.7Ta-2Zr-1.2O (Table 2.6) [62, 63]. The required quantities of O are generally added in titanium alloys through adding titanium oxide ($TiO_2$) [62]. Moreover, the titanium alloys presented in Table 2.5 and Table 2.6 show low elastic modulus (ranges from 36 to 99 GPa) compared to the α type CP-Ti and α+β type Ti-6Al-4V alloys (Table 2.3). This means that β titanium alloys are helpful in obtaining low Young's modulus for biomedical applications.

## 2.5. Titanium alloys for biomedical applications

### 2.5.1. Need of artificial biomedical implants

A biomaterial is a substance that has been engineered to interact with biological systems for therapeutic or diagnostic purposes. Biomedical implants are used in medical applications to perform a body function, augment, repair or replace any hard tissue, organ or function of the body that has been lost through trauma, disease or injury [64]. Thus, a biomaterial helps in improving the fineness and longevity of human life. The field of biomaterials has experienced a very rapid growth due to the following reasons: (a) Incremental growth in the population of aged people who suffer from diseases such as arthritis and need replacement of failed tissue with an implant made up of a biomaterial to gain their functionality back [65], (b) A rise in automobile vehicles and road accidents (approximately tens of millions injuries per year) especially for young people in developing nations [66] and (c) an increase in the amount of leisure time spent on sports activities and resulting physical trauma [67]. Biomaterials are usually designed based on the particular application required in the human body such as cardiac simulator, hip joint, knee joint, heart valve prostheses, shoulder, elbow, dental implants, intraocular lenses and stents [1]. However, implantations of hip, knee and spinal joints are the commonly placed implants amongst all types of implants. Fig. 2.13. briefly displays the applications of titanium alloys as biomedical implants in the human body [68].

There is currently an enormous demand for replacement surgeries of failed tissue among old age people as the liability of hard tissues failure remains high in aged group population. Statistics of biomaterials reveal that more than 7 million Brånemark system implants have been implanted in human bodies [1], where more than 1 million spinal rod implants have been inserted worldwide between the years 1980 and 2000. Moreover, 250 thousands of total hip joint replacements are

being completed every year in the United States of America alone [69]. It has also been observed that the number of revision surgeries for hip and knee joints have increased in the last 20 years. Further, it is predicted that the numbers of revision surgeries for hip and knee joints will rise by 174% (572 thousand procedures) and 673% respectively till the end of 2030 in accordance with the current rate, i.e., 3.48 million procedures [70].

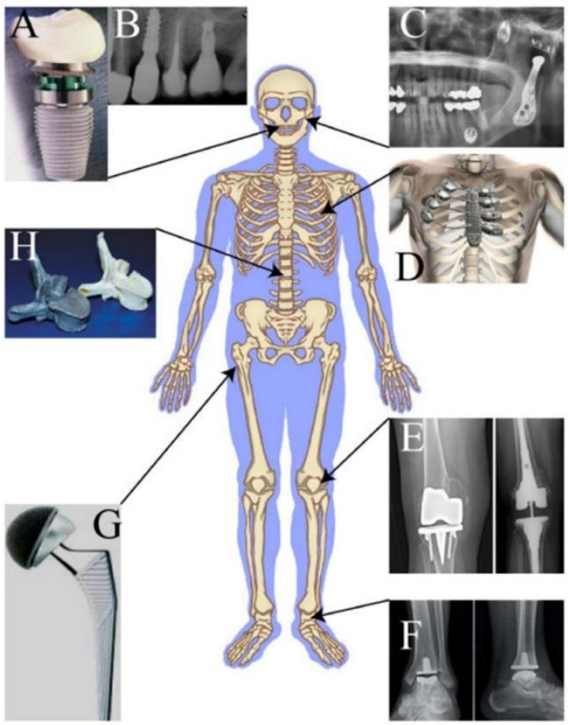


Fig. 2.13. Applications of titanium alloys as biomedical implants in the human body. (a) and (b) Dental implants, (c) Maxillofacial reconstruction, (d) Rib replacement, (e) Knee joints, (f) Ankle joints, (g) Hip joints, (h) Vertebral reconstruction [68].

### 2.5.2. Degenerative diseases and failure of biomedical implants

Degenerative disease is a consequence of a continuous process based on degenerative cell changes, affecting tissues or body parts/organ, which will progressively deteriorate over time, whether as a result of normal bodily wear or lifestyle choices like physical movements, exercise or eating habits [71]. Hence, degenerative disease is the main cause behind the replacement of bone joints. Osteoarthritis (inflammation in the bone joints), osteoporosis (weakening of the bone) and trauma (lead to pain or malfunctioning of human joints) are the kinds of degenerative diseases attributed and approximately 90% of the population above the age of 40 suffers from these kinds of diseases [1]. The solution to these problems is to develop artificial implants made up of biocompatible

materials which can be fabricated in appropriate shapes and with the required properties. The functionality of body parts or tissues can be restored with the help of these biomedical implants. Fig. 2.14 depicts the various components used in artificial hip and knee joint-implants [72].

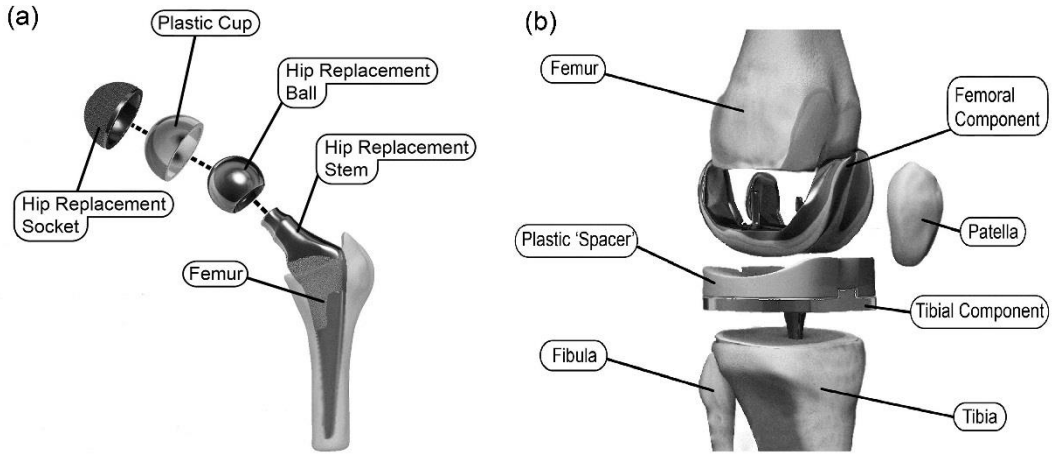


Fig. 2.14. Schematic illustration of components used in artificial (a) hip joint implant and (b) knee joint implant [72].

In current situation, the research findings have been presented with a strong driving force to develop biomaterials of the next generation, which should last for a long period of time because currently used commercial implants have a tendency to fail after around 15 years of service [73, 74]. It is also noteworthy that the number of revision surgeries of hip and knee implants have increased along with the replacement surgeries. The predicted trends of hip and knee revision surgeries suggest that the revision surgeries of hip and knee joints will rise by 137% and 607% respectively between the years 2005 and 2030 [70]. Further, the revision surgeries are costlier, cause a lot of pain to the patients and their success rates are lower. Therefore, biomaterials should be designed in a way that they do not require any revision surgery after the implantation.

Fig. 2.15 depicts various mechanisms responsible for an implant failure, which are illustrated with an example of total hip arthroplasty prosthesis [68]. It is apparent from Fig. 2.15 that an artificial implant usually fails due to (i) Poor mechanical properties, e.g., high Young's modulus and less hardness, strength, ductility, toughness and poor wear resistance, (ii) Poor surface and tribo-corrosion resistance behavior and (iii) Poor biocompatibility. Hence, the orthopedic implants, particularly those used for load bearing applications, should possess outstanding biocompatibility, very good corrosion resistance in the human body environment and should not be having

cytotoxicity. In addition, biomaterials should possess a superior combination of high mechanical strength and low elastic modulus, high fatigue strength as well as wear resistance, high ductility and good fracture toughness [73]. In the last two decades, alloys like cobalt-chromium (Co-Cr), 316L stainless steel (316L SS), CP-Ti and Ti-6Al-4V, have been suggested for biomedical implant applications. Nonetheless, certain limitations such as high elastic modulus, poor biocompatibility, poor corrosive resistance and toxicity associated with these alloys have been identified. Accordingly, many studies on biomedical implant materials have determined that β-type titanium alloys show comparable results to the human bone compared to α type and α+β type titanium alloys. Thus, there is a still scope to develop better biomaterials using β type titanium alloys.

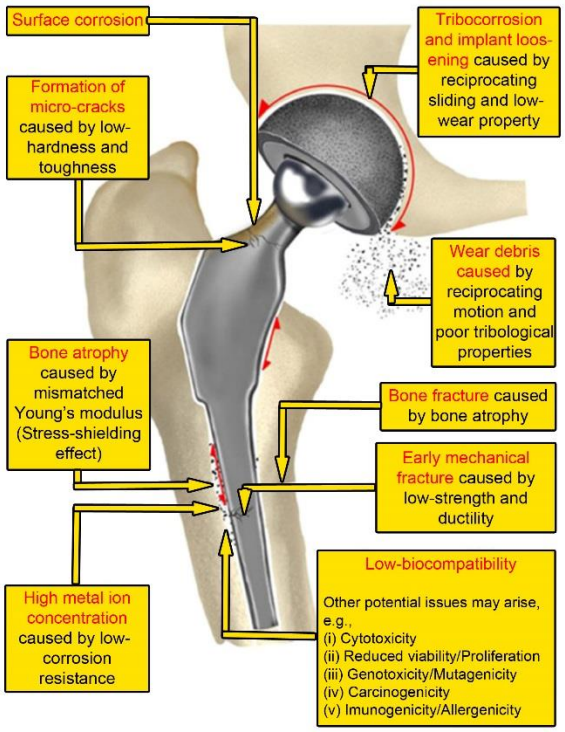


Fig. 2.15. Various mechanisms responsible for an implant failure illustrated with an example of total hip arthroplasty prosthesis [68].

### 2.5.3. Essential requirements of biomaterials

Established literature suggest that the service life of an implant mainly depends on the performance of biomaterials and also on the gender and age of a patient [75]. As revision surgeries are not favorable for patients, biomaterials should last for a long service period and should not cause any

harmful effects to the human body following the implantation [75]. Therefore, a biomaterial should be designed considering the following aspects for a long-term service period.

### *2.5.3.1. Biocompatibility*

Biocompatibility describes properties of biomaterials in many contexts of the human body environment [76]. In this context, the host tissue response with biomaterial and material deterioration are the main factors that affect the biocompatibility. It is expected that biomaterial should be highly non-toxic, non-inflammatory and non-allergic in the human body environment. Furthermore, they should not produce any irritating reactions for surrounding tissues [77]. The success of biomedical implants relies on the response of the human body to the implant. Thrombosis, adhesion of blood platelets to biomaterial and coagulation of blood are the main problems that are commonly related to the biocompatibility. Fig. 2.16 depicts the biological safety of various metals considering (a) cytotoxicity of pure metals and (b) the relationship between polarization resistance and biocompatibility of pure metals, Co-Cr alloys and stainless steel [75, 78]. Fig. 2.16 shows that Ti, B, Mg, Si, P, Ca, Sr, Zr, Nb, Mo, Pd, In, Sn, Ta, Pt, and Au are biocompatible materials [79], whereas, Be, Al, V, Cr, Mn, Fe, Co, Ni, Cu, Zn, and Ag might be harmful biomaterials [79].

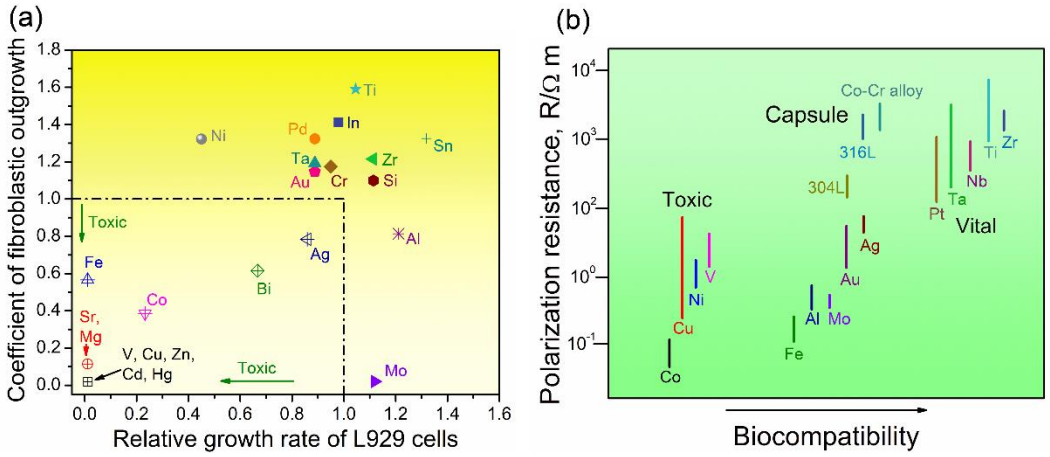


Fig. 2.16. Biological safety of various metals considering (a) cytotoxicity of pure metals and (b) the relationship between polarization resistance and biocompatibility of pure metals, Co-Cr alloys and stainless steels [75, 78].

### *2.5.3.2. Mechanical properties and stress shielding effect*

A biomaterial should be comprised of appropriate mechanical properties such as good tensile strength, fatigue strength, elongation, stiffness, hardness, fracture toughness and low modulus of

elasticity. These mechanical properties should be considered at the time of selection of a biomaterial. Further, the behavior of a material in repetitive cyclic loading and/or straining conditions can be judged by the fatigue strength of a material. A good biomaterial should have superior mechanical compatibility, which means a biomaterial should possess the required mechanical properties and should not fail due to insufficient strength and/or there should not be a mismatch in elastic moduli of an implant and the human bone. For biomaterials, modulus of elasticity is the most important mechanical property and its value should be close to that of the human bone (4 to 30 GPa) [80]. The comparison of the values of elastic modulus for different biomaterials with that of the human bone is presented in Fig. 2.17 [1, 55, 81]. Of note, Ti-24Nb-4Sn-8Zr shows the lowest value of elastic modulus, i.e., 33 GPa, amongst the biomaterials presented in Fig. 2.17.

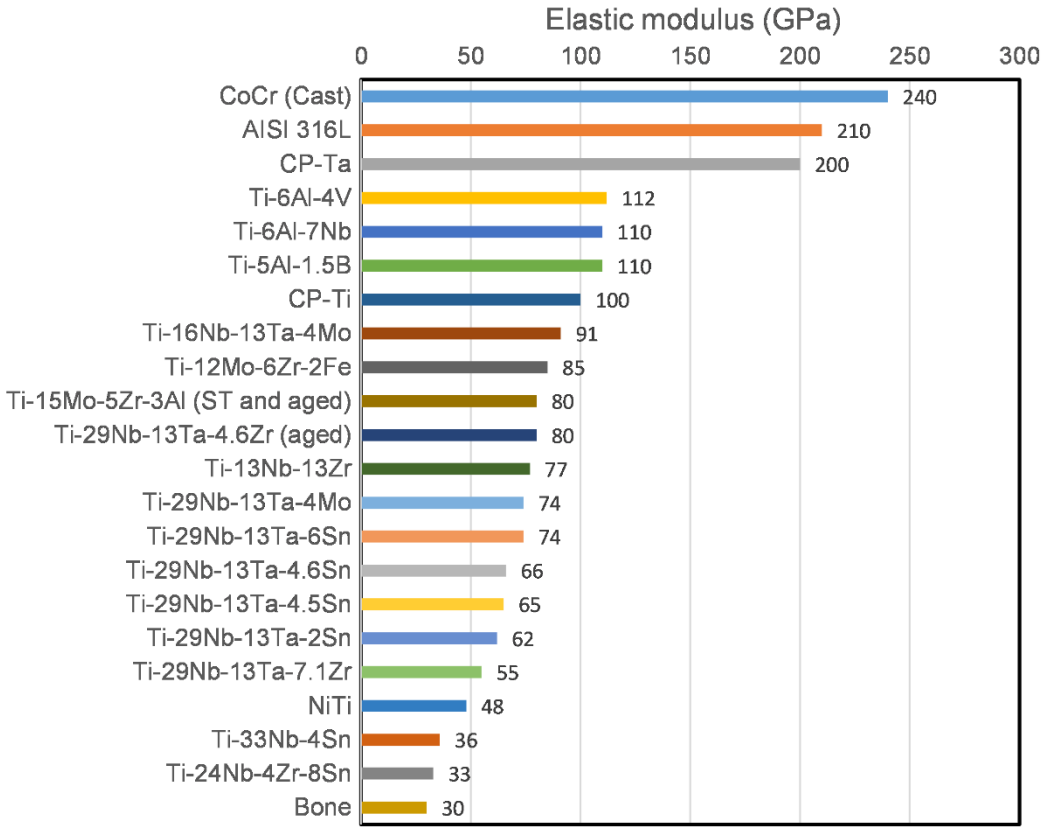


Fig. 2.17. The comparison of the values of elastic modulus for various biomaterials with that of human bone [1, 55, 81].

The problem with current biomaterials is their higher stiffness as compared to bone, which restricts the required stress being transferred to adjacent bone. In this situation, the implant carries most of the applied loads, which leads first to bone resorption nearer to the implant and finally leads to implant loosening. Progressively, as a result, a death of bone cells occurs, this effect is known as the "stress-shielding effect" [82]. In addition, the density of bone eventually decreases if there is a mismatch in elastic moduli of an implant and a bone. Therefore, a biomaterial with superior mechanical strength and low elastic modulus (nearer to that of bone) are highly desirable because it prevents implant loosening and can be used for a long service period to avoid revision surgery.

It is also interesting to know about the age and gender related mechanical properties of the human bone. No noticeable difference has been recorded in gender-based mechanical properties of the human bone [75]. However, a significant difference has been observed in age-related mechanical properties of human cortical bones [75]. The results of the mechanical properties measured for different types of cortical bones (such as fibula, tibia, and femur) in two age groups, i.e., young age group (age-41.5 years) and old age group (age-71 years) suggest that the values of mechanical properties such as $\sigma_{UTS}$, elastic modulus, ultimate strain and density in the old age group are approximately 15 to 40% lower than these in the young age group [75].

#### *2.5.3.3. Corrosion and wear resistance*

A biomaterial should have very good corrosion resistance and high wear resistance properties in the human body because the human body is a complex electrochemical system which is composed of many corrosive substances. The compositional quantities of the human blood serum are presented in Table 2.7 [83]. The degradation of an implant material occurs due to poor corrosion resistance ability after implantation in the corrosive environment of the human body. Consequently, the fatigue life and mechanical strength of an implant decrease, which eventually leads to the failure of an implant.

It has been shown that implants induce non-biocompatible metallic debris ions in the body due to poor wear and corrosion resistance properties, which produce an allergic effect and toxic reactions [84]. Further, low wear resistance also leads to implant loosening as well as wear metallic debris causes harmful reactions in the body [1]. Thus, the service period of an implant can be determined by its wear resistance property.

Table 2.7. The compositional quantities of the human blood serum [83].

| Cations | Quantity (mmol/l) | Anions | Quantity (mmol/l) | Others | Quantity (mmol/l) |
|---|---|---|---|---|---|
| $Na^+$ | 142 | $Cl^-$ | 101 | Organic acids | 6 |
| $K^+$ | 4 | $HCO^{3-}$ | 27 | Proteins | 16 |
| $Ca^{2+}$ | 5 | $HPO_4^{2-}$ | 2 | | |
| $Mg^{2+}$ | 2 | $SO_4^{2-}$ | 1 | | |
| Total | 153 | Total | 131 | | |

#### *2.5.3.4. Osseointegration*

Osseointegration was first referred to by Branemark et al. [85], where three parameters including surface roughness, surface topography and surface chemistry are very important in the development of osseointegration. If an implant is not able to match or integrate with the adjacent bone, as well as with the surrounding tissue, because of micro-motions, then this phenomenon leads to loosening of the implant [86]. Thus, materials with adequate surface quality are required in order to integrate with surrounding tissue and bone.

### 2.5.4. Currently used biomaterials and their limitations

Metals and polyethylene (a type of plastic) are mostly used in orthopaedic implantations. These two materials make a combined joint of an implant in most biomedical implant applications [67]. It has been noted that approximately three-fourth of biomedical implants are made of metallic materials. CP-Ti possesses superior characteristics for its use as an implant in biomedical applications. However, alloys such as 316L SS, Co-Cr alloys and titanium alloys are also used as metallic biomaterials. It has been shown that 316L SS does not comprise the required mechanical properties as well as superior corrosion resistance in the human body. Therefore, it is used in making of bone screws, pins, rods and bone plates. 316L SS and Co-Cr alloys release few elements such as Ni, Cr and Co as a result of corrosive effects in the human body [75, 87] and progressively, these elements produce toxic reactions in the body [88]. Another problem with 316LSS and Co-Cr alloys is their high modulus of elasticity as compared to human bone which results initially in bone resorption and later in loosening of an implant [89]. CP-Ti was earlier used as a biomedical implant material because it is non-toxic, non-corrosive and possesses very good surface property [90], but it has low strength and poor hardness. Due to the limitations of 316LSS, Co-Cr alloys, and CP-Ti, researchers have developed a new titanium-based alloy, i.e., Ti-6Al-4V as a substitute

material of CP-Ti for implant applications with good corrosion resistance and comparable biocompatibility. Ti-6Al-4V has been widely used for many years as an implant material in the biomedical industry [24]. However, it has been shown that Ti-6Al-4V produces toxic effects after several years of usage due to the release of Al and V ions [90]. It has been suggested that the release of these Al and V ions in the human body may lead to long term health diseases such as Alzheimer's disease, haematological alterations, allergic reactions and neurological disorders [18, 23]. Therefore, researchers have been working on developing new titanium alloys as a replacement for currently used implant materials, i.e., Ti-6Al-4V and CP-Ti. Table 2.8 [91] compares the various properties of titanium with 316L SS and Co-Cr alloys. It is apparent from Table 2.8 that titanium comprises superior properties for biomedical applications as compared to 316L SS and Co-Cr alloys. Therefore, research on titanium alloys as biomaterials has been exponentially increased in the last 20 years [92] because titanium alloys serve longevity of human life and improved health care options for patients. Hence, titanium alloys are favorable for their use in biomedical and dental implant applications.

Table 2.8. The comparison between the properties for titanium, 316L SS and Co-Cr alloys [91].

| **Properties** | **Titanium** | **316L SS** | **Co-Cr alloys** |
|---|---|---|---|
| Stiffness | Low | High | Medium |
| Strength | High | Medium | Medium |
| Corrosion resistance | High | Low | Medium |
| Biocompatibility | High | High | Medium |

The advancement in titanium alloys is a very significant phenomenon in the development of new low-cost biomaterials. Many literature studies have suggested that titanium alloys can be a very good substitute for a failed human bone or a hard tissue because titanium alloys possess high mechanical strength, good fatigue resistance, low density, superior corrosion resistance and excellent biocompatibility [1]. Furthermore, titanium alloys possess a lower rigidity as compared to other biomaterials such as Co-Cr alloys and 316L SS [78]. The elastic modulus of titanium alloys varies from 33 to 112 GPa which is closer to that of bone (4 to 30 GPa) and significantly lower than other biomaterials like 316L SS (210 GPa) and Co-Cr alloys (240 GPa) [1, 75]. Hence, the issues of stress-shielding effect and implant loosening associated with other biomaterials can be solved by developing improved titanium alloys.

### 2.5.5. β titanium alloys as biomaterials

Amongst all type of titanium alloys, β titanium alloys possess required attributes for biomedical applications such as excellent biocompatibility, low elastic modulus, non-toxic and non-allergic behavior, good corrosion and wear resistance [82]. In the early development of titanium alloys, many studies have been carried out to find a substitute of Ti-6Al-4V and worked on Ti-6Al-7Nb, Ti-13Nb-13Zr and Ti-12Mo-6Zr alloys [90]. Ti-13Nb-13Zr [93] was the first β titanium alloy developed for biomedical implant applications. Subsequently, plenty of studies have been carried out and many titanium alloys have been developed such as Ti-12Mo-6Zr-2Fe [94], Ti-15Mo [95], Ti-16Nb-10Hf (known as Tiadyne 1610) [29], Ti-15Mo-5Zr-3Al [96], Ti-35.3Nb-5.1Ta-7.1Zr [82], Ti-24Nb-4Zr-8Sn [2], Ti-29Nb-13Ta-4.6Zr [97], Ti-22.3Nb-4.6Zr-1.6Ta-6Fe [98], Ti-25Ta-25Nb [99], Ti-35Nb-7Zr-5Ta [100], Ti-20Mo-7Zr-5Ta [100], Ti-5Mo-4Nb-2Sn [101], Ti-10Mo [101], Ti-7Fe-11Nb [23], Ti-11Nb-9Fe [36], Ti-10Fe-10Ta [18] and many other designs of titanium alloys with a combination of alloying elements such as Nb, Zr, Ta, Mo and Sn. Among the above-mentioned alloys, Ti-29Nb-13Ta-4.6Zr, Ti-24Nb-4Zr-7.9Sn, Ti-22.3Nb-4.6Zr-1.6Ta-6Fe and Ti-35Nb-7Zr-5Ta alloys have been considered as the most promising biomedical alloys. Nonetheless, these alloys have been designed using expensive, rare earth metals and using metals with high melting point temperatures, e.g., Ta, Nb and Mo. The melting point temperature of the elements used in biomedical implant applications are mentioned in Table 2.9. The processing cost of an alloy comprising high melting point temperatures remains high as compared to an alloy comprising low melting point temperatures and therefore, the overall cost of an implant increases. Many orthopedic patients from poor financial backgrounds cannot afford the expensive implantation bills. Hence, in the last 10 years, an enormous demand for a superior low-cost biomedical implant with adequate properties has risen in the implant manufacturing industries. Low-cost, non-toxic, abundant elements such as Fe, Cr, Mn, Sn etc. can effectively be used to reduce the cost of a biomedical implant [24, 75] and interestingly, the melting point temperatures of these inexpensive elements are also less than those of expensive elements such as Ta, Mo, Nb etc.

In addition to this, the solubility of elements in titanium alloys remains a crucial parameter. It has been reported that the high quantities of β eutectoid elements, e.g., Fe, Cr, Mn etc. in titanium alloys form brittle intermetallic phases [16, 25]. Titanium alloys with a high $V_f$ of intermetallic phases exhibit high Young's modulus, which is not desirable for titanium alloys used in biomedical

applications. Therefore, the design of biomedical titanium alloy compositions should be conducted considering both performance and cost parameters.

Table 2.9. Melting point temperatures of elements used in biomedical implant applications.

| Elements | Melting point temperature, $^{o}$C |
|---|---|
| Ti | 1668 |
| Nb | 2469 |
| Ta | 3020 |
| Fe | 1538 |
| Mo | 2623 |
| Zr | 1855 |
| Mn | 1246 |
| Cr | 1907 |
| Sn | 231.9 |

Table 2.10. The stabilizing effect of alloying elements used in titanium alloys [9].

| Element | Phase | Element | Phase |
|---|---|---|---|
| V | β-Isomorphous | Pd | β-Eutectoid |
| Nb | β-Isomorphous | Ag | β-Eutectoid |
| Mo | β-Isomorphous | W | β-Eutectoid |
| Ta | β-Isomorphous | Pt | β-Eutectoid |
| Re | β-Isomorphous | Au | β-Eutectoid |
| Cr | β-Eutectoid | Hf | Neutral/ β-Isomorphous |
| Mn | β-Eutectoid | Zr | Neutral/ β- Isomorphous |
| Fe | β-Eutectoid | Sn | Neutral/β- Eutectoid |
| Co | β-Eutectoid | Al | α |
| Bi | β-Eutectoid | O | α |
| Cu | β-Eutectoid | N | α |

### 2.5.6. Design of titanium alloys for biomedical applications.

In designing β titanium alloys, it is advantageous to select β stabilizers as alloying elements, which help to retain the β phase at room temperature [9]. In ternary and quaternary alloys, it is difficult to study the effect of a particular element on the microstructure and mechanical properties. However, many researchers have obtained the promising results with ternary and quaternary

titanium alloy systems for biomedical applications. Table 2.10 shows the various α stabilizers, neutral elements and β stabilizers including β-isomorphous and β-eutectoid elements [9].

The DV-Xα cluster method [102] has simplified the design of titanium alloys to a great extent for predicting the β stability and deformation mechanisms. This theoretical method (suggested by Morinaga et al. [103]) is based on the molecular orbital calculation of electronic structures. This method determines the two electronic parameters. The first parameter is *Bo* which presents the overlap population between atoms and thereby, the covalent bond strength between elements, e.g., titanium with other alloying elements [9, 45, 78]. The second parameter is *Md* which correlates the electronegativity and the metallic radius of alloying elements. The average values of bond order $(\overline{Bo})$ and metal d-orbital energy level $(\overline{Md})$ are calculated using equations (2.1) and (2.2) respectively [9, 24, 104].

$$\overline{Bo} = \Sigma\, x_i \cdot (Bo)_i \tag{2.1}$$

$$\overline{Md} = \Sigma\, x_i \cdot (Md)_i \tag{2.2}$$

where $x_i$ is the atomic fraction (atomic weight/atomic mass) of the $i^{\text{th}}$ component in the alloy composition, $(Bo)_i$ and $(Md)_i$ are the respective values for the $i^{\text{th}}$ component. This summation extends over the components, $i$ =1, 2, 3, 4…n. The values of *Bo* and *Md* of 3d, 4d, 5d and few non-transition elements from the periodic table are presented in Table 2.11 [103, 105]. The average value of $(\overline{Bo})$ and $(\overline{Md})$ for whole titanium alloy composition is calculated using the individual *Bo* and *Md* values of each element listed in Table 2.11.

Fig. 2.18 illustrates the phase stability diagram suggested by Morinaga et al. [103], which is also known as $\overline{Bo} - \overline{Md}$ map. The phase stability diagram is prepared based on the average values of $\overline{Bo}$ and $\overline{Md}$. The $\overline{Bo} - \overline{Md}$ map clearly separates the regions of α, α+β and β type titanium alloys. Moreover, the prospective deformation mechanisms and the values of elastic modulus for titanium alloys can also be predicted using the $\overline{Bo} - \overline{Md}$ map. Generally, the deformation of β titanium alloys occurs by either slip or twin mechanisms, which depends mostly on the phase stability. As the β stability increases, the deformation mechanism of an alloy changes from twin to slip. In addition, the subregion for the martensite phase transformation is also clearly identified in the $\overline{Bo} - \overline{Md}$ map. It has been observed that the formation of athermal ω phase occurs near the

slip/twin boundary shown in the $\overline{Bo} - \overline{Md}$ map [103]. However, the formation of ω phase can be suppressed by increasing the amount of β stabilizers and improving β phase stability [106].

Table 2.11. The values of *Bo* (bond order) and *Md* (metal d-orbital energy level) of 3d, 4d, 5d and few non-transition elements from the periodic table [103, 105].

| **3d elements** | ***Bo*** | ***Md* (eV)** | **4d elements** | ***Bo*** | ***Md* (eV)** |
|---|---|---|---|---|---|
| Ti | 2.79 | 2.447 | Zr | 3.086 | 2.934 |
| V | 2.805 | 1.872 | Nb | 3.099 | 2.424 |
| Cr | 2.779 | 1.478 | Mo | 3.063 | 1.961 |
| Mn | 2.723 | 1.194 | Tc | 3.026 | 1.294 |
| Fe | 2.651 | 0.969 | Ru | 2.704 | 0.859 |
| Co | 2.529 | 0.807 | Rh | 2.736 | 0.561 |
| Ni | 2.412 | 0.724 | Pd | 2.208 | 0.347 |
| Cu | 2.114 | 0.567 | Ag | 2.094 | 0.196 |
| **5d elements** | ***Bo*** | ***Md* (eV)** | **Other non-transition elements** | ***Bo*** | ***Md* (eV)** |
| Hf | 3.11 | 2.975 | Al | 2.426 | 2.2 |
| Ta | 3.144 | 2.531 | Si | 2.561 | 2.2 |
| W | 3.125 | 2.072 | Sn | 2.283 | 2.1 |
| Re | 3.061 | 1.49 | - | - | - |
| Os | 2.98 | 1.018 | - | - | - |
| Ir | 3.168 | 0.677 | - | - | - |
| Pt | 2.252 | 0.146 | - | - | - |
| Au | 1.953 | 0.258 | - | - | - |

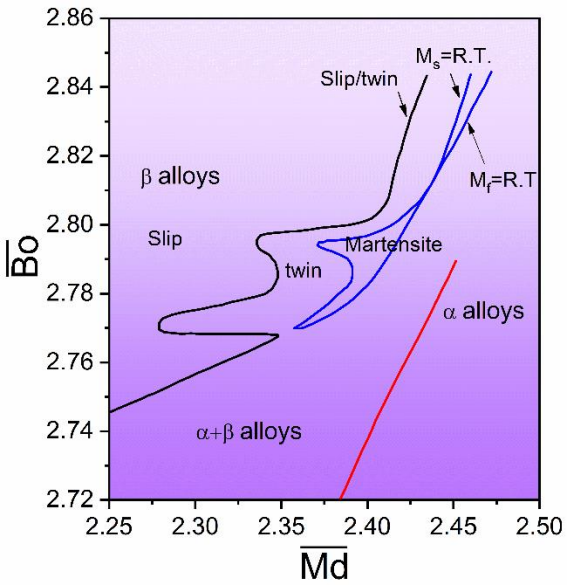


Fig. 2.18. The phase stability diagram based on $\overline{Bo}$ and $\overline{Md}$ parameters for titanium alloys [103].

Fig. 2.19 [74, 78, 103] represents the $\overline{Bo} - \overline{Md}$ map showing the effects of an individual alloying element on the prospective trends of $\overline{Bo}$ and $\overline{Md}$ values for binary titanium alloys. For instance, the prospective trend moves upwards and slightly left for Ti-Mo binary alloys because of the increase in the $\overline{Bo}$ values and the decrease in the $\overline{Md}$ values. Other than the phase stability diagram, Fig. 2.19 is also helpful in selecting alloying elements for titanium alloys.

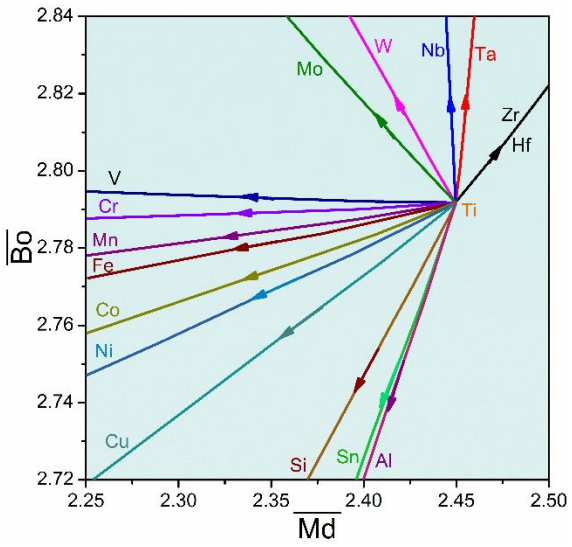


Fig. 2.19. The prospective trends of individual elements based on the values of $\overline{Bo}$ and $\overline{Md}$ on the phase stability diagram [74, 78, 103].

Moreover, $Mo_{eq}$ is also an important parameter to predict the β stability of titanium alloys. The values of $Mo_{eq}$ for a particular alloy composition can be determined using equation (2.3) [107]. An increase in the values of $Mo_{eq}$ improves the stability of the β phase [7, 108]. Table 2.12 shows the critical concentration of various β stabilizers to retain a single β phase in the microstructure [108]. It can be seen in Table 2.12 that Fe, Mn and Cr are strong β stabilizers as their small quantities are enough to retain the β phase in titanium alloys. However, if titanium alloys comprise more than one β stabilizers, then fewer quantities of β stabilizers are required than their critical concentrations presented in Table 2.12 to retain a single β phase.

$$Mo_{eq} = [Mo] + \frac{[Ta]}{5} + \frac{[Nb]}{3.6} + \frac{[W]}{2.5} + \frac{[V]}{1.5} + 1.25\,[Cr] + 1.25[Ni] + 1.7[Mn] + 1.7[Co] + 2.5[Fe] \quad (2.3)$$

where x indicates the concentration of element x in wt%.

Table 2.12. The critical concentration of β stabilizers to retain a single β phase in titanium alloys [108].

| Element | Critical concentration (wt%) |
|---|---|
| Mo | 10 |
| Nb | 36 |
| Ta | 45 |
| V | 15 |
| W | 22.5 |
| Co | 7 |
| Cu | 13 |
| Cr | 6.5 |
| Fe | 3.5 |
| Mn | 6.5 |
| Ni | 9 |

Considering the above designing parameters, the alloying elements of titanium alloys should be selected in a manner, where the designed alloy composition should have high $\overline{Bo}$, low $\overline{Md}$ and high $Mo_{eq}$ values as discussed earlier for improving the β stability [24]. Elements such as Mo, Nb, Ta, Zr and Hf help to achieve high $\overline{Bo}$ values of an alloy composition [82, 105, 109] as illustrated in Fig. 2.19 and thereby, help to achieve low elastic modulus. Moreover, it is apparent from Fig. 2.19 that the $\overline{Md}$ values of binary titanium alloys comprising elements such as Fe, Mn, Cr decrease with a slight fall in $\overline{Bo}$ values as the content of corresponding elements increase in binary titanium alloys. Nonetheless, the problem of slight decrease in $\overline{Bo}$ values can be compensated by adding higher quantities of elements comprising high *Bo* values in titanium alloy compositions. Although the *Md* value of vanadium decreases, it is not still advantageous as it produces toxic reactions in the human body after few years of implantation. It can be noted from equation 2.3 (equation of $Mo_{eq}$) that the addition of low-cost elements, e.g., Fe, Cr and Mn in titanium alloys increase the $Mo_{eq}$ values and therefore, it is advantageous to select these low-cost elements with other elements comprising high *Bo* values, e.g., Nb, Mo and Ta to design an improved low-cost β titanium alloy for biomedical applications.

The tendency of athermal ω phase formation can be predicted based on the ratio of valence electrons to atoms (*e/a*) for titanium alloy compositions [110]. The *e/a* ratio can be determined by equation (2.4) [110].

$$\frac{e}{a} = \Sigma\, x_i \cdot\ e_i \tag{2.4}$$

where $x_i$ is the atomic fraction of the $i^{\text{th}}$ component in the alloy and $e_i$ is the valence electron of $i^{\text{th}}$ element. Previous studies acknowledge that an alloy retains a single β phase in the microstructure at or above the *e/a* value of 4.20 [74]. The consideration of *e/a* values further strengthens the prediction of β phase stability along with the other theoretical β phase stability indicators, e.g., $\overline{Bo}$, $\overline{Md}$ and $Mo_{eq}$.

In summary, it can be deduced that β titanium alloys are suitable for biomedical applications. Therefore, novel β titanium alloys should be designed to overcome the problem of stress-shielding effect. The design of β titanium alloys requires the appropriate selection of alloying elements and their quantities, which can demonstrate low elastic modulus close to that of the human bone. Furthermore, the cost factor should also be considered to reduce the overall price of biomedical implants. Thus, there is a huge demand for low-cost biomaterials in biomedical implant manufacturing industries, which should exhibit a better combination of mechanical, biological and corrosion resistance behaviors.

### 2.6. Titanium alloys for high-strength structural applications

Other than biomedical applications, titanium alloys have also gained much attention as light-weight high-strength materials in automobile and aerospace industries [4, 17]. Titanium, aluminum, magnesium, high-strength steels, nickel based super alloys and carbon fiber composites are commonly used materials in aerospace and automobile applications [111]. Table 2.13 compares the various properties of these aforementioned materials for aerospace and automobile applications [111]. Titanium alloys demonstrate many desirable attributes such as high strength, fracture toughness, fatigue life and corrosion resistance along with low elastic modulus as compared to other materials mentioned in Table 2.13. The cost of titanium alloys is considered high as compared to aluminum, magnesium and high-strength steel. However, there are many drawbacks associated with aluminum, magnesium and high-strength steel (Table 2.13). Contrastingly, titanium alloys demonstrate a wide range of properties which can be tailored by the appropriate selection of processing methods, alloying elements and their quantities.

Table 2.13. The comparison of various properties of aerospace and automobile materials [111].

| Properties | Titanium | Aluminium | Magnesium | High-strength steel | Nickel superalloy | Carbon fibre composite |
|---|---|---|---|---|---|---|
| Cost | Expensive | Cheap | Medium | Medium | Expensive | Expensive |
| Weight (Density) | Medium | Light | Very light | Heavy | Heavy | Very light |
| Stiffness (elastic modulus) | Low/ Medium | Low/ Medium | Low | Very high | Medium | High |
| Strength (yield stress) | Medium/ High | Medium | Low | Very high | Medium | High |
| Fracture toughness | High | Medium | Low/ Medium | Low/ Medium | Medium | Low |
| Fatigue | High | Low/ Medium | Low | Medium/ High | Medium | High |
| Corrosion resistance | High | Medium | Low | Low/ Medium | High | Very high |
| High-temperature creep strength | Medium | Low | Low | High | Very high | Low |
| Ease of recycling | Medium | High | Medium | High | Medium | Very low |

Strength and ductility are two crucial properties for materials used in high-strength structural applications. For metallic materials, ductility usually decreases as strength increases. Therefore, a better blend of strength and ductility is desirable in high-strength structural applications. Strength properties include yield strength, ultimate strength, fatigue strength and creep strength [27, 111]. In high-strength applications, a material should be able to withstand high stress applied on it without plastic deformation [27, 111]. Thus, a material should have high yield strength as plastic deformation starts after yielding. As yield strength and hardness are correlated with each other, hardness also increases as yield strength of a material increases [27, 111].

### 2.6.1. Strengthening mechanisms

A material can be strengthened by hindering the dislocation motion when external load is applied to a material [27]. This indicates that the microstructure of a material should possess a great resistance against a motion of dislocations [27]. There are various mechanisms for producing strengthening effects which increase strength and hardness of materials. The fundamental strengthening mechanisms are described as below.

#### *2.6.1.1. Work (strain) hardening*

Work hardening involves plastic deformation during the processing/manufacturing of a material [27, 111]. The plastic deformation of a material can be executed by forging, cold rolling, hot rolling

and extrusion techniques [27, 111]. This shows that a material experiences a permanent shape change at the manufacturing stage, which creates new dislocations in a material [111]. A high stress intensity is required in the formation of new dislocations, which remains greater than yield stress of a material [111]. The new dislocations then move along the slip planes until any obstacles such as solute particles, grain boundary and/or second particles hinder the movement of dislocations and as a result, the strength of a material increases [27, 111].

#### *2.6.1.2. Solid solution strengthening*

Solid solution strengthening involves the addition of alloying elements with either smaller or larger atomic size than the parent element of an alloy composition [27, 111]. Alloying elements produce either substitutional or interstitial point defects in the crystals [27, 111]. Other than atomic size, crystal structure and electronegativity also influence to produce either substitutional or interstitial point defects in the crystals [3, 27, 111]. According to the Hume-Rothery principle, if the atomic size of an alloying element is either smaller or larger than that of a parent element by around 15%, then atoms of alloying elements occupy interstitial sites in the parent lattice [3, 27, 111]. Contrastingly, if the atomic size of an alloying element is almost identical (within 15%) to that of a parent element, then substitution of atoms occurs in the parent lattice [3, 27, 111]. The presence of substitutional or interstitial atoms in the parent lattice causes lattice distortion, which hinders the dislocation motion passing through them and increases yield strength and hardness [3, 27, 111]. Solid solution strengthening usually depend on the concentration, shear modulus and atomic size of alloying elements [3, 27, 111].

#### *2.6.1.3. Precipitation strengthening*

Precipitation strengthening involves precipitation of hard second phase particles in the parent matrix [27, 111]. The formation of second phase particles depend on the solubility of alloying element in a parent element [27, 111]. The precipitates of the second phase usually impede the dislocation slip activities and therefore, increase the strength of a material [3, 27, 111]. The intensity of hindering dislocation movement depends on crystal structure, size and amount of second phase particles [27, 111]. Heat treatment processes are usually effective in obtaining a dispersion of second phase particles in a parent matrix [3]. An intensive strengthening (increase the strength by more than 300%) can be obtained in a material using second phase precipitates

[111]. Therefore, the precipitation strengthened alloys are used in aerospace, automobile, power generation and chemical industries.

#### *2.6.1.4. Grain boundary strengthening*

The microstructures of polycrystalline materials are usually composed of large sized grains [27, 111]. The arrangement of lattice in each grain remains almost same; however, the orientation of each grain remains different [27, 111]. A boundary which separates two neighboring grains is known as a grain boundary. Grain boundaries usually hinder the dislocation motion passing through them [27, 111]. This indicates that dislocations can easily pass inside the grain until they reach at the grain boundaries. As dislocations usually pass along slip planes, the motion of dislocations disrupts at grain boundaries due to differing crystal orientation [27, 111]. According to the Hall-Petch relationship, yield strength is directly related to the average size of grains in the microstructure [27, 111]. Hence, a greater number of grain boundaries help in increasing yield strength and hardness of a material.

#### *2.6.1.5. Dispersion strengthening*

Dispersion strengthening occurs when small-sized randomly distributed second phase particles hinder the movement of dislocations in the parent matrix [111]. The oxide particles, with size up to 0.1 µm, are usually introduced in a parent matrix using mechanical alloying method, e.g., yttrium oxide [111]. Dislocation cannot pass through the tiny second phase particles due to their different crystal structure and therefore, fine dispersed particles impede the dislocation slip activities [111]. The dispersion strengthening mechanism is also known as Orowan strengthening mechanism [3, 27, 111].

Based on the strengthening mechanisms discussed above, it can be inferred that the second phase plays a crucial role in dislocation pinning and thereby, strength of an alloy. Moreover, as compared to other strengthening mechanisms, second phase particles significantly increase strength of an alloy [111]. As a result, dislocation densities remain higher in alloys with second phase particles than single phase alloys [26]. Therefore, it is worth investigating the detailed deformation behavior of second phase particles to develop an improved titanium alloys for high-strength applications.

### 2.6.2. Strengthening of an alloy using Laves phases

Laves phases are the most abundant type of intermetallic compounds, which form in $AB_2$ type alloy compositions [112]. In $AB_2$ type alloy compositions, the atoms of A remain relatively larger

atoms (e.g., La, Ce, Zr and B) and the atoms of B remain relatively smaller atoms (e.g., Fe, Co, Mn, Ni and Cr) in terms of atomic size [12, 113]. Fritz Laves first described Laves phases, where to date, more than 1400 binary and ternary Laves phases have been documented [114]. Laves phases are basically categorized into three types: (i) C14 with an hcp structure, (ii) C15 with a fcc structure and (iii) C36 with an hcp structure [115]. The prototypes and the packing sequence of a unit layer for C14, C15 and C36 type Laves phases remain $MgZn_2$ with ABABAB type packing sequence, $MgCu_2$ with ABCABC type packing sequence and $MgNi_2$ with ABACABAC type packing sequence respectively [116].

The formation of Laves phase primarily depends on atomic radii ratio of A and B atoms, $R_A/R_B$. The ideal $R_A/R_B$ for the Laves phase formation is 1.225 (i.e., $R_A/R_B = (3/2)^{1/2}$). However, the Laves phase formation has been reported in literature for $R_A/R_B$ from 1.05 to 1.68 with the melting point temperatures from 7 °C to more than 2000 °C. Further, research has also demonstrated that C14 and C36 type Laves phases have mostly been found between $R_A/R_B$ ratio of 1.12 and 1.26, whereas C15 type has mostly been found between $R_A/R_B$ ratio of 1.1 and 1.35 [112]. The general range of $R_A/R_B$ ratio (i.e., 1.12-1.26) for C14 and C36 types of Laves phases is within the general range of $R_A/R_B$ ratio (i.e., 1.1-1.35) for C15 type Laves phases because the geometric parameter, i.e., $R_A/R_B$ ratio, is not the only parameter responsible for the formation of Laves phases. Several other parameters, such as difference in electronegativities of larger (A) and smaller (B) atoms, number of valence electrons and solubility of individual elements in a base element of an alloy composition, also play a crucial role in the formation of a Laves phase [12, 114]. This indicates that all three influential parameters of Laves phase formation apparently depend on alloying elements and their quantities in alloy compositions. Previous literature suggests that C15 type Laves phases remain stable at the values of *e/a* less than 5.77 and greater than 7.56, whereas C14 type Laves phases remain stable at the values *e/a* between 5.85 and 7.50 [117]. The values of *e/a* for the Laves phase and the parent matrix remain different, which can be obtained based on EDX quantitative analysis [12]. Therefore, the values of *e/a* are also important in identifying a specific type of Laves phase based on previous literature [12].

Laves phase alloys demonstrate superior mechanical properties along with very good oxidation and corrosion resistance abilities for structural applications in nuclear, aerospace, chemical and automobile industries [12, 118]. As Laves phases possess high melting temperatures, they are also

suitable for high-temperature applications [12]. Despite comprising these useful attributes, poor ductility and poor fracture toughness are considered as drawbacks of Laves phases [116]. It has been reported in many research findings that the ductility of Laves phase alloys improves when Laves phases precipitate in some soft microstructural matrices [114, 118, 119]. When Laves phase precipitates in soft ductile matrix, Laves phases impede the dislocation slips and behave as a strengthening phase [119].

Takeyama et al. [120] have investigated the behavior of C15 type $Cr_2Nb$ Laves phase in the Cr-Nb alloys. Fig. 2.20 shows the microstructure of the Cr-20Nb alloy in which C15 type $Cr_2Nb$ Laves phase precipitated in the soft Cr rich matrix [120]. It has been reported that the increase in the amount of $Cr_2Nb$ phase increases yield strength and hardness, whereas Cr rich soft phase helps to improve fracture toughness of the Cr-20Nb alloy [120].

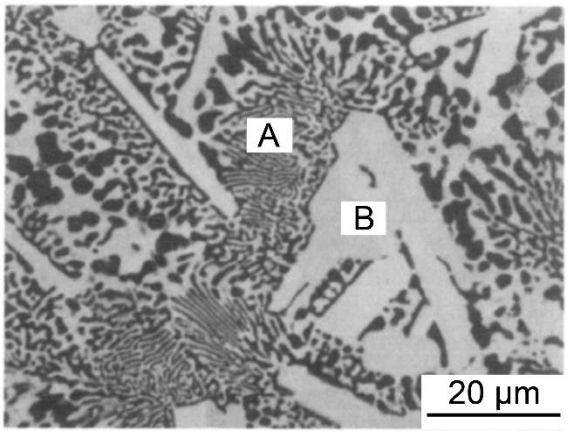


Fig. 2.20. The backscattered SEM image of as-cast Cr-20Nb alloy. The region A shows Cr-$Cr_2Nb$ eutectic phase and the region B (bright) shows primary $Cr_2Nb$ Laves phase [120].

Wasilkowska et al. [121] have examined Laves phases in the as-cast Fe-Al-Zr alloys. Fig. 2.21 shows the SEM microstructural images of Fe-10Al-2.5Zr and Fe-20Al-2.5Zr. The bright eutectic phase in Fig. 2.21 is Zr rich $Zr(Fe,Al)_2$ (C14 type) phase with an hcp structure, which form in the Fe-Al matrix. The high-magnification TEM images of eutectic $Zr(Fe,Al)_2$ phase in the Fe-Al matrix are presented in Fig. 2.22 [121]. Wasilkowska et al. have concluded that the hard skeleton like structure of Laves $Zr(Fe,Al)_2$ phase on grain boundaries is helpful to strengthen the alloy and therefore, suitable for intermediate to high temperature structural applications.

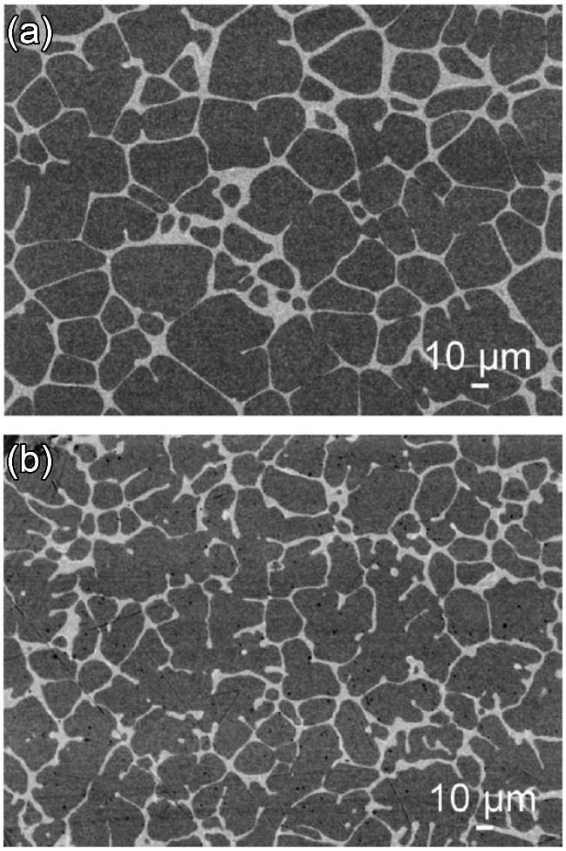


Fig. 2.21. The SEM images of the as-cast (a) Fe-10Al-2.5Zr (b) Fe-20Al-2.5Zr alloys [121].

Scudino et al. [118] have investigated the mechanical behavior of the as-cast $Fe_{90-x}Zr_{10}Cr_x$ alloys and revealed both fcc C15 and hcp C14/C36 type Laves phases in these alloys. Based on this work, it has been noted that the as-cast $Fe_{90-x}Zr_{10}Cr_x$ alloys show 1900 MPa of yield strength, where the addition of Cr enhances plastic strain up to 17% at an expense of only 70 MPa of strength reduction (Fig. 2.23) [118]. Moreover, dislocation activities have not been found in C14/C36 type phases, whereas dislocation bands are found in C15 type Laves phase. This indicates that cubic C15 type Laves phases can be deformed more easily than hcp C14 and C36 type Laves phases [118].

Zhu et al. [117] have studied the mechanical behavior of the $Nb(Cr,Fe)_2$ and $Nb(Cr,Co)_2$ alloys comprising both C14 and C15 type Laves phases. In the $Nb(Cr,Fe)_2$ and $Nb(Cr,Co)_2$ alloys, the quantities of Fe and Co have been varied up to 66.7 at% with the Nb content of 33.3 at% [117]. Fig. 2.24 shows the effect of Fe and Co on Vickers hardness of the $Nb(Cr,Fe)_2$ and $Nb(Cr,Co)_2$ alloys. It is evident from Fig. 2.24 that the $Nb(Cr,Fe)_2$ and $Nb(Cr,Co)_2$ alloys exhibit the impressive Vickers hardness values of more than 850 $kg/mm^2$, which are attributed to the outstanding

strengthening ability of Laves phases [117]. Zhu et al. have also found that the fracture toughness of C15 type Laves phases remain higher than that of C14 type Laves phases because C15 type Laves phases are composed with a cubic structure, where C14 type Laves phases are composed with a hexagonal structure [117]. Liu et al. [116] have also studied Vickers hardness and fracture toughness of $NbFe_2$, $NbCr_2$, $TaCr_2$ and $ZrCr_2$ type Laves phases in the Cr rich matrix. They found the superior Vickers hardness values close to 1000 $kg/mm^2$ and the fracture toughness values up to 14.3 $MPam^{-1/2}$ in the Laves phase alloys [116].

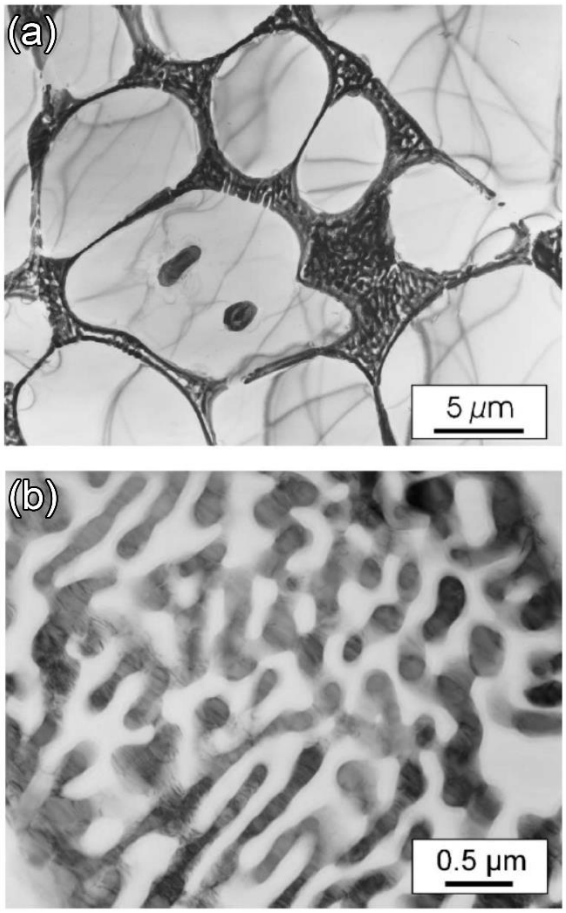


Fig. 2.22. High-voltage TEM images of the as-cast Fe-10Al-2.5Zr. (a) Morphology of eutectic phase on grain boundaries, (b) Eutectic region [121].

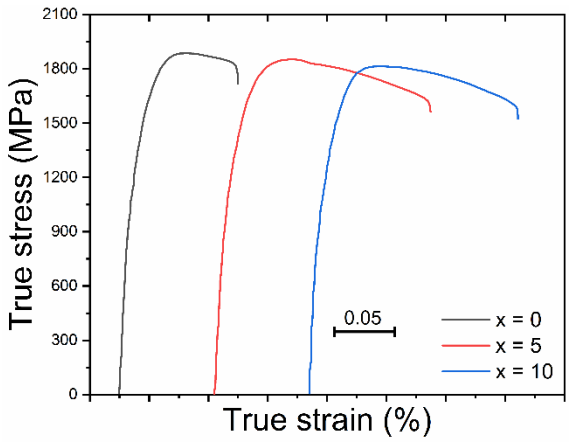


Fig. 2.23. True compressive stress versus strain curves of the $Fe_{90-x}Zr_{10}Cr_x$ alloys [118].

It can be deduced when considering the superior attributes of Laves phases that they can produce superior strengthening effects in alloys. Therefore, Laves phase alloys are suitable for high-strength applications at room temperature and at elevated temperatures. The bulk ductility and toughness of Laves phase alloys can be enhanced by alloying Laves phases/particles with the ductile matrix, e.g., bcc matrix [119]. Hence, it is of emerging research value to investigate the various properties of Laves phases to develop an improved high-strength structural alloy.

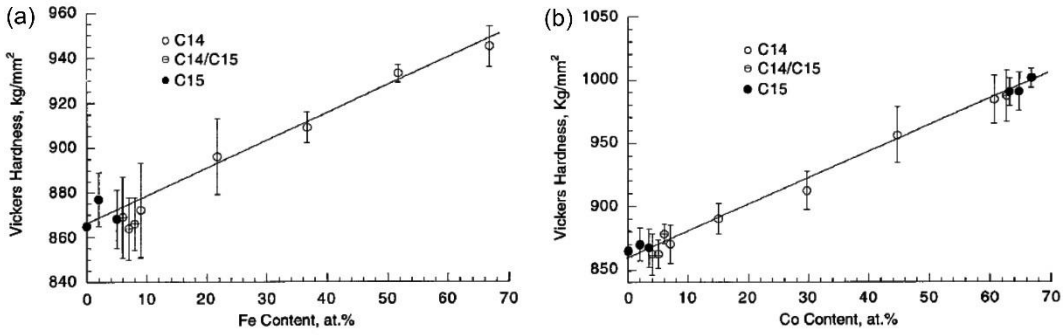


Fig. 2.24. (a) The effects of Fe on Vickers hardness of the $Nb(Cr,Fe)_2$ alloys and (b) Effect of Co on Vickers hardness of the $Nb(Cr,Co)_2$ alloys [117].

## 2.7. Application-specific effects of alloying elements

Alloying elements play a crucial role in tailoring the microstructure and thereby, mechanical and corrosion properties of titanium alloys. Each alloying element in titanium alloys behaves

differently to one another. Hence, an alloying element suitable for one application may not be suitable for other applications. The effect of many individual alloying elements for biomedical and high-strength structural applications are discussed below.

### 2.7.1. Biomedical applications

Based on the characteristics of different alloying elements discussed in preceding sections, it can be inferred that elements such as Nb, Ta and Mo are the most promising alloying elements for titanium alloys used in biomedical implant applications as these elements are biocompatible, non-toxic and improve the stability of β phase as well as reduce elastic modulus, whereas small quantities (up to 8 wt%) of Zr and Sn are also advantageous in titanium alloy compositions for biomedical applications. Among the three most promising alloying elements for biomedical applications, i.e., Nb, Ta and Mo, Nb comprises the best combination of required characteristics when properties including biocompatibility, melting point, corrosion resistance, mechanical strength and elastic modulus are considered. Moreover, the strong β-stabilizing elements such as Fe, Mn and Cr exhibit sufficient biocompatibility and corrosion resistance and simultaneously, reduce the elastic modulus of titanium alloys when the small quantities (up to 8 wt%) of these elements are added to titanium alloy compositions. Moreover, small quantities of Fe, Mn and Cr are enough to produce the required strengthening effects in titanium alloys used for biomedical applications. Although Fe, Mn and Cr are inexpensive as compared to Nb, Ta and Mo, they display intermetallic phases and eventually, increase the elastic modulus when high quantities (more than 8 wt%) of these elements are added in titanium alloys. Therefore, high quantities of Fe, Mn and Cr in titanium alloys are not desirable for biomedical applications.

### 2.7.2. High-strength structural applications

A better combination of yield strength, hardness and plasticity is essential in high-strength structural applications. Yield strength and hardness relate directly to each other, whereas plasticity relate inversely with yield strength and hardness. Therefore, an alloy with high yield strength and hardness usually fails to exhibit large plasticity. Considering these points, elements with lower atomic radius, e.g., Fe, Mn, V and Cr and higher atomic radius, e.g., Zr, than titanium can produce solid solution strengthening which increases yield strength and hardness of titanium alloys. Moreover, due to the size misfit effect, the chances of second phase formation remain high if elements with lower atomic radius (Fe, Mn, V and Cr) and/or higher atomic radius (Zr) than

titanium are added to titanium alloys. The presence of the second phase in the matrix produces precipitation strengthening which also increases yield strength and hardness. As a result, elements such as Fe, Mn, Cr and Zr are promising elements to increase yield strength and hardness in titanium alloys. In addition to this, elements such as Al, Nb, Ta and Mo soften the microstructure matrix and help to improve plasticity and corrosion resistance. Zr also shows superior mechanical (including high strength and large plasticity) and corrosion properties in titanium alloys and therefore, Zr can also be a promising element in titanium alloys. In addition, for elevated-temperature applications, titanium based Laves phase alloys are effective because Laves phases are able to demonstrate high-mechanical strength and very good corrosion and oxidation resistance even at elevated-temperatures. In order to obtain the Laves phase in titanium alloys, adequate quantities of alloying elements are necessary. Considering the above points, in high-strength titanium alloys, a combination of alloying elements is desirable in order to obtain a better blend of yield strength, hardness and plasticity along with very good corrosion resistance.

**Page deliberately left blank**

# Chapter 3. Research applicability and objectives

This chapter describes the applicability and objectives of the present research derived based on the literature review.

### 3.1. Ti-Nb-Fe-Cr alloys for biomedical applications

In the last two decades, researchers have engaged in endeavors to develop β titanium alloys using non-toxic β stabilizing elements (e.g., Nb, Ta, Mo, Zr etc.) for biomedical applications. These alloys exhibit superior properties including elastic moduli of around 40-60 GPa for surgical implant applications. Nonetheless, these elements are expensive rare earth elements. Thus, over the last few years, researchers have focused on the design of titanium alloys using abundant, inexpensive elements such as Fe, Mn, Cr and Sn [24, 82], but without compromising the performance requirements of surgical implant materials. Therefore, both the factors-the performance and the cost should be considered while designing titanium alloys for surgical implants.

Nb exhibits excellent performance attributes such as low modulus, superior corrosion resistance and biocompatibility along with good superelastic and shape memory behaviors. Further, Nb is non-allergic, non-toxic and non-cytotoxic. These aforementioned properties are essential for an improved surgical implant material [9]. In addition, the melting point of Nb is lower than the melting points of Mo and Ta, where it has also been reported that high Nb content strengthens the β phase stability of titanium alloys [109, 122]. The addition of Fe, which is a low-cost and is a strong β stabilizing element in titanium alloys, improves tensile and bending strength [109]. Fe also reduces the α phase precipitation, decreases the martensitic start temperature and thereby, favors the retention of the β phase at room temperature [109]. Many previous research findings have reported Fe as a biocompatible element in titanium alloys [123, 124]. The addition of Cr to titanium also has attractive attributes such as being low-cost and having β stabilization ability and improved corrosion resistance [125]. Moreover, the addition of Cr in titanium alloy composition suppresses the formation of an undesired athermal ω phase [126]. Consequently, it appears to be an appropriate choice based on the points discussed above to select Nb, Fe and Cr as alloying elements of titanium alloys because these three elements may offer a better combination of properties such as improved mechanical strength, plasticity and hardness along with low elastic

modulus, superior biocompatibility and corrosion resistance. Hence, in the present work, the quaternary Ti-Nb-Fe-Cr system has been chosen for the investigation.

Nb is a rare earth element even though it has been chosen in the present work with an aim to achieve superior performance behavior of titanium alloys. The selection of Nb, Fe and Cr elements as alloying elements of titanium alloys represents an optimized selection based on both factors of performance and cost as discussed above. Previous research findings have reported an elastic modulus of around 50 GPa using an amount of Nb between 25% and 30% in titanium alloys [99, 127, 128]. Therefore, in the present work, the amount of Nb has been selected as 27% in the Ti-Nb-Fe-Cr alloys. Moreover, it has also been reported in previous research findings that small amounts of Fe and Cr are sufficient to create a significant impact on the stability of the β phase [36, 109, 129, 130]. Hence, the present work has used 7 wt% quantity of Fe and the amount of Cr has been varied from 0 to 8 wt% in the Ti-Nb-Fe-Cr alloys.

In the present work, the Ti-27Nb-7Fe-xCr (x = 0, 2, 4, 6, 8 wt%) alloys were theoretically designed using the DV-Xα cluster method [103]. In addition to the cluster method, $Mo_{eq}$ and *e/a* have also been taken into consideration while designing the Ti-27Nb-7Fe-xCr alloys. Moreover, this work investigates the microstructure and mechanical properties of the Ti-27Nb-7Fe-xCr alloys with a Cr content varying from 0 to 8%. Furthermore, the analysis of the deformation induced slip bands around the hardness indentation has been studied to a limited degree to date for titanium alloys. Therefore, the analysis of slip bands around the micro-hardness indentation of each alloy composition has been studied in the present work. Additionally, the evaluations of the wear resistance indices (i.e., H/E and $H^3/E^2$) and elastic energies of the Ti-27Nb-7Fe-xCr alloys have also been carried out in the present work.

### 3.2. Ti-Zr-Fe-Cr, Ti-Zr-Fe-Mn and Ti-Zr-Fe-Sn alloys for high-strength applications

Research and development activities on Laves phase alloys have received significant attention during the last two decades, especially relating to their atomic structural aspects and attractive properties such as superior mechanical strength, hardness, corrosion resistance and oxidation resistance [118, 131]. However, Laves phase alloys still experience extreme brittleness because less than five independent slip systems remain active in Laves phase alloys and this number should usually be greater than five in order to accommodate plastic deformation [132]. The undesirable problem of embrittlement in Laves phase alloys can be solved by alloying Laves particles with any

ductile metallic matrix, particularly with a material with a bcc phase [118]. In this case, the Laves phase plays the role of a strength-bearing component and a bcc matrix improves plasticity [118].

β titanium alloys comprising a bcc structure, are often the first choice for researchers to overcome the problem of severe brittleness in Laves phase alloys. Alloying of the β titanium matrix with the Laves phase [119] can lead to exhibit superior plasticity along with high strength, very good fatigue behavior and superior corrosion resistance [6, 16, 38, 133]. Therefore, the investigations on the alloy composition comprising the β titanium matrix and the Laves phase can provide insightful research outcomes in present and future generations of aerospace and automobile applications [134]. Recently, many researchers have also studied the mechanical properties of Laves phase alloys which had been alloyed with titanium to improve their ductile behavior [5, 119, 135].

The selection of elements is a vital phenomenon in designing β titanium alloys because an improved β phase stability can only be achieved using β stabilizing elements [18, 23, 36]. Among other β stabilizers, the elements such as Mn, Fe and Cr are inexpensive and strong β stabilizers that increase the stability of the β phase even when small quantities of these elements are added to titanium alloys [7, 17, 136]. These inexpensive β stabilizers work as solute constituents to increase the yield strength and hardness of titanium alloys [25, 137]. Furthermore, although Zr and Sn are recognized as neutral elements, Zr and Sn can also improve the mechanical and corrosion properties when alloyed with titanium [138-141]. Additionally, Sn works as a β stabilizer even when only small quantities of Sn are added to titanium alloys [10, 138]. Considering the above points, three quaternary alloy systems, i.e., (i) Ti-Zr-Fe-Cr, (ii) Ti-Zr-Fe-Mn and (iii) Ti-Zr-Fe-Sn, have been selected with an aim to obtain the Laves phase in the microstructure first and then to investigate their corresponding microstructure, mechanical and fracture behavior.

The ideal value of $R_A/R_B$ for the Laves phase formation in alloys is 1.225 [112]. The value of $R_A/R_B$ for ternary and quaternary alloys is generally estimated by taking a ratio of average atomic radius of larger elements to average atomic radius of smaller elements present in an alloy composition [5, 12, 142]. This means that the value of $R_A/R_B$ is dependent only on the geometric parameter (i.e., atomic radius) of the elements present in an alloy composition, but not on the quantities of the alloying elements present in an alloy composition as suggested by Ishimasa et al. [142]. However, the quantities of alloying elements affect the formation of Laves phase as well as the volume fraction of Laves phase ($V_{f,\,Laves}$) based on the solubility of alloying elements in a base

element as suggested by Thoma et al. [112]. Further, an improved strength-plasticity trade-off can be achieved in titanium alloys by appropriately varying the $V_{f,\ Laves}$ [5, 11, 143].

The values of $R_A/R_B$ for Ti-Zr-Fe-Cr, Ti-Zr-Fe-Mn and Ti-Zr-Fe-Sn systems are close to the ideal value (1.225) of $R_A/R_B$ for the Laves phase formation. Based on the values of $R_A/R_B$ for Ti-Zr-Fe-Cr, Ti-Zr-Fe-Mn and Ti-Zr-Fe-Sn systems, the chances of Laves phase formation are high. However, the quantities of alloying elements have been selected considering the binary and ternary phase diagrams of the corresponding alloy systems. The following are the three groups of alloys, which have been designed to check their suitability based on microstructure, mechanical and fracture behavior for high-strength applications.

(i) Ti-33Zr-xFe-yCr (x = 3, 5, 7 wt% and y = 2, 4 wt%) alloys

(ii) Ti-35Zr-5Fe-xMn (x = 0, 2, 4, 6, 8 wt%) alloys

(iii) Ti-xZr-7Fe-ySn (x = 25, 30, 35 wt% and y = 2, 4 wt%) alloys

### 3.3. Research objectives

This work mainly focuses on the design and development of new metastable β titanium alloys suitable for biomedical and high-strength structural applications using inexpensive solute elements. The following are the main objectives of this work:

1) To design the metastable β titanium alloys (four groups) for biomedical and high-strength structural applications (discussed in this chapter).
2) To investigate the microstructure and mechanical behavior of the new Ti-27Nb-7Fe-xCr (x = 0, 2, 4, 6, 8 wt%) alloys for biomedical applications (results and discussion related to this objective are presented in Chapter 5).
3) To investigate the effects of C15 type Laves phase on the microstructure, mechanical and fracture behavior of the new Ti-33Zr-xFe-yCr (x = 3, 5, 7 wt% and y = 2, 4 wt%) alloys for high-strength structural applications (results and discussion related to this objective are presented in Chapter 6).
4) To investigate the effects of C14 type Laves phase on the microstructure, mechanical and fracture behavior of the new Ti-35Zr-5Fe-xMn (x = 0, 2, 4, 6, 8 wt%) alloys for high-strength structural applications (results and discussion related to this objective are presented in Chapter 7).

5) To investigate the deformation and strengthening characteristics of C14 and C15 type Laves phases in β titanium alloys using a micro-indentation method (results and discussion related to this objective are presented in Chapter 8).
6) To investigate the effects of varying the concentrations of Zr and Sn in the new Ti-xZr-7Fe-ySn (x = 25, 30, 35 wt% and y = 2, 4 wt%) alloys (results and discussion related to this objective are presented in Chapter 9).

Fig. 3.1 presents a brief overview of the design, fabrication, characterization/investigations executed for the investigated titanium alloys, research outcomes, applications and benefits of this work.

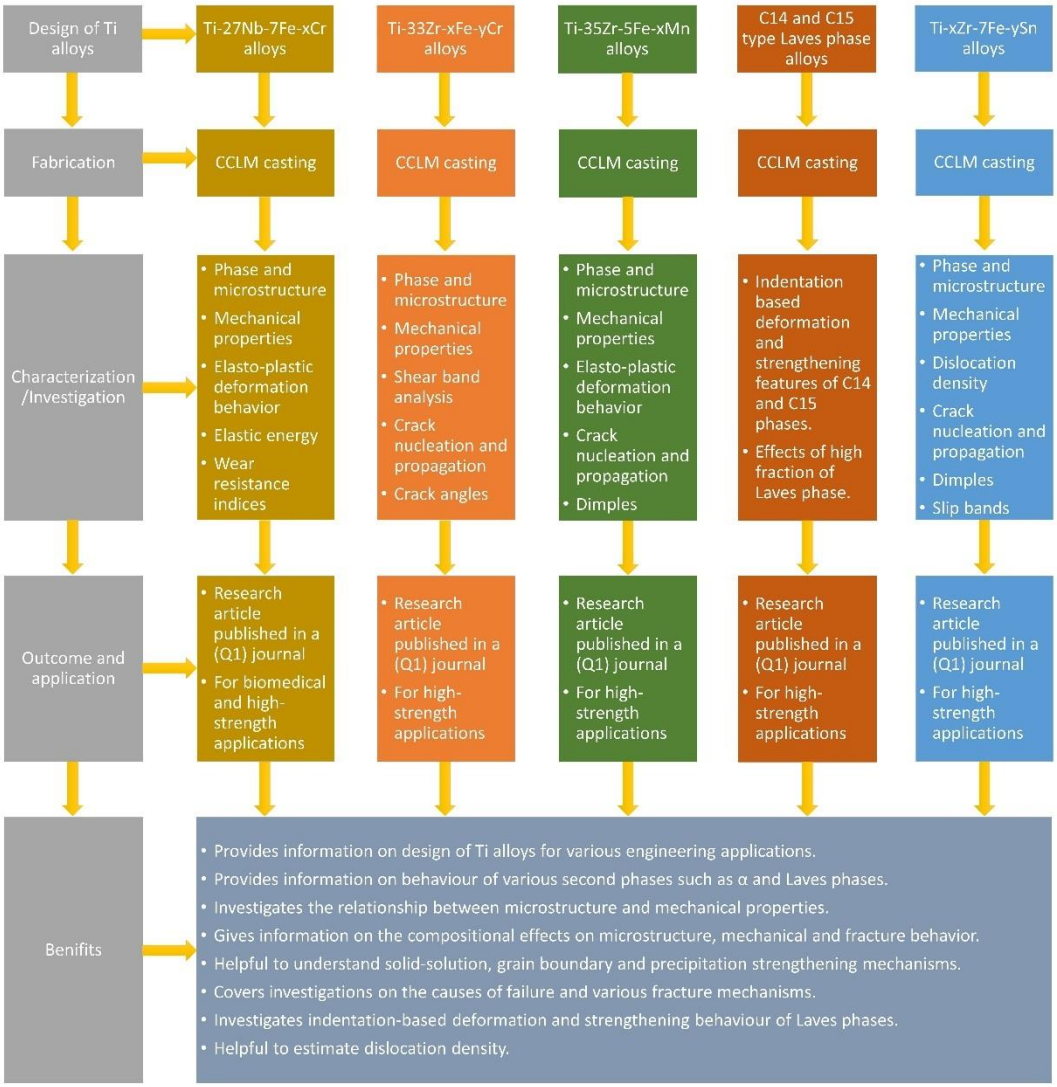


Fig. 3.1. The highlights of design, fabrication, characterizations, outcomes and benefits of the present work.

**Page deliberately left blank**

# Chapter 4. Materials and methods

This chapter provides information on the fabrication of the designed Ti-Nb-Fe-Cr, Ti-Zr-Fe-Cr, Ti-Zr-Fe-Mn and Ti-Zr-Fe-Sn alloys, methods used for phase, microstructure, mechanical and fracture analyses along with the sample preparation technique for each analysis.

## 4.1. Fabrication and sample preparation

The series of Ti-27Nb-7Fe-xCr (x = 0, 2, 4, 6, 8 wt%), Ti-33Zr-xFe-yCr (x = 3, 5, 7 wt% and y = 2, 4 wt%), Ti-35Zr-5Fe-xMn (x = 0, 2, 4, 6, 8 wt%) and Ti-xZr-7Fe-ySn (x = 25, 30, 35 wt% and y = 2, 4 wt%) alloys were cast from 99.9% pure alloying elements under an argon atmosphere using a cold crucible levitation melting (CCLM) furnace. The CCLM furnace is a kind of induction furnace which can effectively melt elements having high melting point temperatures to achieve homogeneous chemical composition of the produced alloy without contaminations after a strong stirring process provided by electromagnetic force. The alloy ingots of all the designed alloys were flipped and remelted at least four times to obtain homogeneous chemical compositions. After melting and proper mixing of molten raw metals, a rapid quenching was carried out in a water-cooled copper crucible for all the designed alloys. The Ti-27Nb-7Fe-xCr alloys were produced in the form of cylindrical rods with approximately 8 mm in diameter. For the Ti-33Zr-xFe-yCr, Ti-35Zr-5Fe-xMn and Ti-xZr-7Fe-ySn alloys, the cylindrical rods with approximately 4.5 mm diameter were produced from their corresponding ingots using wire electrical discharge machining. Note that the cylindrical rods were taken out from the center of the ingots in order to avoid the rapid cooling effect at outer regions of the ingots in the Ti-33Zr-xFe-yCr, Ti-35Zr-5Fe-xMn and Ti-xZr-7Fe-ySn alloys.

The cylindrical rods of all the designed alloys were cut using a Buehler Isomet 1000 low-speed precision saw in order to evaluate their microstructure and mechanical behavior. For microstructural analyses, the samples were ground using silicon carbide papers up to 4000 grits and then polished using a Struers MD-Chem polishing cloth with a suspension liquid of Struers OP-S colloidal silica. For all the designed alloys, all the grinding and polishing operations were performed using standard metallographic procedures. The samples of the Ti-27Nb-7Fe-xCr alloys were etched after polishing using Kroll's reagent (30 vol.% nitric acid, 5 vol.% hydrofluoric acid and 65 vol.% water) for the microstructure analyses.

### 4.2. Phase and microstructure analyses

X-ray diffraction (XRD) tests were carried out for the phase analyses using a PANalytical EMPYREAN diffractometer, operated at 40 kV and 40 mA with Co Kα source (λ = 0.1789 nm). The XRD profiles for all the designed alloys were obtained in a 2θ range from 30° to 110°. The XRD tests for the Ti-27Nb-7Fe-xCr and Ti-33Zr-xFe-yCr alloys were performed at a scan speed of 0.011°/s with a step size of 0.013°, whereas the XRD tests for the Ti-35Zr-5Fe-xMn and Ti-xZr-7Fe-ySn alloys were performed at a scan speed of 0.016°/s with a step size of 0.013° and a scan speed of 0.011°/s with a step size of 0.003° respectively. The size of the slits used in the XRD tests was selected (based on sample diameter and minimum scan angle) in such a manner that the area of the XRD beam spot remained smaller than the surface area of the sample and therefore, the XRD beam spot did not spill out of the surface area of the sample during XRD tests. The XRD peaks were matched with JCPDS powder diffraction files for the phase and structural parameters.

The lattice parameters ($a$) corresponding to the β phase peaks were calculated using equation (4.1) [144]:

$$\alpha = \frac{\lambda\sqrt{h^2+k^2+l^2}}{2\ sin\ \theta} \tag{4.1}$$

where $\lambda$ is the X-ray wavelength, (h, k, l) are the miller indices of the diffraction planes and $\theta$ is the Bragg angle. To obtain the precise $a$ of the β phase, the calculated $a$ values corresponding to the β phase peaks were first plotted against the Nelson-Riley function $((\cos^2\theta/\sin\theta) + (\cos^2\theta/\theta))$ [5, 144]. The trendline obtained from the plotted values of $a$ was then extrapolated to find the value of the $a$ at $\theta=90^\circ$ [144] and then the $a$ value obtained after extrapolation (at $\theta=90^\circ$) was considered to be the respective $a$ of the alloy.

Scanning electron microscopy (SEM) was carried out using a FEI Verios XHR 460 for the microstructure analyses. Energy dispersive X-ray spectroscopy (EDX) quantitative point analyses and EDX elemental mapping were performed using an Oxford Instruments X-Max SDD detector which is equipped with a FEI Verios XHR 460. From the SEM images, the $V_f$ of the constituent phases present in all the designed alloys were estimated using ImageJ software. For the Ti-35Zr-5Fe-xMn alloys, the $V_f$ of the phases present in the alloys were also estimated using integrated areas of the diffraction peaks corresponding to the phases present [23, 36]. The integrated areas of the diffraction peaks were obtained using a peak fitting program of Origin software with a Pearson

VII function [145]. The $V_f$ of the β ($V_{f,\,\beta}$) and C14 ($V_{f,\,C14}$) phases from the integrated areas of the diffraction peaks were estimated using equations (4.2) and (4.3) respectively [23, 36, 45].

$$V_{f,\ \beta} = \frac{A_\beta}{A_{C14}+A_\beta} \tag{4.2}$$

$$V_{f,\ C14} = \frac{A_{C14}}{A_{C14}+A_\beta} \tag{4.3}$$

where $V_{f,\ \beta}$ and $V_{f,\ C14}$ are the volume fractions and $A_\beta$ and $A_{C14}$ are the total integrated areas (including all the peaks), corresponding to β and C14 phases respectively.

For Ti-35Zr-5Fe-6Mn (wt%) and Ti-33Zr-7Fe-4Cr (wt%), transmission electron microscopy (TEM), selected area electron diffraction (SAED) and EDX were performed using a JEOL JEM-2100 microscope. Specimens for TEM were prepared from the 3 mm discs by electropolishing in a mixture of ethanol and perchloric acid with a respective proportion of 9:1 by volume at a temperature of -30 °C with an electrode voltage of 30–90 V [146].

The XRD line profile analyses were carried out to estimate dislocation density of the β phase after compression testing using equation (4.4) which was derived based on the Williamson-Smallman method [147-149].

$$\rho_d = \frac{2\sqrt{3}\,\xi}{Db} \tag{4.4}$$

where $\rho_d$ is dislocation density, $\xi$ is lattice strain, $D$ is crystallite size and $b$ is burgers vector, $b = (a/2)\sqrt{h^2+k^2+l^2}$ for bcc and fcc crystal structures (where $a$ is lattice parameter and $h$, $k$ and $l$ are miller indices) [3]. The values of lattice strain and crystallite size were estimated using equation (4.5) suggested by Williamson and Hall [150-153] based on the broadening of XRD peaks.

$$B_{St} \cdot cos\theta = \frac{k\lambda}{D} + 2\xi \cdot sin\theta \tag{4.5}$$

where $B_{St}$ is broadening of XRD peaks that has occurred due to lattice strain and crystallite size, $\theta$ is diffraction angle of a peak, $k$ is constant (~ 1), $D$ is crystallite size and $\xi$ is lattice strain. The broadening of peaks can usually be measured in terms of a full-width half maximum, FWHM, which is a width of a peak (in radians) at the half of the maximum intensity of a peak. However,

the total broadening of XRD peaks usually occurs due to crystallite size, lattice strain as well as due to the instrument used in a XRD test according to equation (4.6) [151, 152].

$$B_O = B_{St} + B_I \tag{4.6}$$

where $B_O$ is the observed/total broadening of peaks, $B_{St}$ is the broadening of peaks that occurs due to lattice strain and crystallite size and $B_I$ is the broadening of peaks that occurs due to the instrument used. This means that $B_I$ should be subtracted from $B_O$ in order to obtain the value of $B_{St}$. The value of $B_I$ can be obtained from the observed peak broadening that occurs in a standard $LaB_6$ sample provided by the manufacturer of the diffractometer. The values of $B_{St}$ in the present work were obtained directly from Highscore software provided by the manufacturer of the diffractometer, which gives the values of $B_{St}$ after subtracting$B_I$. According to the Williamson-Hall plot [150-152], the values of $B_{St} \cdot cos\theta$ were plotted against the values of $2sin\theta$ for the peaks associated with the β phase. The crystallite size was then estimated using the value of y-intercept and the lattice strain was estimated from the slope of the Williamson-Hall plot [151, 152]. The dislocation densities in the β phase for each alloy (after compression testing) were estimated considering the burgers vector, $b$ = ($a$/2) <111> [154].

## 4.3. Mechanical characterization

### 4.3.1. Compression testing

For all the designed alloys, compression tests were performed at ambient temperature on at least three cylindrical samples at a crosshead speed of 0.1 mm/min using an Instron 5982 universal testing machine. The cylindrical samples with 8 mm in diameter and 15 mm length were used in compression testing of the Ti-27Nb-7Fe-xCr alloys, whereas the cylindrical samples with 4.5 mm in diameter and 8 mm length were used in compression testing of the Ti-33Zr-xFe-yCr, Ti-35Zr-5Fe-xMn and Ti-xZr-7Fe-ySn alloys. Prior to compression tests, both end faces of each cylindrical sample were ground such that these faces became flat, perpendicular to the loading direction as well as parallel to each other. For all the designed alloys, the values of 0.2% compressive yield strength, plastic strain and ultimate compressive strength were calculated from the engineering stress-strain curve and the average values of properties were considered. A clip-on extensometer was used to obtain elastic modulus of the Ti-27Nb-7Fe-xCr alloys.

### 4.3.2. Hardness testing

For the Ti-27Nb-7Fe-xCr, Ti-35Zr-5Fe-xMn and Ti-xZr-7Fe-ySn alloys, Vickers micro-hardness testing was carried out on a polished specimen of each alloy using a Zwick Roell ZHU micro-hardness testing machine at a load of 5 kgf and at a dwell time of 30 s. At least eight measurements of micro-hardness were taken for each alloy and then the average value of hardness was considered for each alloy. Optical microscopy (OM) was performed using a Zeiss Axiocam to analyze the elasto-plastic deformation mechanisms around the micro-hardness indentations of the Ti-27Nb-7Fe-xCr and Ti-35Zr-5Fe-xMn alloys. Moreover, the bonding-interface technique was used to study the subsurface deformation features of the Ti-35Zr-5Fe-6Mn (wt%), Ti-35Zr-5Fe-8Mn (wt%) and Ti-33Zr-7Fe-4Cr (wt%) [155, 156].

To obtain elastic modulus and hardness of the Ti-33Zr-xFe-yCr alloys, nanoindentation tests were carried out on a polished sample (approximately 4.5 mm in diameter and 1.2 mm long) using a Hysitron TI-950 TriboIndenter with a Berkovich indenter. A total of 10 indentations were taken at random places covering maximum surface area of the samples with a maximum force of 10 mN.

### 4.3.3. Fracture analyses

For the Ti-33Zr-xFe-yCr, Ti-35Zr-5Fe-xMn and Ti-xZr-7Fe-ySn alloys, the Fracture analyses were carried out on the samples after compression testing using a FEI Verios XHR 460 scanning electron microscope in order to obtain the information about fracture, deformation and shear band patterns. To examine the shear band patterns and crack propagation, a sample after compression testing of each investigated alloy was cut first into two halves, where one of these two halves was polished. Furthermore, a sample after compression testing was carefully cleaned to analyze the fractured morphologies on the outer surfaces and/or to obtain the information on dimples.

**Page deliberately left blank**

Chapters 5 to 9 are not included in this version of the thesis.

These Chapters have been published, and are listed on the ECU Repository.

**Page deliberately left blank**

# Chapter 10. Summary and future work

This chapter summarizes the concluding remarks of the present research as well as provides recommendations for the future work.

## 10.1. Summary

In the present work, the Ti-27Nb-7Fe-xCr alloys have been designed for surgical implant applications considering the performance and cost parameters, whereas the Ti-33Zr-xFe-yCr, Ti-35Zr-5Fe-xMn and Ti-xZr-7Fe-ySn alloys have been designed for high-strength applications. Inexpensive β stabilizing elements such as Fe, Cr and Mn have been used in the investigated alloys to further improve the performance of the designed alloys. Following are the concluding remarks of the present work.

1) In the Ti-27Nb-7Fe-xCr alloys, the alloying of Cr renders a dual phase microstructure composed of a dominant β and a small amount of orthorhombic α" formed in the Ti-27Nb-7Fe alloy to a single β phase microstructure formed in the alloys containing Cr. None of the investigated alloys fail until the load reaches to 100 kN and all demonstrate impressive maximum compressive strength (~2 GPa) as well as plastic strain (> 26%). Among the Ti-27Nb-7Fe-xCr alloys, the highest plastic strain (40.3%) is found in Ti-27Nb-7Fe, whereas the lowest Young's modulus (72 GPa) is achieved in Ti-27Nb-7Fe-8Cr. The Ti-27Nb-7Fe-xCr alloys with a single β phase show a greater number of slip bands in the morphologies around the Vickers indentation than the Ti-27Nb-7Fe alloy with a dual phase microstructure.
2) In the Ti-33Zr-xFe-yCr alloys, Ti-33Zr-3Fe-2Cr retains a complete β phase in the microstructure, whereas the rest of the investigated Ti-33Zr-xFe-yCr alloys show dual phase microstructures including C15 type Laves and β phases. Moreover, a C14 type Laves and β phases feature in the microstructures of all the Ti-35Zr-5Fe-xMn alloys. The volume fraction of C15 and C14 type Laves phases increase as the quantities of Fe and Cr increase in the Ti-33Zr-xFe-yCr alloys and the quantities of Mn increase in the Ti-35Zr-5Fe-xMn alloys respectively. The mechanical properties are influenced by the volume fraction of the corresponding Laves phase present in the Ti-33Zr-xFe-yCr and Ti-35Zr-5Fe-xMn alloys.

The increase in the corresponding quantities of Fe, Cr and Mn in the Ti-33Zr-xFe-yCr and Ti-35Zr-5Fe-xMn alloys produce solid solution and precipitation strengthening.

3) It can be deduced that hcp C14 and fcc C15 type Laves phases produce strong strengthening effects in the β titanium matrix. Hence, the deformation and strength characteristics of C14 (hcp) and C15 (fcc) type Laves phases have been investigated using an indentation method in the Ti-35Zr-5Fe-6Mn and Ti-33Zr-7Fe-4Cr alloys respectively. It has been found that the C15 type Laves phase deforms better than the C14 type Laves phase and therefore, the C15 type Laves phase contributes in enhancing bulk plasticity of an alloy. Further, an alloy with relatively high-volume fraction of Laves phase shows a smaller indentation-based deformation zone than an alloy with relatively low-volume fraction of Laves phase.
4) The quantities of Zr and Sn have been varied in the Ti-xZr-7Fe-ySn alloys in order to obtain an improved trade-off between strength and plasticity by controlling the volume fraction of a C14 type Laves phase in the β matrix. The values of dislocation density increase as the volume fraction of C14 phase increases, which indicates the strong dislocation pinning ability of C14 type Laves phase. The volume fraction of Laves phase significantly influence the mechanical properties of the Ti-xZr-7Fe-ySn alloys, which is useful in achieving a wide range of strength and plasticity values.
5) Fracture analyses reveal the hard nature of corresponding Laves phases present in the Ti-33Zr-xFe-yCr, Ti-35Zr-5Fe-xMn and Ti-xZr-7Fe-ySn alloys compared to soft β phase as the alloys comprising Laves phase fail in an intergranular mode. It has also been noticed that the microstructure, mechanical and fracture properties correlate with one another.
6) The Ti-33Zr-xFe-yCr, Ti-35Zr-5Fe-xMn and Ti-xZr-7Fe-ySn alloys exhibit yield strength from 1048 to 1580 MPa, ultimate compressive strength from 1498 to 2140 MPa and plastic strain from 2.6 to 33.6%. Interestingly, the β matrix is useful to enhance the bulk plasticity of the Laves phase alloys.
7) Finally, based on the results obtained in the present work, it can be inferred that Ti-27Nb-7Fe-8Cr possesses a better blend of required properties for biomedical applications, whereas the Ti-33Zr-7Fe-4Cr, Ti-35Zr-5Fe-8Mn and Ti-35Zr-7Fe-2Sn alloys possess a better blend of strength characteristics for high-strength structural applications.

## 10.2. Recommendations for the future work

This thesis answers all the research questions presented in this work. However, further investigations are still required to examine other necessary properties of the investigated alloys and/or to further improve the properties of the investigated alloys. The following are recommendations for the future work on the designed alloys.

1) Investigating the corrosion resistance and wear resistance properties of all the studied alloys. The corrosion resistance properties of the Ti-27Nb-7Fe-xCr alloys (in the simulated body fluid) are useful in biomedical applications, whereas the corrosion properties of the Ti-33Zr-7Fe-4Cr, Ti-35Zr-5Fe-8Mn and Ti-35Zr-7Fe-2Sn alloys (in the sea water) are useful in aerospace, automobile and chemical industries. Further, the wear resistance properties are useful for biomedical and high-strength structural applications because poor wear resistance leads to failure of the alloys.
2) Investigating the fatigue properties of all the studied alloys. The fatigue properties of all the studied alloys are useful in studying the behavior of these alloys during the cyclic/fluctuating loading conditions depending on the end application of an alloy.
3) Investigating the tensile properties of all the studied alloys is useful for all engineering and biomedical applications as the tensile properties are considered more reliable than the compressive properties.
4) Investigating the fracture toughness properties of all the studied alloys, which are useful for biomedical as well as high-strength structural applications.
5) Producing the studied alloys using selective laser melting and spark plasma sintering to further improve their mechanical behavior.
6) Processing of the studied alloys using heat treatment and work hardening techniques such as hot rolling, cold rolling, annealing and forging to further improve their mechanical behavior.

**Page deliberately left blank**

# Bibliography


[1] M. Geetha, A.K. Singh, R. Asokamani, A.K. Gogia, Ti based biomaterials, the ultimate choice for orthopaedic implants – A review, *Prog. Mater. Sci.* 54 (**2009**) 397-425.

[2] L.C. Zhang, D. Klemm, J. Eckert, Y.L. Hao, T.B. Sercombe, Manufacture by selective laser melting and mechanical behavior of a biomedical Ti–24Nb–4Zr–8Sn alloy, *Scr. Mater.* 65 (**2011**) 21-24.

[3] W.D. Callister, Fundamentals of materials science and engineering, John Wiley & Sons. Inc., New York, **2000**.

[4] L.C. Zhang, Y. Liu, S. Li, Y. Hao, Additive Manufacturing of Titanium Alloys by Electron Beam Melting: A Review, *Adv. Eng. Mater.* 20 (**2018**) 1700842.

[5] C.D. Rabadia, Y.J. Liu, L. Wang, H. Sun, L.C. Zhang, Laves phase precipitation in Ti-Zr-Fe-Cr alloys with high strength and large plasticity, *Mater. Des.* 154 (**2018**) 228-238.

[6] P. Qin, Y. Liu, T.B. Sercombe, Y. Li, C. Zhang, C. Cao, H. Sun, L.C. Zhang, Improved Corrosion Resistance on Selective Laser Melting Produced Ti-5Cu Alloy after Heat Treatment, *ACS Biomater. Sci. Eng.* 4 (**2018**) 2633-2642.

[7] C.D. Rabadia, Y.J. Liu, G.H. Cao, Y.H. Li, C.W. Zhang, T.B. Sercombe, H. Sun, L.C. Zhang, High-strength β stabilized Ti-Nb-Fe-Cr alloys with large plasticity, *Mater. Sci. Eng. A* 732 (**2018**) 368-377.

[8] Y. Liu, S. Li, H. Wang, W. Hou, Y. Hao, R. Yang, T. Sercombe, L.C. Zhang, Microstructure, defects and mechanical behavior of beta-type titanium porous structures manufactured by electron beam melting and selective laser melting, *Acta Mater.* 113 (**2016**) 56-67.

[9] A. Biesiekierski, J. Wang, M.A. Gepreel, C. Wen, A new look at biomedical Ti-based shape memory alloys, *Acta Biomater.* 8 (**2012**) 1661-1669.

[10] S.F. Jawed, C.D. Rabadia, Y.J. Liu, L.Q. Wang, Y.H. Li, X.H. Zhang, L.C. Zhang, Mechanical characterization and deformation behavior of β-stabilized Ti-Nb-Sn-Cr alloys, *J. Alloys Compd.* 792 (**2019**) 684-693.

[11] C.D. Rabadia, Y.J. Liu, S.F. Jawed, L. Wang, Y.H. Li, X.H. Zhang, T.B. Sercombe, H. Sun, L.C. Zhang, Improved deformation behavior in Ti-Zr-Fe-Mn alloys comprising the C14 type Laves and β phases, *Mater. Des.* 160 (**2018**) 1059-1070.

[12] J. Nei, K. Young, S.O. Salley, K.Y.S. Ng, Determination of C14/C15 phase abundance in Laves phase alloys, *Mater. Chem. Phys.* 136 (**2012**) 520-527.

[13] F. Stein, G. Sauthoff, M. Palm, Experimental determination of intermetallic phases, phase equilibria, and invariant reaction temperatures in the Fe-Zr system, *J. Phase Equilibria* 23 (**2002**) 480.

[14] M. Peters, J. Hemptenmacher, J. Kumpfert, C. Leyens, Structure and Properties of Titanium and Titanium Alloys, in: C. Leyens, M. Peters (Eds.), Titanium and Titanium Alloys: Fundamentals and Applications, Wiley-VCH, Weinheim, **2003**, pp. 1-36.

[15] M. Balazic, J. Kopac, M.J. Jackson, W. Ahmed, Review: Titanium and titanium alloy applications in medicine, *Int. J. Nano and Biomater.* 1 (**2007**) 3-34.

[16] L. Zhang, J. Das, H. Lu, C. Duhamel, M. Calin, J. Eckert, High strength Ti–Fe–Sn ultrafine composites with large plasticity, *Scr. Mater.* 57 (**2007**) 101-104.

[17] L.C. Zhang, L.Y. Chen, A Review on Biomedical Titanium Alloys: Recent Progress and Prospect, *Adv. Eng. Mater.* 21 (**2019**) 1801215.

[18] S. Ehtemam-Haghighi, H.B. Lu, G.Y. Jian, G.H. Cao, D. Habibi, L.C. Zhang, Effect of α″ martensite on the microstructure and mechanical properties of beta-type Ti–Fe–Ta alloys, *Mater. Des.* 76 (**2015**) 47-54.
[19] F. Guillemot, F. Prima, R. Bareille, D. Gordin, T. Gloriant, M.C. Porte-Durrieu, D. Ansel, C. Baquey, Design of new titanium alloys for orthopaedic applications, *Med. Biol. Eng. Comput.* 42 (**2004**) 137-141.
[20] E.W. Collings, The physical metallurgy of titanium alloys, American Society for Metals, Metals Park, Ohio, **1984**.
[21] G. Lütjering, J. Williams, A. Gysler, Microstructure and mechanical properties of titanium alloys, in: J.C.M. Li (Ed.), Microstructure and Properties of Materials: (Volume 2), World Scientific, Singapore, **2000**, pp. 1-77.
[22] M. Balazic, J. Kopac, M.J. Jackson, W. Ahmed, Titanium and titanium alloy applications in medicine, *Int. J. Nano and Biomater.* 1 (**2007**) 3-34.
[23] S. Ehtemam-Haghighi, K.G. Prashanth, H. Attar, A.K. Chaubey, G.H. Cao, L.C. Zhang, Evaluation of mechanical and wear properties of TixNb7Fe alloys designed for biomedical applications, *Mater. Des.* 111 (**2016**) 592-599.
[24] S. Ehtemam-Haghighi, Y. Liu, G. Cao, L.C. Zhang, Influence of Nb on the β→ α ″ martensitic phase transformation and properties of the newly designed Ti-Fe-Nb alloys, *Mater. Sci. Eng. C* 60 (**2016**) 503-510.
[25] L. Zhang, H.-B. Lu, C. Mickel, J. Eckert, Ductile ultrafine-grained Ti-based alloys with high yield strength, *Appl. Phys. Lett.* 91 (**2007**) 051906.
[26] C.D. Rabadia, Y.J. Liu, L.Y. Chen, S.F. Jawed, L.Q. Wang, H. Sun, L.C. Zhang, Deformation and strength characteristics of Laves phases in titanium alloys, *Mater. Des.* 179 (**2019**) 107891.
[27] D. Hull, D.J. Bacon, Introduction to Dislocations, fifth ed., Butterworth-Heinemann, Oxford, **2011**.
[28] F.C. Campbell, Elements of metallurgy and engineering alloys, ASM International, Ohio, **2008**.
[29] K. Wang, The use of titanium for medical applications in the USA, *Mater. Sci. Eng. A* 213 (**1996**) 134-137.
[30] M. Niinomi, Mechanical properties of biomedical titanium alloys, *Mater. Sci. Eng. A* 243 (**1998**) 231-236.
[31] Q. Chen, G.A. Thouas, Metallic implant biomaterials, *Mater. Sci. Eng. R* 87 (**2015**) 1-57.
[32] G. Lütjering, J.C. Williams, Titanium, Springer Science & Business Media, Berlin, **2007**.
[33] J.R. Davis, Handbook of materials for medical devices, ASM International, Metals Park, Ohio, **2003**.
[34] M. Niinomi, Metals for biomedical devices, Woodhead publishing, UK, **2019**.
[35] R. Narayan, Biomedical materials, Springer Science & Business Media, Berlin, **2009**.
[36] S. Ehtemam-Haghighi, Y. Liu, G. Cao, L.C. Zhang, Phase transition, microstructural evolution and mechanical properties of Ti-Nb-Fe alloys induced by Fe addition, *Mater. Des.* 97 (**2016**) 279-286.
[37] Y. Liu, S. Li, W. Hou, S. Wang, Y. Hao, R. Yang, T.B. Sercombe, L.-C. Zhang, Electron Beam Melted Beta-type Ti–24Nb–4Zr–8Sn Porous Structures With High Strength-to-Modulus Ratio, *J. Mater. Sci. Technol.* 32 (**2016**) 505-508.

[38] Y.J. Liu, H.L. Wang, S.J. Li, S.G. Wang, W.J. Wang, W.T. Hou, Y.L. Hao, R. Yang, L.C. Zhang, Compressive and fatigue behavior of beta-type titanium porous structures fabricated by electron beam melting, *Acta Mater.* 126 (**2017**) 58-66.
[39] P. Qin, Y. Chen, Y.-J. Liu, J. Zhang, L.-Y. Chen, Y. Li, X. Zhang, C. Cao, H. Sun, L.-C. Zhang, Resemblance in Corrosion Behavior of Selective Laser Melted and Traditional Monolithic β Ti-24Nb-4Zr-8Sn Alloy, *ACS Biomater. Sci. Eng.* 5 (**2019**) 1141-1149.
[40] S. Banerjee, P. Mukhopadhyay, Phase transformations: examples from titanium and zirconium alloys, Elsevier, Oxford, **2010**.
[41] G. Welsch, R. Boyer, E. Collings, Materials properties handbook: titanium alloys, ASM international, Metals Park, Ohio, **1994**.
[42] Y.L. Zhou, M. Niinomi, T. Akahori, Effects of Ta content on Young's modulus and tensile properties of binary Ti–Ta alloys for biomedical applications, *Mater. Sci. Eng. A* 371 (**2004**) 283-290.
[43] Y. Zhu, X. Wang, L. Wang, Y. Fu, J. Qin, W. Lu, D. Zhang, Influence of forging deformation and heat treatment on microstructure of Ti–xNb–3Zr–2Ta alloys, *Mater. Sci. Eng. C* 32 (**2012**) 126-132.
[44] L.C. Zhang, High performance ultrafine-grained Ti-Fe-based alloys with multiple length-scale phases, *Adv. Mater. Res.* 1 (**2012**) 13-29.
[45] S. Ehtemam-Haghighi, G. Cao, L.C. Zhang, Nanoindentation study of mechanical properties of Ti based alloys with Fe and Ta additions, *J. Alloys Compd.* 692 (**2017**) 892-897.
[46] Y.B. Wang, Y.F. Zheng, The microstructure and shape memory effect of Ti–16 at.%Nb alloy, *Mater. Lett.* 62 (**2008**) 269-272.
[47] A. Ramarolahy, P. Castany, F. Prima, P. Laheurte, I. Péron, T. Gloriant, Microstructure and mechanical behavior of superelastic Ti–24Nb–0.5O and Ti–24Nb–0.5N biomedical alloys, *J. Mech. Behav. Biomed.* 9 (**2012**) 83-90.
[48] Y. Bai, Y. Deng, Y. Zheng, Y. Li, R. Zhang, Y. Lv, Q. Zhao, S. Wei, Characterization, corrosion behavior, cellular response and in vivo bone tissue compatibility of titanium–niobium alloy with low Young's modulus, *Mater. Sci. Eng. C* 59 (**2016**) 565-576.
[49] Y.-H. Hon, J.-Y. Wang, Y.-N. Pan, Composition/phase structure and properties of titanium-niobium alloys, *Mater. Trans.* 44 (**2003**) 2384-2390.
[50] W.-F. Ho, A comparison of tensile properties and corrosion behavior of cast Ti–7.5Mo with CP-Ti, Ti–15Mo and Ti–6Al–4V alloys, *J. Alloys Compd.* 464 (**2008**) 580-583.
[51] Y.-L. Zhou, D.-M. Luo, Microstructures and mechanical properties of Ti–Mo alloys cold-rolled and heat treated, *Mater. Charact.* 62 (**2011**) 931-937.
[52] Y.L. Zhou, M. Niinomi, T. Akahori, Decomposition of martensite α″ during aging treatments and resulting mechanical properties of Ti−Ta alloys, *Mater. Sci. Eng. A* 384 (**2004**) 92-101.
[53] H. Matsumoto, S. Watanabe, S. Hanada, Beta TiNbSn alloys with low Young's modulus and high strength, *Mater. Trans.* 46 (**2005**) 1070-1078.
[54] S. Hanada, N. Masahashi, T.K. Jung, Effect of stress-induced α″ martensite on Young's modulus of β Ti–33.6Nb–4Sn alloy, *Mater. Sci. Eng. A* 588 (**2013**) 403-410.
[55] S. Guo, Q. Meng, X. Zhao, Q. Wei, H. Xu, Design and fabrication of a metastable β-type titanium alloy with ultralow elastic modulus and high strength, *Sci. Rep.* 5 (**2015**) 14688.
[56] A.H. Hussein, M.A.H. Gepreel, M.K. Gouda, A.M. Hefnawy, S.H. Kandil, Biocompatibility of new Ti–Nb–Ta base alloys, *Mater. Sci. Eng. C* 61 (**2016**) 574-578.

[57] E. Bertrand, T. Gloriant, D.M. Gordin, E. Vasilescu, P. Drob, C. Vasilescu, S.I. Drob, Synthesis and characterisation of a new superelastic Ti–25Ta–25Nb biomedical alloy, *J. Mech. Behav. Biomed.* 3 (**2010**) 559-564.
[58] J. Málek, F. Hnilica, J. Veselý, B. Smola, S. Bartáková, J. Vaněk, Microstructure and mechanical properties of Ti-35Nb-6Ta alloy after thermomechanical treatment, *Mater. Charact.* 66 (**2012**) 75-82.
[59] C.A.R.P. Baptista, S.G. Schneider, E.B. Taddei, H.M. da Silva, Fatigue behavior of arc melted Ti–13Nb–13Zr alloy, *Int. J. Fatigue* 26 (**2004**) 967-973.
[60] C. Ning, D. Ding, K. Dai, W. Zhai, L. Chen, The effect of Zr content on the microstructure, mechanical properties and cell attachment of Ti–35Nb–xZr alloys, *Biomed. Mater.* 5 (**2010**) 045006.
[61] J. Zhang, F. Sun, Y. Hao, N. Gozdecki, E. Lebrun, P. Vermaut, R. Portier, T. Gloriant, P. Laheurte, F. Prima, Influence of equiatomic Zr/Nb substitution on superelastic behavior of Ti–Nb–Zr alloy, *Mater. Sci. Eng. A* 563 (**2013**) 78-85.
[62] M. Besse, P. Castany, T. Gloriant, Mechanisms of deformation in gum metal TNTZ-O and TNTZ titanium alloys: A comparative study on the oxygen influence, *Acta Mater.* 59 (**2011**) 5982-5988.
[63] T. Furuta, S. Kuramoto, J. Hwang, K. Nishino, T. Saito, M. Niinomi, Mechanical properties and phase stability of Ti-Nb-Ta-Zr-O alloys, *Mater. Trans.* 48 (**2007**) 1124-1130.
[64] S. Bose, A. Bandyopadhyay, Characterization of Biomaterials, first ed., Academic Press, Oxford, **2013**.
[65] R. Yang, Y. Hao, S. Li, Development and Application of Low-Modulus Biomedical Titanium Alloy Ti2448, , in: A.N. Laskovski (Ed.), Biomedical Engineering, Trends in Materials Science, InTech, London, **2011**.
[66] WHO, Global status report on road safety 2015, World Health Organization, Geneva, **2015**.
[67] M. Abdel-Hady Gepreel, M. Niinomi, Biocompatibility of Ti-alloys for long-term implantation, *J. Mech. Behav. Biomed.* 20 (**2013**) 407-415.
[68] W. Weng, A. Biesiekierski, Y. Li, C. Wen, Effects of selected metallic and interstitial elements on the microstructure and mechanical properties of beta titanium alloys for orthopedic applications, *Materialia* 6 (**2019**) 100323.
[69] C.P. Delaunay, Metal-on-metal bearings in cementless primary total hip arthroplasty, *J. Arthroplasty* 19 (**2004**) 35-40.
[70] S. Kurtz, K. Ong, E. Lau, F. Mowat, M. Halpern, Projections of primary and revision hip and knee arthroplasty in the United States from 2005 to 2030, *J. Bone Jt. Surg.* 89 (**2007**) 780-5.
[71] Degenerative Nerve Diseases, 2017. https://medlineplus.gov/degenerativenervediseases.html.
[72] The Hip and Knee Handbook, 2017. http://hipandkneehandbook.com/images-of-mechanical-joint-implants.
[73] G. Manivasagam, D. Dhinasekaran, A. Rajamanickam, Biomedical Implants: Corrosion and its Prevention - A Review, *Recent Pat. Corros. Sci* 2 40-54.
[74] P. Laheurte, F. Prima, A. Eberhardt, T. Gloriant, M. Wary, E. Patoor, Mechanical properties of low modulus beta titanium alloys designed from the electronic approach, *J. Mech. Behav. Biomed.* 3 (**2010**) 565-573.
[75] Y. Li, C. Yang, H. Zhao, S. Qu, X. Li, Y. Li, New Developments of Ti-Based Alloys for Biomedical Applications, *Mater.* 7 (**2014**) 1709-1800.

[76] J. Black, Biological Performance of Materials: Fundamentals of Biocompatibility, 4 ed., CRC Publisher, Taylor and Fransis Group, New York, **2005**.
[77] H. Hermawan, D. Ramdan, J.R. Djuansjah, Metals for Biomedical Applications, Biomedical Engineering - From Theory to Applications, InTech, London, **2011**.
[78] D. Kuroda, M. Niinomi, M. Morinaga, Y. Kato, T. Yashiro, Design and mechanical properties of new beta type titanium alloys for implant materials, *Mater. Sci. Eng. A* 243 (**1998**) 244-249.
[79] M. Calin, A. Gebert, A.C. Ghinea, P.F. Gostin, S. Abdi, C. Mickel, J. Eckert, Designing biocompatible Ti-based metallic glasses for implant applications, *Mater. Sci. Eng. C* 33 (**2013**) 875-883.
[80] J. Currey, Cortical bone, Handbook of Biomaterial Properties, Springer US, Boston, **1998**, pp. 3-14.
[81] Y. Hao, S. Li, S. Sun, C. Zheng, Q. Hu, R. Yang, Super-elastic titanium alloy with unstable plastic deformation, *Appl. Phys. Lett.* 87 (**2005**) 091906.
[82] M. Niinomi, M. Nakai, J. Hieda, Development of new metallic alloys for biomedical applications, *Acta Biomater.* 8 (**2012**) 3888-3903.
[83] S. Affatato, Wear of orthopaedic implants and artificial joints, Elsevier, Cambridge, **2012**.
[84] N.J. Hallab, S. Anderson, T. Stafford, T. Glant, J.J. Jacobs, Lymphocyte responses in patients with total hip arthroplasty, *J. Orthop. Res.* 23 (**2005**) 384-391.
[85] P.I. Branemark, R. Adell, T. Albrektsson, U. Lekholm, S. Lundkvist, B. Rockler, Osseointegrated Titanium Fixtures in the Treatment of Edentulousness, *Biomater.* 4 (**1983**) 25-28.
[86] M. Viceconti, R. Muccini, M. Bernakiewicz, M. Baleani, L. Cristofolini, Large-sliding contact elements accurately predict levels of bone–implant micromotion relevant to osseointegration, *J. Biomech.* 33 (**2000**) 1611-1618.
[87] Y. Okazaki, E. Gotoh, Comparison of metal release from various metallic biomaterials in vitro, *Biomater.* 26 (**2005**) 11-21.
[88] K.L. Wapner, Implications of metallic corrosion in total knee arthroplasty, *Clin. Orthop. Relat. Res.* (**1991**) 12-20.
[89] S.H. Teoh, Fatigue of biomaterials: a review, *Int. J. Fatigue* 22 (**2000**) 825-837.
[90] C.N. Elias, J.H.C. Lima, R. Valiev, M.A. Meyers, Biomedical applications of titanium and its alloys, *JOM* 60 (**2008**) 46-49.
[91] A. Nouri, Hodgson, Peter D. and Wen, Cui'e, Biomimetic porous titanium scaffolds for orthopaedic and dental applications, InTech, Croatia, **2010**.
[92] M.T. Mohammed, Z.A. Khan, A.N. Siddiquee, Titanium and its Alloys, the Imperative Materials for Biomedical Applications, International Conference on Recent Trends in Engineering & Technology, **2012**.
[93] ASTM, Mechanical and tribological properties and biocompatibility of diffusion hardened Ti–13Nb–13Zr – a new titanium alloy for surgical implants, ASTM STP 1272, Medical applications of titanium and its alloys, West Conshohocken, PA: ASTM International, **1996**, pp. 96-116.
[94] ASTM, Microstructure and properties of a new beta titanium alloy, Ti–12Mo–6Zr–2Fe, developed for surgical implants, ASTM STP 1272, Medical applications of titanium and its alloys, West Conshohocken, PA: ASTM International, **1996**, pp. 76-87.

[95] ASTM, Characterization of Ti–15Mo beta titanium alloy for orthopedic implant, ASTM STP 1272, Medical applications of titanium and its alloys, West Conshohocken, PA: ASTM International, **1996**, pp. 60-75.
[96] S.G. Steinemann, P.A. Mausli, S. Szmuklermoncler, M. Semlitsch, O. Pohler, H.E. Hintermann, S.M. Perren, Beta-Titanium Alloy for Surgical Implants, *Titanium '92: Science and Technology, Vols 1-3* (**1993**) 2689-2696.
[97] D. Kuroda, H. Kawasaki, S. Hiromoto, T. Hanawa, Development of new Ti-Fe-Ta and Ti-Fe-Ta-Zr system alloys for biomedical applications, *Mater. Trans.* 46 (**2005**) 1532-1539.
[98] M. Ikeda, M. Ueda, R. Matsunaga, M. Ogawa, M. Niinomi, Isothermal Aging Behavior of Beta Titanium-Manganese Alloys, *Mater. Trans.* 50 (**2009**) 2737-2743.
[99] E. Bertrand, T. Gloriant, D.M. Gordin, E. Vasilescu, P. Drob, C. Vasilescu, S.I. Drob, Synthesis and characterisation of a new superelastic Ti-25Ta-25Nb biomedical alloy, *J. Mech. Behav. Biomed.* 3 (**2010**) 559-564.
[100] D. Raabe, B. Sander, M. Friak, D. Ma, J. Neugebauer, Theory-guided bottom-up design of beta-titanium alloys as biomaterials based on first principles calculations: Theory and experiments, *Acta Mater.* 55 (**2007**) 4475-4487.
[101] K. Taneichi, M. Taira, E. Sukedai, T. Narushima, Y. Iguchi, C. Ouchi, Alloy design and property evaluation of new β type titanium alloy with excellent cold workability and biocompatibility, *ISIJ Int.* 46 (**2006**) 292-301.
[102] M. Morinaga, Y. Murata, H. Yukawa, Alloy Design Based on the DV-Xα Cluster Method, in: H. Adachi, T. Mukoyama, J. Kawai (Eds.), Hartree-Fock-Slater Method for Materials Science: The DV-Xα Method for Design and Characterization of Materials, Springer Berlin Heidelberg, Berlin, Heidelberg, **2006**, pp. 23-48.
[103] M. Morinaga, M. Kato, T. Kamimura, M. Fukumoto, I. Harada, K. Kubo, Theoretical Design of Beta-Type Titanium-Alloys, in: F. Froes, I. Caplan (Eds.) Titanium '92: Science and Technology, Minerals, Metals & Materials Soc, San Diego, CA, **1993**, pp. 217-224.
[104] C. Li, D.-G. Lee, X. Mi, W. Ye, S. Hui, Y. Lee, Phase transformation and age hardening behavior of new Ti–9.2Mo–2Fe alloy, *J. Alloys Compd.* 549 (**2013**) 152-157.
[105] M. Abdel-Hady, K. Hinoshita, M. Morinaga, General approach to phase stability and elastic properties of β-type Ti-alloys using electronic parameters, *Scr. Mater.* 55 (**2006**) 477-480.
[106] X.H. Min, S. Emura, L. Zhang, K. Tsuzaki, Effect of Fe and Zr additions on ω phase formation in β-type Ti–Mo alloys, *Mater. Sci. Eng. A* 497 (**2008**) 74-78.
[107] R. Boyer, G. Welsch, E.W. Collings, Materials Properties Handbook - Titanium Alloys, ASM International, Metals Park, Ohio, **1994**.
[108] R.P. Kolli, A. Devaraj, A Review of Metastable Beta Titanium Alloys, *Metals* 8 (**2018**) 506.
[109] C.A. Salvador, M.R. Dal Bo, F.H. Costa, M.O. Taipina, E.S. Lopes, R. Caram, Solute lean Ti-Nb-Fe alloys: An exploratory study, *J. Mech. Behav. Biomed.* 65 (**2016**) 761-769.
[110] S.F. Jawed, C.D. Rabadia, Y.J. Liu, L. Wang, Y.H. Li, X.H. Zhang, L.C. Zhang, Beta-type Ti-Nb-Zr-Cr alloys with large plasticity and significant strain hardening, *Mater. Des.* 181 (**2019**) 108064.
[111] A.P. Mouritz, Introduction to aerospace materials, Elsevier, Cambridge, **2012**.
[112] D.J. Thoma, J.H. Perepezko, A geometric analysis of solubility ranges in Laves phases, *J. Alloys Compd.* 224 (**1995**) 330-341.
[113] S. Banerjee, A. Kumar, P. Ruz, P. Sengupta, Influence of Laves phase on microstructure and hydrogen storage properties of Ti–Cr–V based alloy, *Int. J. Hydrogen Energy* 41 (**2016**) 18130-18140.

[114] F. Stein, M. Palm, G. Sauthoff, Structure and stability of Laves phases. Part I. Critical assessment of factors controlling Laves phase stability, *Intermetallics* 12 (**2004**) 713-720.
[115] F. Chu, D.J. Thoma, P.G. Kotula, S. Gerstl, T.E. Mitchell, I.M. Anderson, J. Bentley, Phase stability and defect structure of the C15 Laves phase $Nb(Cr,V)_2$, *Acta Mater.* 46 (**1998**) 1759-1769.
[116] C.T. Liu, J.H. Zhu, M.P. Brady, C.G. McKamey, L.M. Pike, Physical metallurgy and mechanical properties of transition-metal Laves phase alloys, *Intermetallics* 8 (**2000**) 1119-1129.
[117] J.H. Zhu, C.T. Liu, P.K. Liaw, Phase stability and mechanical behavior of $NbCr_2$-based Laves phases, *Intermetallics* 7 (**1999**) 1011-1016.
[118] S. Scudino, P. Donnadieu, K.B. Surreddi, K. Nikolowski, M. Stoica, J. Eckert, Microstructure and mechanical properties of Laves phase-reinforced Fe-Zr-Cr alloys, *Intermetallics* 17 (**2009**) 532-539.
[119] A.J. Knowles, A. Bhowmik, S. Purkayastha, N.G. Jones, F. Giuliani, W.J. Clegg, D. Dye, H.J. Stone, Laves phase intermetallic matrix composite in situ toughened by ductile precipitates, *Scr. Mater.* 140 (**2017**) 59-62.
[120] M. Takeyama, C.T. Liu, Microstructure and Mechanical-Properties of Laves-Phase Alloys Based on $Cr_2Nb$, *Mater. Sci. Eng. A* 132 (**1991**) 61-66.
[121] A. Wasilkowska, M. Bartsch, F. Stein, M. Palm, K. Sztwiertnia, G. Sauthoff, U. Messerschmidt, Plastic deformation of Fe-Al polycrystals strengthened with Zr-containing Laves phases - I. Microstructure of undeformed materials, *Mater. Sci. Eng. A* 380 (**2004**) 9-19.
[122] P.S. Nnamchi, C.S. Obayi, I. Todd, M.W. Rainforth, Mechanical and electrochemical characterisation of new Ti-Mo-Nb-Zr alloys for biomedical applications, *J. Mech. Behav. Biomed.* 60 (**2016**) 68-77.
[123] Y. Abd-elrhman, M.A.H. Gepreel, A. Abdel-Moniem, S. Kobayashi, Compatibility assessment of new V-free low-cost Ti–4.7Mo–4.5Fe alloy for some biomedical applications, *Mater. Des.* 97 (**2016**) 445-453.
[124] D. Kuroda, H. Kawasaki, A. Yamamoto, S. Hiromoto, T. Hanawa, Mechanical properties and microstructures of new Ti–Fe–Ta and Ti–Fe–Ta–Zr system alloys, *Mater. Sci. Eng. C* 25 (**2005**) 312-320.
[125] Y. Kusano, T. Inamura, H. Kanetaka, S. Miyazaki, H. Hosoda, Phase Constitution and Mechanical Properties of Ti-(Cr, Mn)-Sn Biomedical Alloys, *Mater. Sci. Forum* 654 (**2010**) 2118-2121.
[126] X.F. Zhao, M. Niinomi, M. Nakai, J. Hieda, Young's Modulus Changeable β-Type Binary Ti-Cr Alloys for Spinal Fixation Applications, *Key Eng. Mater.* 508 (**2012**) 117-123.
[127] D. Kent, G. Wang, Z. Yu, M.S. Dargusch, Pseudoelastic behaviour of a β Ti–25Nb–3Zr–3Mo–2Sn alloy, *Mater. Sci. Eng. A* 527 (**2010**) 2246-2252.
[128] S. Ozan, Y. Li, J. Lin, Y. Zhang, H. Jiang, C. Wen, Microstructural evolution and its influence on the mechanical properties of a thermomechanically processed β Ti–32Zr–30Nb alloy, *Mater. Sci. Eng. A* 719 (**2018**) 112-123.
[129] P. Wang, Y. Feng, F. Liu, L. Wu, S. Guan, Microstructure and mechanical properties of Ti–Zr–Cr biomedical alloys, *Mater. Sci. Eng. C* 51 (**2015**) 148-152.
[130] X. Zhao, M. Niinomi, M. Nakai, J. Hieda, T. Ishimoto, T. Nakano, Optimization of Cr content of metastable β-type Ti–Cr alloys with changeable Young's modulus for spinal fixation applications, *Acta Biomater.* 8 (**2012**) 2392-2400.

[131] W. Huo, H. Zhou, F. Fang, Z. Xie, J. Jiang, Microstructure and mechanical properties of $CoCrFeNiZr_x$ eutectic high-entropy alloys, *Mater. Des.* 134 (**2017**) 226-233.
[132] A.I. Taub, R.L. Fleischer, Intermetallic Compounds for High-Temperature Structural Use, *Science* 243 (**1989**) 616-621.
[133] L. Wang, L. Xie, Y. Lv, L. Zhang, L. Chen, Q. Meng, J. Qu, D. Zhang, W. Lu, Microstructure evolution and superelastic behavior in Ti-35Nb-2Ta-3Zr alloy processed by friction stir processing, *Acta Mater.* 131 (**2017**) 499-510.
[134] S. Huang, X. Zhang, Y. Jiang, Y. Jiang, C. Mao, D. Wu, L. Zhang, L. Liu, Experimental investigation of Ti-Nb-Co ternary system at 1000°C, *Mater. Des.* 115 (**2017**) 170-178.
[135] C. Liu, J.Q. Qin, Z.H. Feng, S.L. Zhang, M.Z. Ma, X.Y. Zhang, R.P. Liu, Improving the microstructure and mechanical properties of Zr-Ti alloy by nickel addition, *J. Alloys Compd.* 737 (**2018**) 405-411.
[136] J. Wang, Z. Qin, F. Xiong, S. Wang, X. Lu, C. Li, Design and preparation of low-cost $\alpha + \beta$ titanium alloy based on assessment of Ti-Al-Fe-Cr system, *Mater. Sci. Eng. A* 732 (**2018**) 63-69.
[137] X.H. Min, S. Emura, N. Sekido, T. Nishimura, K. Tsuchiya, K. Tsuzaki, Effects of Fe addition on tensile deformation mode and crevice corrosion resistance in Ti–15Mo alloy, *Mater. Sci. Eng. A* 527 (**2010**) 2693-2701.
[138] Y.D. Shi, L.N. Wang, S.X. Liang, Q. Zhou, B. Zheng, A high Zr-containing Ti-based alloy with ultralow Young's modulus and ultrahigh strength and elastic admissible strain, *Mater. Sci. Eng. A* 674 (**2016**) 696-700.
[139] L. Chen, J. Li, Y. Zhang, L.-C. Zhang, W. Lu, L. Zhang, L. Wang, D. Zhang, Effects of alloyed Si on the autoclave corrosion performance and periodic corrosion kinetics in Zr–Sn–Nb–Fe–O alloys, *Corros. Sci.* 100 (**2015**) 651-662.
[140] L. Chen, J. Li, Y. Zhang, L.-C. Zhang, W. Lu, L. Wang, L. Zhang, D. Zhang, Zr–Sn–Nb–Fe–Si–O alloy for fuel cladding candidate: Processing, microstructure, corrosion resistance and tensile behavior, *Corros. Sci.* 100 (**2015**) 332-340.
[141] Y.J. Liu, X.P. Li, L.C. Zhang, T.B. Sercombe, Processing and properties of topologically optimised biomedical Ti–24Nb–4Zr–8Sn scaffolds manufactured by selective laser melting, *Mater. Sci. Eng. A* 642 (**2015**) 268-278.
[142] T. Ishimasa, Chapter 3 New group of icosahedral quasicrystals, in: T. Fujiwara, Y. Ishii (Eds.), Handbook of Metal Physics, Elsevier, Oxford, **2008**, pp. 49-74.
[143] C. Zehnder, K. Czerwinski, K.D. Molodov, S. Sandlöbes-Haut, J.S.K.L. Gibson, S. Korte-Kerzel, Plastic deformation of single crystalline C14 $Mg_2Ca$ Laves phase at room temperature, *Mater. Sci. Eng. A* 759 (**2019**) 754-761.
[144] B.D. Cullity, S.R. Stock, Elements of X-Ray Diffraction, third ed., Prentice-Hall, New York, **2001**.
[145] L.C. Zhang, Z.Q. Shen, J. Xu, Glass formation in a (Ti, Zr, Hf)–(Cu, Ni, Ag)–Al high-order alloy system by mechanical alloying, *J. Mater. Res.* 18 (**2003**) 2141-2149.
[146] L.C. Zhang, J. Xu, Glass-forming ability of melt-spun multicomponent (Ti, Zr, Hf)–(Cu, Ni, Co)–Al alloys with equiatomic substitution, *J. Non-Cryst. Solids* 347 (**2004**) 166-172.
[147] G.K. Williamson, R.E. Smallman, III. Dislocation densities in some annealed and cold-worked metals from measurements on the X-ray debye-scherrer spectrum, *The Philosophical Magazine: A Journal of Theoretical Experimental and Applied Physics* 1 (**1956**) 34-46.

[148] A. Shabani, M.R. Toroghinejad, A. Shafyei, P. Cavaliere, Effect of cold-rolling on microstructure, texture and mechanical properties of an equiatomic FeCrCuMnNi high entropy alloy, *Materialia* 1 (**2018**) 175-184.
[149] A.P. Zhilyaev, A.A. Samigullina, A.A. Nazarov, E.R. Shayakhmetova, Structure evolution in coarse-grained nickel under ultrasonic treatment, *Mater. Sci. Eng. A* 731 (**2018**) 231-238.
[150] K. Bazzi, A. Rathi, V.M. Meka, R. Goswami, T.V. Jayaraman, Significant reduction in intrinsic coercivity of high-entropy alloy FeCoNiAl0.375Si0.375 comprised of supersaturated f.c.c. phase, *Materialia* 6 (**2019**) 100293.
[151] C. Suryanarayana, M.G. Norton, X-ray diffraction: a practical approach, Springer Science & Business Media, Berlin, **2013**.
[152] G.K. Williamson, W.H. Hall, X-ray line broadening from filed aluminium and wolfram, *Acta Metall.* 1 (**1953**) 22-31.
[153] Y.J. Yin, J.Q. Sun, J. Guo, X.F. Kan, D.C. Yang, Mechanism of high yield strength and yield ratio of 316 L stainless steel by additive manufacturing, *Mater. Sci. Eng. A* 744 (**2019**) 773-777.
[154] F. Laliberte, M. Li, J. Almer, L. Liu, In-situ synchrotron X-ray study of microstructural evolution during creep deformation in Grade 91 steel, *Mater. Sci. Eng. A* 737 (**2018**) 115-123.
[155] H. Zhang, X. Jing, G. Subhash, L.J. Kecskes, R.J. Dowding, Investigation of shear band evolution in amorphous alloys beneath a Vickers indentation, *Acta Mater.* 53 (**2005**) 3849-3859.
[156] U. Ramamurty, S. Jana, Y. Kawamura, K. Chattopadhyay, Hardness and plastic deformation in a bulk metallic glass, *Acta Mater.* 53 (**2005**) 705-717.
[157] S. Sadeghpour, S.M. Abbasi, M. Morakabati, A. Kisko, L.P. Karjalainen, D.A. Porter, On the compressive deformation behavior of new beta titanium alloys designed by d-electron method, *J. Alloys Compd.* 746 (**2018**) 206-217.
[158] M. Morinaga, 1.3 - The molecular orbital approach and its application to biomedical titanium alloy design A2 - Froes, Francis H, in: M. Qian (Ed.), Titanium in Medical and Dental Applications, Woodhead Publishing, **2018**, pp. 39-64.
[159] D.J. Lin, J.H. Chern Lin, C.P. Ju, Structure and properties of Ti–7.5Mo–xFe alloys, *Biomater.* 23 (**2002**) 1723-1730.
[160] A. Cremasco, P.N. Andrade, R.J. Contieri, E.S.N. Lopes, C.R.M. Afonso, R. Caram, Correlations between aging heat treatment, ω phase precipitation and mechanical properties of a cast Ti–Nb alloy, *Mater. Des.* 32 (**2011**) 2387-2390.
[161] S. Gabriel, J. Panaino, I. Santos, L. Araujo, P. Mei, L. De Almeida, C. Nunes, Characterization of a new beta titanium alloy, Ti–12Mo–3Nb, for biomedical applications, *J. Alloys Compd.* 536 (**2012**) S208-S210.
[162] A. Biesiekierski, J. Lin, Y. Li, D. Ping, Y. Yamabe-Mitarai, C. Wen, Investigations into Ti–(Nb, Ta)–Fe alloys for biomedical applications, *Acta Biomater.* 32 (**2016**) 336-347.
[163] D.Q. Martins, M.E.P. Souza, S.A. Souza, D.C. Andrade, C.M.A. Freire, R. Caram, Solute segregation and its influence on the microstructure and electrochemical behavior of Ti–Nb–Zr alloys, *J. Alloys Compd.* 478 (**2009**) 111-116.
[164] P.E.L. Moraes, R.J. Contieri, E.S.N. Lopes, A. Robin, R. Caram, Effects of Sn addition on the microstructure, mechanical properties and corrosion behavior of Ti–Nb–Sn alloys, *Mater. Charact.* 96 (**2014**) 273-281.

[165] Y.-Q. Ma, S.-Y. Yang, W.-J. Jin, Y.-N. Wang, C.-P. Wang, X.-J. Liu, Microstructure, mechanical and shape memory properties of Ti-55Ta-xSi biomedical alloys, *Trans. Nonferrous Met. Soc. China* 21 (**2011**) 287-291.
[166] B. Liu, Y.P. Li, H. Matsumoto, Y.B. Liu, Y. Liu, A. Chiba, Thermomechanical characterization of P/M Ti–Fe–Mo–Y alloy with a fine lamellar microstructure, *Mater. Sci. Eng. A* 528 (**2011**) 2345-2352.
[167] P. Zhang, S.X. Li, Z.F. Zhang, General relationship between strength and hardness, *Mater. Sci. Eng. A* 529 (**2011**) 62-73.
[168] P. Manda, U. Chakkingal, A.K. Singh, Hardness characteristic and shear band formation in metastable β-titanium alloys, *Mater. Charact.* 96 (**2014**) 151-157.
[169] J. Xu, G.d. Wang, X. Lu, L. Liu, P. Munroe, Z.-H. Xie, Mechanical and corrosion-resistant properties of Ti–Nb–Si–N nanocomposite films prepared by a double glow discharge plasma technique, *Ceram. Int.* 40 (**2014**) 8621-8630.
[170] R.P. Kolli, W.J. Joost, S. Ankem, Phase Stability and Stress-Induced Transformations in Beta Titanium Alloys, *JOM* 67 (**2015**) 1273-1280.
[171] V. Raghavan, Fe-Nb-Ti (Iron-Niobium-Titanium), *J. Phase Equilibria* 33 (**2012**) 404-406.
[172] C. Yang, T. Wei, Y.P. Yao, Y.H. Li, S.G. Qu, L.C. Zhang, Bulk multimodal-grained irons with large plasticity fabricated by spark plasma sintering, *Mater. Sci. Eng. A* 591 (**2014**) 54-58.
[173] H. Attar, M. Calin, L.C. Zhang, S. Scudino, J. Eckert, Manufacture by selective laser melting and mechanical behavior of commercially pure titanium, *Mater. Sci. Eng. A* 593 (**2014**) 170-177.
[174] J.S. Keist, T.A. Palmer, Development of strength-hardness relationships in additively manufactured titanium alloys, *Mater. Sci. Eng. A* 693 (**2017**) 214-224.
[175] P.J. Bardziński, P. Błyskun, Mechanical properties and structure of rapidly solidified bulk $Fe_{89-x}Hf_4Ta_1Cu_1Gd_1Si_xB_4$ (x=0–15) and $Fe_{74}Hf_4Ta_1Cu_1Gd_1La_ySi_{15-y}B_4$ (y=7) alloys, *Mater. Des.* 103 (**2016**) 377-390.
[176] C. Ai, F. He, M. Guo, J. Zhou, Z.J. Wang, Z.W. Yuan, Y.J. Guo, Y.L. Liu, L. Liu, Alloy design, micromechanical and macromechanical properties of $CoCrFeNiTa_x$ eutectic high entropy alloys, *J. Alloys Compd.* 735 (**2018**) 2653-2662.
[177] Y. Tian, B. Ouyang, A. Gontcharov, R. Gauvin, P. Lowden, M. Brochu, Microstructure evolution of Inconel 625 with 0.4 wt% boron modification during gas tungsten arc deposition, *J. Alloys Compd.* 694 (**2017**) 429-438.
[178] D.D. Risanti, G. Sauthoff, Strengthening of iron aluminide alloys by atomic ordering and Laves phase precipitation for high-temperature applications, *Intermetallics* 13 (**2005**) 1313-1321.
[179] C.C. Silva, H.C. de Miranda, M.F. Motta, J.P. Farias, C.R.M. Afonso, A.J. Ramirez, New insight on the solidification path of an alloy 625 weld overlay, *J. Mater. Res. Technol.* 2 (**2013**) 228-237.
[180] X.J. Zhang, Y.B. Li, X.D. He, Y. Sun, S.P. Pang, G.H. Su, X.R. Liu, Z.R. Yang, Influence of Cr addition on microstructure and mechanical properties of Zr-based alloys corresponding to Zr-C-Cr system, *J. Alloys Compd.* 640 (**2015**) 240-245.
[181] J.J. Schirra, R.H. Caless, R.W. Hatala, The effect of Laves phase on the mechanical properties of wrought and cast+ HIP Inconel 718, in: E.A. Loria (Ed.), Superalloys 718, 625, 706 and Various Derivates, TMS, Warrendale, PA, **1991**, pp. 375-388.

[182] J.M. Park, K.B. Kim, W.T. Kim, M.H. Lee, J. Eckert, D.H. Kim, High strength ultrafine eutectic Fe-Nb-Al composites with enhanced plasticity, *Intermetallics* 16 (**2008**) 642-650.
[183] P. Donnadieu, C. Pohlmann, S. Scudino, J.J. Blandin, K.B. Surreddi, J. Eckert, Deformation at ambient and high temperature of in situ Laves phases-ferrite composites, *Sci. Technol. Adv. Mater.* 15 (**2014**) 034801.
[184] J. Strasky, P. Harcuba, K. Vaclavova, K. Horvath, M. Landa, O. Srba, M. Janecek, Increasing strength of a biomedical Ti-Nb-Ta-Zr alloy by alloying with Fe, Si and O, *J. Mech. Behav. Biomed.* 71 (**2017**) 329-336.
[185] Y.J. Hwang, S.H. Hong, Y.S. Kim, H.J. Park, Y.B. Jeong, J.T. Kim, K.B. Kim, Influence of silicon content on microstructure and mechanical properties of Ti-Cr-Si alloys, *J. Alloys Compd.* 737 (**2018**) 53-57.
[186] A.L. Greer, Y.Q. Cheng, E. Ma, Shear bands in metallic glasses, *Mater. Sci. Eng., R* 74 (**2013**) 71-132.
[187] M.A. Meyers, G. Subhash, B.K. Kad, L. Prasad, Evolution of Microstructure and Shear-Band Formation in Alpha-Hcp Titanium, *Mech. Mater.* 17 (**1994**) 175-193.
[188] D.M. Kochmann, K.C. Le, A continuum model for initiation and evolution of deformation twinning, *J. Mech. Phys. Solids* 57 (**2009**) 987-1002.
[189] Y. Yang, X.M. Li, X.L. Tong, Q.M. Zhang, C.Y. Xu, Effects of microstructure on the adiabatic shearing behaviors of titanium alloy, *Mater. Sci. Eng. A* 528 (**2011**) 3130-3133.
[190] B.A. Sun, W.H. Wang, The fracture of bulk metallic glasses, *Prog. Mater. Sci.* 74 (**2015**) 211-307.
[191] L.H. Liu, C. Yang, F. Wang, S.G. Qu, X.Q. Li, W.W. Zhang, Y.Y. Li, L.C. Zhang, Ultrafine grained Ti-based composites with ultrahigh strength and ductility achieved by equiaxing microstructure, *Mater. Des.* 79 (**2015**) 1-5.
[192] Y.K. Xu, H. Ma, J. Xu, E. Ma, Mg-based bulk metallic glass composites with plasticity and gigapascal strength, *Acta Mater.* 53 (**2005**) 1857-1866.
[193] I.V. Okulov, H. Wendrock, A.S. Volegov, H. Attar, U. Kuhn, W. Skrotzki, J. Eckert, High strength beta titanium alloys: New design approach, *Mater. Sci. Eng. A* 628 (**2015**) 297-302.
[194] G.H. Zhao, S.V. Ketov, J. Jiang, H. Mao, A. Borgenstam, D.V. Louzguine-Luzgin, New beta-type Ti-Fe-Sn-Nb alloys with superior mechanical strength, *Mater. Sci. Eng. A* 705 (**2017**) 348-351.
[195] M.E. Schlesinger, The Mn-Zr (manganese-zirconium) system, *J. Phase Equilibria* 20 (**1999**) 79-83.
[196] V. Ivanchenko, Mn-Ti-Zr (Manganese-Titanium-Zirconium), in: G. Effenberg, S. Ilyenko (Eds.), Non-Ferrous Metal Systems. Part 3: Selected Soldering and Brazing Systems, Springer Berlin Heidelberg, Berlin, Heidelberg, **2007**, pp. 475-485.
[197] V. Raghavan, Fe-Ti-Zr (Iron-Titanium-Zirconium), *J. Phase Equilibria* 31 (**2010**) 469.
[198] G. Li, N. Nishimiya, H. Satoh, N. Kamegashira, Crystal structure and hydrogen absorption of $Ti_xZr_{1-x}Mn_2$, *J. Alloys Compd.* 393 (**2005**) 231-238.
[199] H. Flandorfer, J. Grobner, A. Stamou, N. Hassiotis, A. Saccone, P. Rogl, R. Wouters, H. Seifert, D. Maccio, R. Ferro, G. Haidemenopoulos, L. Delaey, G. Effenberg, Experimental investigation and thermodynamic calculation of the ternary system Mn-Y-Zr, *Z. Metallk.* 88 (**1997**) 529-538.
[200] E.L. Stevens, J. Toman, A.C. To, M. Chmielus, Variation of hardness, microstructure, and Laves phase distribution in direct laser deposited alloy 718 cuboids, *Mater. Des.* 119 (**2017**) 188-198.

[201] Y.D. Wu, Y.H. Cai, X.H. Chen, T. Wang, J.J. Si, L. Wang, Y.D. Wang, X.D. Hui, Phase composition and solid solution strengthening effect in TiZrNbMoV high-entropy alloys, *Mater. Des.* 83 (**2015**) 651-660.
[202] D. Aboudi, S. Lebaili, M. Taouinet, J. Zollinger, Microstructure evolution of diffusion welded 304L/Zircaloy4 with copper interlayer, *Mater. Des.* 116 (**2017**) 386-394.
[203] G. Gottstein, Physical foundations of materials science, first ed., Springer Science & Business Media, Berlin, **2013**.
[204] A. Devaraj, W. Wang, R. Vemuri, L. Kovarik, X. Jiang, M. Bowden, J.R. Trelewicz, S. Mathaudhu, A. Rohatgi, Grain Boundary Segregation and Intermetallic Precipitation in Coarsening Resistant Nanocrystalline Aluminum Alloys, *Acta Mater.* (**2018**).
[205] N.Y. Yurchenko, N.D. Stepanov, A.O. Gridneva, M.V. Mishunin, G.A. Salishchev, S.V. Zherebtsov, Effect of Cr and Zr on phase stability of refractory Al-Cr-Nb-Ti-V-Zr high-entropy alloys, *J. Alloys Compd.* 757 (**2018**) 403-414.
[206] X. Li, J.J. Shi, C.H. Wang, G.H. Cao, A.M. Russell, Z.J. Zhou, C.P. Li, G.F. Chen, Effect of heat treatment on microstructure evolution of Inconel 718 alloy fabricated by selective laser melting, *J. Alloys Compd.* 764 (**2018**) 639-649.
[207] P. Xie, M. Han, C.L. Wu, Y.Q. Yin, K. Zhu, R.H. Shen, J.H. Chen, A high-performance TRIP steel enhanced by ultrafine grains and hardening precipitates, *Mater. Des.* 127 (**2017**) 1-7.
[208] F.C. Campbell, Chapter 5: Eutectic Alloy Systems, in: F.C. Campbell (Ed.), Phase diagrams: understanding the basics, ASM International, Ohio, **2012**.
[209] F.G. Coury, T. Butler, K. Chaput, A. Saville, J. Copley, J. Foltz, P. Mason, K. Clarke, M. Kaufman, A. Clarke, Phase equilibria, mechanical properties and design of quaternary refractory high entropy alloys, *Mater. Des.* 155 (**2018**) 244-256.
[210] B. Gwalani, V. Soni, M. Lee, S.A. Mantri, Y. Ren, R. Banerjee, Optimizing the coupled effects of Hall-Petch and precipitation strengthening in a $Al_{0.3}$CoCrFeNi high entropy alloy, *Mater. Des.* 121 (**2017**) 254-260.
[211] L.Y. Du, L. Wang, W. Zhai, L. Hu, J.M. Liu, B. Wei, Liquid state property, structural evolution and mechanical behavior of TiFe alloy solidified under electrostatic levitation condition, *Mater. Des.* 160 (**2018**) 48-57.
[212] R.L. Fleisgher, Solution hardening, *Acta Metall.* 9 (**1961**) 996-1000.
[213] L.Y. Sheng, J.T. Guo, H.Q. Ye, Microstructure and mechanical properties of NiAl–Cr(Mo)/Nb eutectic alloy prepared by injection-casting, *Mater. Des.* 30 (**2009**) 964-969.
[214] A. Ruiz-Moreno, P. Hähner, Indentation size effects of ferritic/martensitic steels: A comparative experimental and modelling study, *Mater. Des.* 145 (**2018**) 168-180.
[215] A. Das, S. Tarafder, Geometry of dimples and its correlation with mechanical properties in austenitic stainless steel, *Scr. Mater.* 59 (**2008**) 1014-1017.
[216] J.L. Sun, P.W. Trimby, F.K. Yan, X.Z. Liao, N.R. Tao, J.T. Wang, Shear banding in commercial pure titanium deformed by dynamic compression, *Acta Mater.* 79 (**2014**) 47-58.
[217] Y.J. Liu, S.J. Li, L.C. Zhang, Y.L. Hao, T.B. Sercombe, Early plastic deformation behaviour and energy absorption in porous β-type biomedical titanium produced by selective laser melting, *Scr. Mater.* 153 (**2018**) 99-103.
[218] R. Vaidyanathan, M. Dao, G. Ravichandran, S. Suresh, Study of mechanical deformation in bulk metallic glass through instrumented indentation, *Acta Mater.* 49 (**2001**) 3781-3789.
[219] A. Hasnaoui, H. Van Swygenhoven, P.M. Derlet, Dimples on Nanocrystalline Fracture Surfaces As Evidence for Shear Plane Formation, *Science* 300 (**2003**) 1550-1552.

[220] J. Fan, J. Li, H. Kou, K. Hua, B. Tang, Y. Zhang, Microstructure and mechanical property correlation and property optimization of a near β titanium alloy Ti-7333, *J. Alloys Compd.* 682 (**2016**) 517-524.
[221] P. Sellappan, T. Rouxel, F. Celarie, E. Becker, P. Houizot, R. Conradt, Composition dependence of indentation deformation and indentation cracking in glass, *Acta Mater.* 61 (**2013**) 5949-5965.
[222] D. Ćorić, M. Majić Renjo, L. Ćurković, Vickers indentation fracture toughness of Y-TZP dental ceramics, *Int. J. Refract. Met. Hard Mater.* 64 (**2017**) 14-19.
[223] Y. Yang, L. Wang, L. Snead, S.J. Zinkle, Development of novel Cu-Cr-Nb-Zr alloys with the aid of computational thermodynamics, *Mater. Des.* 156 (**2018**) 370-380.
[224] T. To, F. Célarié, C. Roux-Langlois, A. Bazin, Y. Gueguen, H. Orain, M. Le Fur, V. Burgaud, T. Rouxel, Fracture toughness, fracture energy and slow crack growth of glass as investigated by the Single-Edge Precracked Beam (SEPB) and Chevron-Notched Beam (CNB) methods, *Acta Mater.* 146 (**2018**) 1-11.
[225] R. Bhowmick, R. Raghavan, K. Chattopadhyay, U. Ramamurty, Plastic flow softening in a bulk metallic glass, *Acta Mater.* 54 (**2006**) 4221-4228.
[226] A.E. Giannakopoulos, S. Suresh, Determination of elastoplastic properties by instrumented sharp indentation, *Scr. Mater.* 40 (**1999**) 1191-1198.
[227] E. Jumaev, S.H. Hong, J.T. Kim, H.J. Park, Y.S. Kim, S.C. Mun, J.-Y. Park, G. Song, J.K. Lee, B.H. Min, T. Lee, K.B. Kim, Chemical evolution-induced strengthening on AlCoCrNi dual-phase high-entropy alloy with high specific strength, *J. Alloys Compd.* 777 (**2019**) 828-834.
[228] C. Yang, L.M. Kang, X.X. Li, W.W. Zhang, D.T. Zhang, Z.Q. Fu, Y.Y. Li, L.C. Zhang, E.J. Lavernia, Bimodal titanium alloys with ultrafine lamellar eutectic structure fabricated by semi-solid sintering, *Acta Mater.* 132 (**2017**) 491-502.
[229] Y. Zhang, D. Kent, G. Wang, D. St John, M. Dargusch, An investigation of the mechanical behaviour of fine tubes fabricated from a Ti–25Nb–3Mo–3Zr–2Sn alloy, *Mater. Des.* 85 (**2015**) 256-265.
[230] C. Yang, O. Muránsky, H. Zhu, G.J. Thorogood, H. Huang, X. Zhou, On the origin of strengthening mechanisms in Ni-Mo alloys prepared via powder metallurgy, *Mater. Des.* 113 (**2017**) 223-231.
[231] Y.B. Jeong, H.R. Jo, J.T. Kim, S.H. Hong, K.B. Kim, A study on the micro-evolution of mechanical property and microstructures in (Cu-30Fe)-2X alloys with the addition of minor alloying elements, *J. Alloys Compd.* 786 (**2019**) 341-345.
[232] W. Niu, M.J. Bermingham, P.S. Baburamani, S. Palanisamy, M.S. Dargusch, S. Turk, B. Grigson, P.K. Sharp, The effect of cutting speed and heat treatment on the fatigue life of Grade 5 and Grade 23 Ti–6Al–4V alloys, *Mater. Des.* 46 (**2013**) 640-644.
[233] L. Chen, Q. Zeng, J. Li, J. Lu, Y. Zhang, L.-C. Zhang, X. Qin, W. Lu, L. Zhang, L. Wang, D. Zhang, Effect of microstructure on corrosion behavior of a Zr–Sn–Nb–Fe–Cu–O alloy, *Mater. Des.* 92 (**2016**) 888-896.
[234] B.D. Beake, A.J. Harris, J. Moghal, D.E.J. Armstrong, Temperature dependence of strain rate sensitivity, indentation size effects and pile-up in polycrystalline tungsten from 25 to 950 °C, *Mater. Des.* 156 (**2018**) 278-286.
[235] Y. Cao, Z. Xue, X. Chen, D. Raabe, Correlation between the flow stress and the nominal indentation hardness of soft metals, *Scr. Mater.* 59 (**2008**) 518-521.

[236] M.C. Li, M.Q. Jiang, F. Jiang, L. He, J. Sun, Testing effects on hardness of a Zr-based metallic glass under nanoindentation, *Scr. Mater.* 138 (**2017**) 120-123.
[237] K.C. Chen, S.M. Allen, J.D. Livingston, Factors affecting the room-temperature mechanical properties of $TiCr_2$-base Laves phase alloys, *Mater. Sci. Eng. A* 242 (**1998**) 162-173.
[238] D. Kramer, H. Huang, M. Kriese, J. Robach, J. Nelson, A. Wright, D. Bahr, W.W. Gerberich, Yield strength predictions from the plastic zone around nanocontacts, *Acta Mater.* 47 (**1998**) 333-343.
[239] S. Xie, E.P. George, Hardness and shear band evolution in bulk metallic glasses after plastic deformation and annealing, *Acta Mater.* 56 (**2008**) 5202-5213.
[240] Z. Yan, K. Wang, Y. Zhou, X. Zhu, R. Xin, Q. Liu, Crystallographic orientation dependent crack nucleation during the compression of a widmannstätten-structure α/β titanium alloy, *Scr. Mater.* 156 (**2018**) 110-114.
[241] L. Lu, Y. Shen, X. Chen, L. Qian, K. Lu, Ultrahigh Strength and High Electrical Conductivity in Copper, *Science* 304 (**2004**) 422-426.
[242] C.R. Hutchinson, J.F. Nie, S. Gorsse, Modeling the precipitation processes and strengthening mechanisms in a Mg-Al-(Zn) AZ91 alloy, *Metall. Mater. Trans. A* 36 (**2005**) 2093-2105.
[243] J. Wang, M.R.G. Ferdowsi, S.R. Kada, C.R. Hutchinson, M.R. Barnett, Influence of precipitation on yield elongation in Mg-Zn alloys, *Scr. Mater.* 160 (**2019**) 5-8.
[244] S. Shukla, T. Wang, S. Cotton, R.S. Mishra, Hierarchical microstructure for improved fatigue properties in a eutectic high entropy alloy, *Scr. Mater.* 156 (**2018**) 105-109.
[245] Y.J. Liu, Y.S. Zhang, L.C. Zhang, Transformation-induced plasticity and high strength in beta titanium alloy manufactured by selective laser melting, *Materialia* 6 (**2019**) 100299.
[246] J.C. Wang, Y.J. Liu, P. Qin, S.X. Liang, T.B. Sercombe, L.C. Zhang, Selective laser melting of Ti–35Nb composite from elemental powder mixture: Microstructure, mechanical behavior and corrosion behavior, *Mater. Sci. Eng. A* 760 (**2019**) 214-224.
[247] C.L. Yang, Z.J. Zhang, P. Zhang, C.Y. Cui, Z.F. Zhang, Synchronous improvement of the strength and plasticity of Ni-Co based superalloys, *Mater. Sci. Eng. A* 736 (**2018**) 100-104.
[248] L. Zeng, G. Xu, L. Liu, W. Bai, L. Zhang, Experimental investigation of phase equilibria in the Ti-Fe-Zr system, *Calphad* 61 (**2018**) 20-32.
[249] O.N. Senkov, S. Rao, K.J. Chaput, C. Woodward, Compositional effect on microstructure and properties of NbTiZr-based complex concentrated alloys, *Acta Mater.* 151 (**2018**) 201-215.
[250] D.H. Krinsley, K. Pye, S. Boggs Jr, N.K. Tovey, Backscattered scanning electron microscopy and image analysis of sediments and sedimentary rocks, Cambridge University Press, Cambridge, **2005**.
[251] J. Chakrabarty, Applied plasticity, Springer, New York, **2000**.
[252] Y.H. Li, C. Yang, F. Wang, H.D. Zhao, S.G. Qu, X.Q. Li, W.W. Zhang, Y.Y. Li, Biomedical TiNbZrTaSi alloys designed by d-electron alloy design theory, *Mater. Des.* 85 (**2015**) 7-13.
[253] H. Zhan, W. Zeng, G. Wang, D. Kent, M. Dargusch, On the deformation mechanisms and strain rate sensitivity of a metastable β Ti–Nb alloy, *Scr. Mater.* 107 (**2015**) 34-37.
[254] D. Udler, D.N. Seidman, Solute-atom interactions with low-angle twist boundaries, *Scripta Metallurgica et Materialia* 26 (**1992**) 449-454.
[255] M.I. Isik, A. Kostka, V.A. Yardley, K.G. Pradeep, M.J. Duarte, P.P. Choi, D. Raabe, G. Eggeler, The nucleation of Mo-rich Laves phase particles adjacent to M23C6 micrograin boundary carbides in 12% Cr tempered martensite ferritic steels, *Acta Mater.* 90 (**2015**) 94-104.

[256] L. Wang, W. Lu, J. Qin, F. Zhang, D. Zhang, Influence of cold deformation on martensite transformation and mechanical properties of Ti–Nb–Ta–Zr alloy, *J. Alloys Compd.* 469 (**2009**) 512-518.
[257] L.M. Kang, C. Yang, F. Wang, S.G. Qu, X.Q. Li, W.W. Zhang, Deformation induced precipitation of $MgZn_2$-type laves phase in Ti-Fe-Co alloy, *J. Alloys Compd.* 778 (**2019**) 795-802.
[258] D.V. Louzguine-Luzgin, L.V. Louzguina-Luzgina, V.I. Polkin, A. Inoue, Deformation-induced transformations in $Ti_{60}Fe_{20}Co_{20}$ alloy, *Scr. Mater.* 57 (**2007**) 445-448.
[259] X. Li, R. Song, N. Zhou, J. Li, An ultrahigh strength and enhanced ductility cold-rolled medium-Mn steel treated by intercritical annealing, *Scr. Mater.* 154 (**2018**) 30-33.
[260] S. Liu, Z. Xiong, H. Guo, C. Shang, R.D.K. Misra, The significance of multi-step partitioning: Processing-structure-property relationship in governing high strength-high ductility combination in medium-manganese steels, *Acta Mater.* 124 (**2017**) 159-172.
[261] R.W. Hertzberg, R.P. Vinci, J.L. Hertzberg, Deformation and fracture mechanics of engineering materials, fifth ed., Wiley, Hoboken, NJ, **2013**.

# Personal details

**Educational history**

- Doctor of philosophy: Mechanical and Materials Engineering, Edith Cowan University, Australia.
- Master of Technology: Mechanical Engineering, Nirma University, India
- Bachelor of Engineering: Mechanical Engineering, Saurashtra University, India

**Personal experience**

This is the last section of my PhD thesis which provides my personal details. Today is 7$^{th}$ of January 2020 and my PhD thesis is finally being submitted after examination which suggest the end point of my PhD study and the beginning of a new era in my career. I will remember and follow the most insightful words/suggestions of respected Lai-Chang in progressing my career. I will remember the formulae: $1.001^{365}=1.440$, $1.002^{365}=2.073$ and increase my skills daily considering these formulae. I will stick to reading one research paper daily in enhancing my knowledge and research skills because research paper reading is a key to success in academic career. I will also remember the ECU-Joondalup campus and especially my office 5.222, where I have worked hard, spent many sleepless nights and learnt many valuable skills. Therefore, I want to cherish all these unforgettable sweet memories.

From these 3 years and 2 months of PhD journey, I have published 5 first-authored (including 3 in Materials & Design) and 2 second-authored journal articles as well as 1 International conference paper. I also have 6+ years of lecturing experience and 1 year of industrial experience.

At the end, I would like to extend my sincere gratitude to all my mentors and friends, thank you very much for being an important part of my life.